CERN–2005–009
5 September 2005

ORGANISATION EUROPÉENNE POUR LA RECHERCHE NUCLÉAIRE
CERN EUROPEAN ORGANIZATION FOR NUCLEAR RESEARCH

The REX-ISOLDE Facility: Design and Commissioning Report

Editors: F. Ames
J. Cederkall (Convenor)
T. Sieber
F. Wenander

Contributors: F. Ames, J. Cederkall, O. Kester, T. Sieber, R. von Hahn, P. van den Bergh, F. Wenander

CERN–850 copies printed–September 2005

Abstract

This report describes the design and commissioning phases of the REX-ISOLDE post-accelerator. The project was initiated in 1993 as a pilot experiment for the post-acceleration of radioactive beams produced by the ISOLDE facility at CERN. Machine construction began in 1995 and commissioning was completed in 2002. In 2004 the experiment (including machine development and physics issues related to beam preparation), which originally resided in the Experimental Physics Division, was incorporated in the Accelerators and Beams Department as a user facility. This report focuses on the technical issues related to construction and commissioning of the machine but also briefly addresses the physics cases for radioactive nuclear beams.

Foreword

Soon after ISOLDE came into operation in 1967, it was realized that some of the highest intensity radioactive ion beams lend themselves to post-acceleration. But it was only in the mid 1980s that a strong interest for post-accelerated radioactive beams was revealed by nuclear astrophysics, later followed by nuclear physics. The topic was vigorously discussed at many workshops and conferences and the first post-accelerated radioactive ion beam, produced in 1989 with coupled cyclotrons in Belgium, boosted the field of research. In the same year the PRIMA proposal to post-accelerate the ISOLDE beams was presented. However, it coincided with the shutdown of the SC and the move of ISOLDE to the PS Booster, and thus was not pursued.

In 1993, new life was given to the idea to post-accelerate the ISOLDE beams. Groups from Germany, Sweden, and Belgium, together with the ISOLDE Collaboration and CERN proposed a radically different concept of post-acceleration that would allow for efficient and cost-effective acceleration of radioactive ions from ISOLDE. The concept was based on bunching and cooling in a Penning trap, on charge breeding in an EBIS source, and on a linear accelerator that would bring the 60 keV, radioactive, singly-charged ions to 2.2 MeV/u in about 40 ms.

Low-multiplicity Coulomb excitation and transfer reaction experiments were proposed using a novel, high-efficiency detector array based on highly segmented germanium and silicon detectors; the so-called MINIBALL detector array. MINIBALL became possible by enlarging the original collaboration to include groups from France and the UK. The whole accelerator and detector system was proposed to the ISOLDE Scientific Committee as an experiment in November 1994. The proposal had two main aims: to show the feasibility of this new acceleration scheme and to perform the first Coulomb excitation measurements on neutron-rich magnesium isotopes ultimately reaching the short-lived ($T_{1/2}$ = 120 ms) ^{32}Mg isotope. In 1995 the CERN Research Board approved this Radioactive EXperiment at ISOLDE (REX-ISOLDE) and construction of the hall extension began.

It took several years of hard work to efficiently produce the first energetic radioactive beams (in 2001). In the same year, data taking with MINIBALL began on a number of different short-lived isotopes and in October 2004 the first high-quality data were collected on the Coulomb excitation of ^{32}Mg. This event marked the fulfilment of the goals put forward in the original REX-ISOLDE proposal.

Since then, the energy of REX-ISOLDE has been increased to 3.0 MeV/u, and even higher energies and intensities are currently being developed with HIE-ISOLDE. This will open a wide spectrum of new experiments of interest for nuclear physics and astrophysics as well as for applications in other fields of science. Ultimately, this will pave the way for the construction of the advanced radioactive ion-beam facility EURISOL.

Piet Van Duppen
Leuven, 9 December 2004

REX-ISOLDE and MINIBALL Collaborations

Associated institutes and universities

Catholic University, Leuven, Belgium

CERN, Geneva, Switzerland

Chalmers University, Gothenburg, Sweden

CSIC, Madrid, Spain

Darmstadt Technical University, Darmstadt, Germany

GSI, Darmstadt, Germany

Johann Wolfgang Goethe University, Frankfurt, Germany

Johannes Gutenberg University, Mainz, Germany

Louis Pasteur University, Strasbourg, France

Ludwig Maximilian University, Munich, Germany

Lund University, Lund, Sweden

Manne Siegbahn Laboratory, Stockholm, Sweden

Max Planck Institute for Nuclear Physics, Heidelberg, Germany

University of Aarhus, Aarhus, Denmark

University of Edinburgh, Edinburgh, UK

University of Cologne, Cologne, Germany

University of Liverpool, Liverpool, UK

Contents

Abbreviations and Acronyms

ADC	analog-to-digital converter
ANC	asymptotic normalization coefficient
API	application programmer's interface
BTS	beam transport system
CCV	current control value
CNO	carbon–nitrogen–oxygen cycle
CRYSIS	Cryogenic Stockholm Ion Source
DCOM	distributed component object model
DLL	dynamic link library
DP	distributed peripheral
DSC	device stub controller
EBIS	electron beam ion source
EURISOL	EURopean Isotope Separation On-Line Radioactive Ion Beam Facility
FEC	front-end computer
FWHM	full-width half-maximum
GDG	gate and delay generator
GFAS	simple analog function generator
GPIB	general-purpose interface bus
GUI	graphical user interface
HLI	HochLadungsInjektor
HV	high voltage
IKS	Institute for Nuclear and Reactor Physics (Catholic University Leuven)
ISA	industry standard architecture
ISO	International Organization for Standardization
ISOL	Isotope Separation On-Line
ISOLDE	On-Line Isotope Mass Separator
KONUS	KOmbinierte NUll Grad Sollteilchen Struktur
LMU	Ludwig Maximilian University
LORASR	LOngitudinale und RAdiale Strahldynamikrechnungen mit Raumladung
MACOR	machinable glass ceramic (registered trademark)
MAFF	Munich Accelerator for Fission Fragments
MCP	microchannel plate
MCR	main control room

MLL	Maier Leibnitz Laboratory
MPI	Max Planck Institute
NEG	non-evaporable getter
NMR	nuclear magnetic resonance
OFHC	oxygen-free high-conductive
OLE	object linking and embedding
OPC	object linking and embedding for process control
PARMTEQ	phase and radial motion in a transverse electric quadrupole
PB DP	PROFIBUS distributed peripheral
PCI	peripheral component interconnect
PID	proportional integral derivative
PLC	programmable logic controller
REX	Radioactive beam EXperiment
RFQ	radio frequency quadrupole
RIA	Rare Isotope Accelerator
RIB	radioactive ion beam
RIKRBF	RIKen Radioactive Beam Facility
RPC	remote procedure call
TCP/IP	transmission control protocol/internet protocol
TOF	time of flight
TRANSPORT	third order transport
TTL	transistor–transistor logic
TTF	transit time factor
UHV	ultra-high vacuum
VB	Visual Basic
VME	VERSAmodule Eurocard

1 Motivation and physics case

1.1 Introduction to the physics case for accelerated radioactive beams

Physics with Radioactive Ion Beams (RIBs) is a subject that incorporates many different subfields. Radioactive beams are of interest not only to pure nuclear physics; they are also vital for progress in nuclear astrophysics, fundamental physics, and for the application of nuclear physics in solid-state physics and the life sciences. The On-Line Isotope Mass Separator (ISOLDE) has been at the forefront of radioactive beam research for the past 30 years, using slow beams produced by the Isotope Separator On-Line (ISOL) method, and thus has contributed extensively to developments in many of these subfields.

The new trend in ISOL-based radioactive beam physics is a move towards the post-acceleration of beams with well-defined emittance. The aim is to perform precision experiments with radioactive beams of a kind that have until now been possible only with stable beams. Post-acceleration of a well-defined RIB will open up new territory for nuclear physics: territory that has remained unexplored for the past 50 years. Several projects for the next generation of post-accelerated RIBs are therefore under way or planned around the world, including the Riken Radioactive Beam Facility (RIKRBF) in Japan, the Rare Isotope Accelerator (RIA) project in the US, and the European Isotope Separation On-Line Radioactive Ion Beam Facility (EURISOL) in Europe. Several facilities with lower intensity beams, using both ISOL and fragmentation methods for ion beam production, are already active in Canada, Europe, Japan, and the US.

The ISOL method involves the bombardment of a thick target (g/cm^2) of a heavier element with a lighter driver beam. The radioactive isotopes are produced in spallation, fragmentation, or fission reactions. The advantage of this method is the high yields that can be achieved, particularly for isotopes with lifetimes down to the millisecond range. The limitation of the ISOL method lies in its chemical sensitivity. A number of interesting isotopes of so-called refractive elements cannot currently be extracted from a thick ISOL target using this classical approach. Likewise, beams of very short-lived isotopes experience decay losses during diffusion and effusion through the target-ion source assembly. Nevertheless, over the years, some 600 different isotopes of approximately 70 elements have been produced at ISOLDE, which shows the intrinsic strength of the method.

The complementary method to ISOL is production via fragmentation of a heavy-ion beam in a thin target. This method is not chemically sensitive and can be used for very short-lived isotopes. However, in many cases the yield is lower than the ISOL yield and the beams do not have such attractive properties as the post-accelerated ISOL beam. These technical differences indicate the complementary physics that can be pursued at the two different types of facility. There are physics cases both on the neutron-rich and on the proton-rich side of stability that benefit from an ISOL facility, but the same is also true for a fragmentation-based machine. It is thought that a fragmentation facility in combination with a gas-stopper and re-acceleration could improve the properties of fragmentation beams, but this field is still developing. For the moment, a large number of isotopes can be produced using the ISOL method, and post-accelerated beams of good quality are available for experiments. The main future development in the ISOL technique will be the production of high-power targets to increase the production yield.

1.1.1 Pure nuclear physics

As mentioned above, post-accelerated beams are particularly important for pure nuclear physics and nuclear astrophysics. Therefore, before moving to a new, high-intensity machine, it has been valuable to consider to what extent combinations of new beam manipulation technology can be used at existing facilities to produce beams with the required properties, and to investigate what experiments can be carried out at these facilities. The Radioactive beam EXperiment (REX) at ISOLDE was proposed in 1992. The design and construction of REX began in 1995 and the first commissioning experiments

were carried out in 2000 (see Fig. 1). The project was at first a pilot experiment to test novel ideas for beam cooling, charge breeding and post-acceleration, but following successful commissioning it was turned into a CERN User facility in 2004.

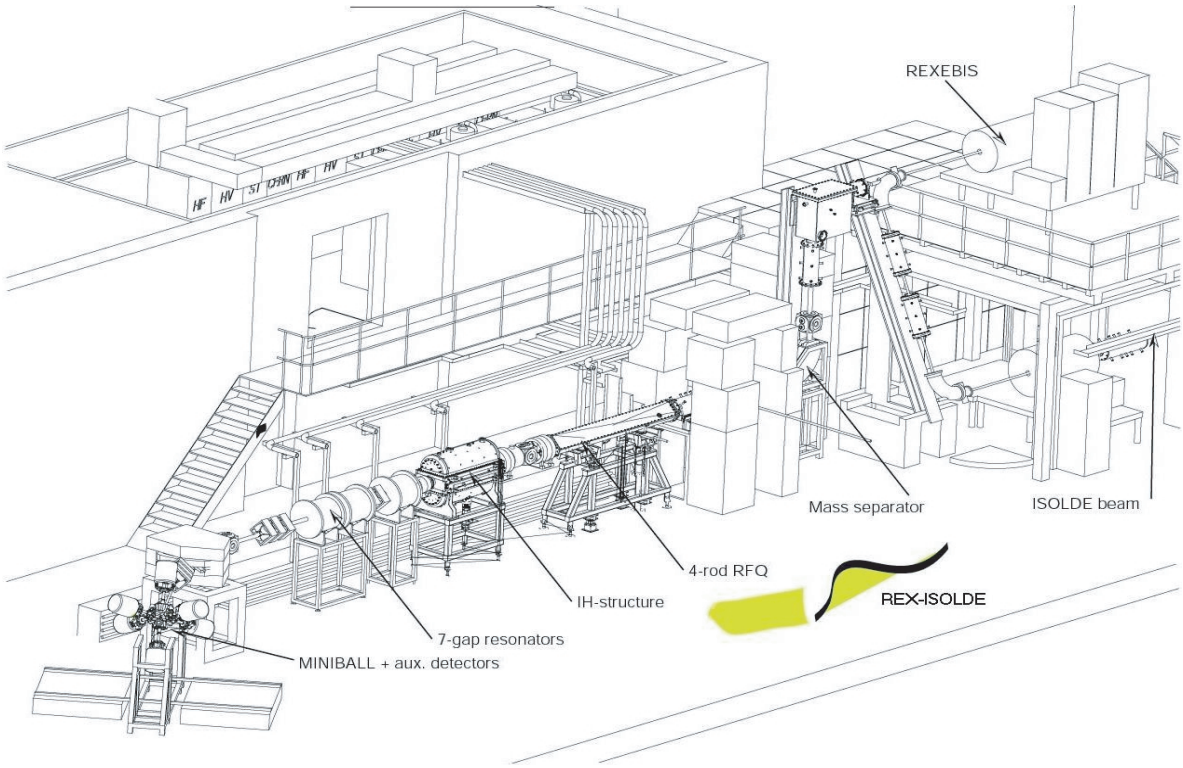

Fig. 1: Overview of the REX-ISOLDE post-accelerator. The configuration shown was used for the proof-of-principle tests for radioactive beam post-acceleration as well as in the first experiments at 2.2 MeV/u beam energy. The accelerator has since been upgraded to reach energies of approximately 3.0 MeV/u

The REX physics programme now includes a list of 13 approved experiments and 50% of beam time is dedicated to REX experiments. This report details some of the principles and techniques used by REX-ISOLDE, but the present section also outlines in more detail the physics case for radioactive beams. The information given here draws on the many reports and white papers produced by groups in Europe and the US over the past few years and the reader is encouraged to consult those documents for a more complete view of the pursued physics (see the Bibliography for references).

Several issues of pure nuclear physics interest can be studied with radioactive beams. It is, for example, well established that shell gaps at stability are formed by the influence of the nuclear spin-orbit force. In a mean field approach to the nuclear many-body problem, the nuclear spin-orbit force is usually introduced as the derivate of this field. It is thus clear that isotopes lying further away from stability will have a different nucleon distribution and therefore one may expect the shape of the potential to change. The predicted behaviour is where the Woods–Saxon potential, confirmed closer to stability by electron scattering experiments, gradually approaches a parabolic shape. As a consequence the nuclear spin-orbit force changes and new shell gaps occur. This raises two interesting questions. First, can the well-established shell structure at stability, which has been used to build all nuclear models to date, correctly predict behaviour at the drip lines? This requires the connection of nuclear data at stability with similar data far from stability—using a model in a way that has been impossible until now. The second question is related to nuclear astrophysics. The production of heavy elements beyond iron is believed to occur in the so-called rapid neutron capture process (r-process). Important data for reproducing the mass flow in the r-process include separation energies, decay rates, and

neutron capture rates for isotopes far from stability. Relevant data can be delivered by a high-intensity RIB facility. Current predictions of isotopic abundance in the A ~ 120 and A ~ 180 regions show underproduction of some isotopes, in particular those with masses just below the waiting-point masses. On the other hand, similar network calculations using quenched N = 82 and N = 126 shells reproduce the abundance pattern better—although far from perfectly. One indication of shell closure is the amount of collectivity in the first excited 2^+ state. This can be looked at using Coulomb excitation. One of the aims at REX is to study shell evolution at different closed neutron shells. This includes studies in the ^{78}Ni, ^{100}Sn, and ^{132}Sn regions.

Another phenomenon of interest in pure nuclear physics is the creation of low-lying intruder states far from stability. These states, typically of 2p–2h character, induce strong core polarization and drive the nucleus towards deformation. One particularly interesting area is the so-called island-of-inversion around ^{32}Mg. A series of experiments have been carried out at Michigan State University using relativistic Coulomb excitation and low-resolution γ-ray detectors. The results of these experiments confirm the intruder structure of the ground state of ^{32}Mg. However, relativistic Coulomb excitation relies on more involved data analysis; access to the first 2^+ state in, for example ^{32}Mg and its neighbours, using low-energy Coulomb excitation with a well-defined safe-distance, can address the physics question more purely. One of the programmes pursued at REX is therefore to study neutron-rich Na and Mg isotopes with Coulomb excitation using a low-energy beam in order to reduce the error bar of the extracted B(E2) value. This is done using a set of highly segmented Ge detectors and sample Analog-to-Digital Converters (ADCs) for interaction point determination, which ensures excellent Doppler correction and therefore contributes to better experimental accuracy.

Some light, neutron-rich nuclei exhibit the so-called halo phenomenon. These nuclei constitute particle-bound systems that can be decomposed into a core and two, or more, so-called halo neutrons, whose wave function extends into the classically forbidden region. In ^{11}Li the system decomposes if one of the two halo neutrons is removed, indicating that the ^{10}Li nucleus is particle unbound. ^{11}Li is therefore bound by a force of higher order than the normal two-body interaction. Studies of the halo phenomenon at REX include resonance scattering of ^{9}Li on a proton-rich target to find the composition of the unbound ground state of ^{10}Li. It is intended that similar physics questions will be studied for neutron-rich He and C isotopes.

Another long-standing question is that of double-shell-closure nuclei. Studies of the double-shell closure at ^{78}Ni and ^{100}Sn have been a hot topic in pure nuclear physics for the past decade. With radioactive nuclear beams it is, for example, now possible to extend Coulomb excitation studies of the first excited 2^+ states in the Sn isotopic chain to unstable isotopes. Previous studies of shell evolution on the proton-rich side of stability have relied on fusion–evaporation reactions and population of the so-called yrast-cascade that de-excites the nucleus to the ground state. Measurements of the lifetime of some pure 6^+ states have been carried out for even–even isotopes in this chain to as far as ^{102}Sn. These states provide a measure of the effective neutron charge as the shell closure is approached and thus indicate to what extent the core is inert. Radioactive beams make it possible to compare the structure and influence of core polarization using Coulomb excitation to previous lifetime measurements. ISOLDE also provides a unique opportunity to study similar effects close to ^{132}Sn. It is therefore possible to cover a full isotopic chain from the very proton-rich to the very neutron-rich. Analogous studies for the very neutron-rich Ni isotopes are interesting, and a programme for Coulomb excitation of neutron-rich Zn isotopes is also being pursued at REX, with similar arguments.

Other physics cases that have been brought up since the commissioning of REX include shape studies in proton-rich Se isotopes and mixed symmetry states in heavy Kr isotopes. The physics case for the latter is based on the so-called Interacting Boson Model (IBM), which in principle is a truncation scheme of the full nuclear shell model, where the fermions of the nucleus form pairs with spin 0. The IBM model draws heavily on symmetries of the nuclear Hamiltonian and includes such concepts as supersymmetry.

1.1.2 Nuclear astrophysics

One of the most interesting aspects of RIB physics is its application to nuclear astrophysics. In explosive scenarios such as X-ray bursts and novae the thermonuclear runaway leads to neutron and proton capture on unstable isotopes. So far, it has not been possible to study the rates of these reactions by direct methods in the laboratory, therefore the isotopic abundance ratios and the energy output of explosive stellar scenarios have been only approximately determined. High-intensity radioactive beams will make direct studies possible. Reactions originally proposed for REX include the ^{35}Ar(p,γ) reaction, which is considered to be a bottleneck reaction in the rapid proton capture process (rp-process). This process is significant at high temperatures, when the seed nuclei of the CNO cycle overcome the Coulomb barrier and capture protons. The process is similar to the r-process, but occurs when the temperature and density become high enough to trigger reactions such as the ^{15}O(α,γ) reaction. If this so-called break-out occurs and the pick-up process continues to the light Na isotopes, then the cyclic reaction chain, which is vital for catalysing H into He, will not be completed. Instead, heavier elements will be produced. Interesting reactions in this context are also the ^{17}F(p,γ) and ^{14}O(α,p)^{17}F reactions. The inelastic branch of the latter reaction can be studied via proton scattering into excited states of ^{17}F. An experiment using REX and MINIBALL is planned to investigate this. Note that the production of the ^{17}F beam has required the testing of a new method for beam preparation, in which a molecular beam of LaF is extracted, cooled, and bunched before being post-accelerated. Finally, there is substantial potential at REX for the study of astrophysical reaction rates using indirect methods: not only for studies of resonance structures and extraction of spectroscopic factors, but also for the deduction of optical model potential parameters for unstable isotopes and the determination of reaction rates using the Asymptotic Normalization Coefficient (ANC) method.

2 The REX-ISOLDE beam preparation system

Charge breeding is a key element of the concept used for the post-acceleration of the radioactive ion beam at REX-ISOLDE. This approach provides several benefits. A first acceleration step, boosting the ion-beam energy before stripping (which is typical of traditional heavy-ion acceleration schemes), can be avoided. Furthermore, with fairly easily attainable specifications for the charge breeder it is possible to extend the mass range of the ion beams that can be post-accelerated, without introducing several stripping stages or increasing the length of the accelerator. As a consequence we can keep the size of the post-accelerator small while retaining maximum flexibility. This flexibility will allow the physics programme to take advantage of the substantial know-how in radioactive ion-beam production already existing at ISOLDE, where more than 600 isotopes of approximately 70 elements are available.

2.1 The Penning trap (REXTRAP)

ISOLDE delivers a quasi-continuous beam, with a time structure dictated by the half-life of and the effusion and diffusion times for the specific isotope in the primary target. The low-energy beam typically consists of singly charged ions at an energy of 60 keV. As the transversal emittance of the beam is approximately 30 π·mm·mrad, the beam preparation stage first matches the beam to fulfil the injection criteria of the charge breeder, after which the charge breeder stage matches the ion-beam properties to the requirements of the linear accelerator. For this purpose, REX-ISOLDE uses a unique system consisting of a Penning trap (for accumulation, bunching, and cooling of the ion beam) combined with an electron-beam ion source (EBIS) for charge-state breeding. The constituents of this system are described in some detail in the following section. The design and construction of the REX-ISOLDE Penning trap (REXTRAP) was undertaken at Mainz University and draws on the design of the ISOLTRAP mass spectrometer located at ISOLDE.

2.1.1 Principle of operation

REXTRAP [1] is a large, cylindrical, gas-filled Penning trap located on a high-voltage (HV) platform. The trapping volume, comprising a local longitudinal electrostatic minimum, resides in the room-temperature bore of a 3 T superconducting solenoid. The potential at the beam entrance of the HV platform is slightly lower than that of the ISOLDE ion source. The ions are therefore electrostatically decelerated when they pass the potential barrier of the trap. Inside the trap they move through a high-pressure region close to the trap entrance. If the buffer gas pressure in this region is properly tuned, the energy loss due to collisions with buffer gas atoms will be sufficient for the injected ions not to overcome the potential barrier again after reflection at the exit barrier (on the other side of the trap). The ions will thus oscillate and eventually accumulate in the potential minimum mentioned above. The overall effect is a longitudinal cooling of the ions. After accumulation and additional radial cooling the potential barrier at the exit of the trap is lowered and the ions are released in a short bunch. The principle of operation is demonstrated in Fig. 2. In order to handle short-lived nuclides the cycle time is designed to be as short as 20 ms.

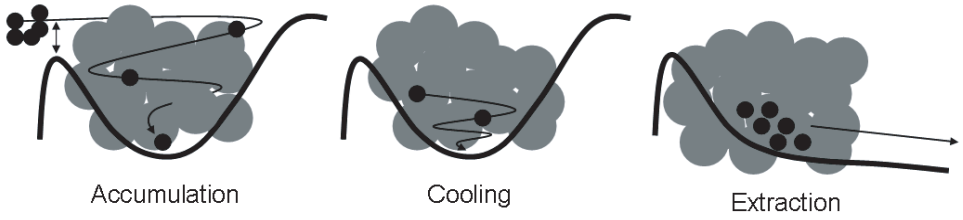

Fig. 2: A schematic representation of the three steps of REXTRAP operation

The equation-of-motion for a single ion in a Penning trap can be solved analytically [2]. It results in a superposition of three eigenmotions, one oscillation in the longitudinal direction and two circular motions in the azimuthal plane. The latter two are denoted as the magnetron and reduced cyclotron motions, respectively. The sum frequency of these two motions is the true cyclotron frequency, $\nu_c = qB/2\pi m$. It depends solely on the mass m, and the charge q, of the ion, and on the magnetic field B. With the introduction of a damping force, like the viscous force provided by the buffer gas, the magnetron motion becomes unstable and its radius increases. Thus, the extension of the ion cloud increases. An effective injection into the EBIS requires a small transversal emittance, since the acceptance of REXEBIS is ~10 π·mm·mrad at 60 keV. Therefore, not only is longitudinal cooling and bunching necessary, but also transversal cooling.

Most experiments at REXTRAP have been performed using a so-called sideband cooling technique. In this method the magnetron and reduced cyclotron motions of the ions are coupled to each other by applying a Radio Frequency (RF) field, at the sum frequency, to a split-ring electrode in the trap centre. This method has been developed at ISOLDE [3] to cool radioactive ions prior to precise mass measurements. As the sum frequency is also the cyclotron frequency of the ion, the technique is mass selective and can be used to clean the ion cloud of species of different mass. The main advantage of REXTRAP is that the ions can be centred very quickly. With an adequate RF amplitude the cooling time depends only on the damping force of the buffer gas. For a typical gas pressure of approximately 10^{-4} mbar Ne in the trap centre, this is of the order of a few milliseconds. The final energy of the ions is determined by the temperature of the buffer gas. A disadvantage of this method is that it is related to single-ion motion. The technique works well if this motion is well defined and no perturbations exist (such perturbations being, for example, ion–ion interactions in a dense ion cloud). The effect of perturbations is a limited, final, ion density. As the trapping volume is limited in size this also limits the number of stored and cooled ions.

Another way to create a high-density ion cloud is to apply a rotating multipole field (i.e. a rotating wall). In this case the field forces the ion cloud to rotate around the longitudinal axis. The

resulting Lorentz force balances the Coulomb repulsion of the ions and the centrifugal forces. With this technique ion densities as high as the Brillouin limit can be attained [4] and the ion cloud can be considered as a rigid, rotating ellipsoid. At the limiting density the cloud rotates at half the cyclotron frequency. Plasma oscillation modes can also occur, resulting in heating or cooling. They can be used for a better coupling of the rotating multipole field with the ion cloud. Until now rotating wall cooling has mostly been used for dense clouds of electrons or positrons. It has been used for ions in combination with laser cooling to reach very low temperatures. With this combination, ordering effects like Coulomb crystallization can be studied.

2.1.2 Ion optical design

The transfer of ions to the homogeneous part of the magnetic field is a crucial step in the trap injection process. The inhomogeneous fringe field at the trap entrance couples the longitudinal and transversal phase spaces of the ions, resulting in an increased longitudinal energy spread. As the ions are to be stopped in the buffer gas, the energy spread is also related to the minimum energy loss provided by the buffer gas collisions. Consequently, the energy spread determines the minimum gas pressure necessary for ion capture. Ion optical simulations have been performed to minimize the energy pick-up, mainly using the ray tracing code SIMION 3D [5]. It is assumed in the calculations that the incoming beam has a focus in front of the trap. A two-step deceleration and final focusing using an Einzel lens has been selected for the beam optics. For a typical ISOLDE beam this solution gives a 50 eV maximum energy pick-up. It also provides a narrow beam focus after the first deceleration stage, which enables the installation of a small diaphragm for differential pumping, necessary to insulate the buffer gas region from the ISOLDE beam line. The position of this focal point can be adjusted using the first electrode after the main deceleration. After the ions enter the magnetic field, at an energy of about 1.5 keV, they are re-focused with an Einzel lens into the entrance diaphragm of the high-pressure region. The geometry of the ejection part is similar to the injection part, with the difference being that at the exit side the electrode potentials can be switched for capturing, accumulating, and ejecting ions.

2.1.3 REXTRAP set-up

The secondary beam from ISOLDE enters REXTRAP via the central beam line. It branches off into the RA0 line at the switchyard that follows the CA0 section. Directly after the switchyard a 90° electrostatical deflector can be moved into the beam path to enable the introduction of a beam from a test ion source into the trap. This ensures the possibility of optimizing the system independently of the ISOLDE ion sources and beam lines. A standard ISOLDE quadrupole triplet lens focuses the beam. A beam kicker, consisting of two pairs of parallel plates, is also installed in front of the trap high-voltage cage. In the horizontal direction it is necessary to correct for a 3° misalignment between the RA0 and the REX-ISOLDE beam lines. In the vertical direction one plate is used as a beam gate using a fast high-voltage switch. Parts of the ISOLDE beam lines and REXTRAP are shown in Fig. 3.

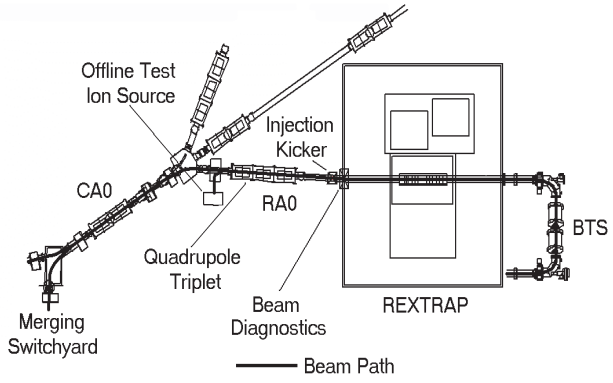

Fig. 3: Beam line layout at the merging point of ISOLDE and REX-ISOLDE

The trap electrodes and the surrounding vacuum tubes are shown in Fig. 4. The outer electrodes, used for deceleration and acceleration, are made of stainless steel and fixed inside the vacuum chamber. The large insulators on each side, which separate the high-voltage part from the ground potential, are made of polyethylene and are shielded on the inner side with stainless steel rings. The electrodes of the main trap structure are made of oxygen-free copper and are gold plated. They are separated and insulated from each other by ceramic (MACOR) rings. Some of the cylindrical electrodes have holes to attain better pumping conditions inside the structure or to improve the inlet of the buffer gas. The central electrode is divided into eight sectors to allow the application of the azimuthal multipole fields for the cooling. The trap electrodes are divided into five subunits, where each is held together by an outside support structure made of aluminium. The subunits are screwed together to form the complete trap structure, which has an overall length of about 1.3 m.

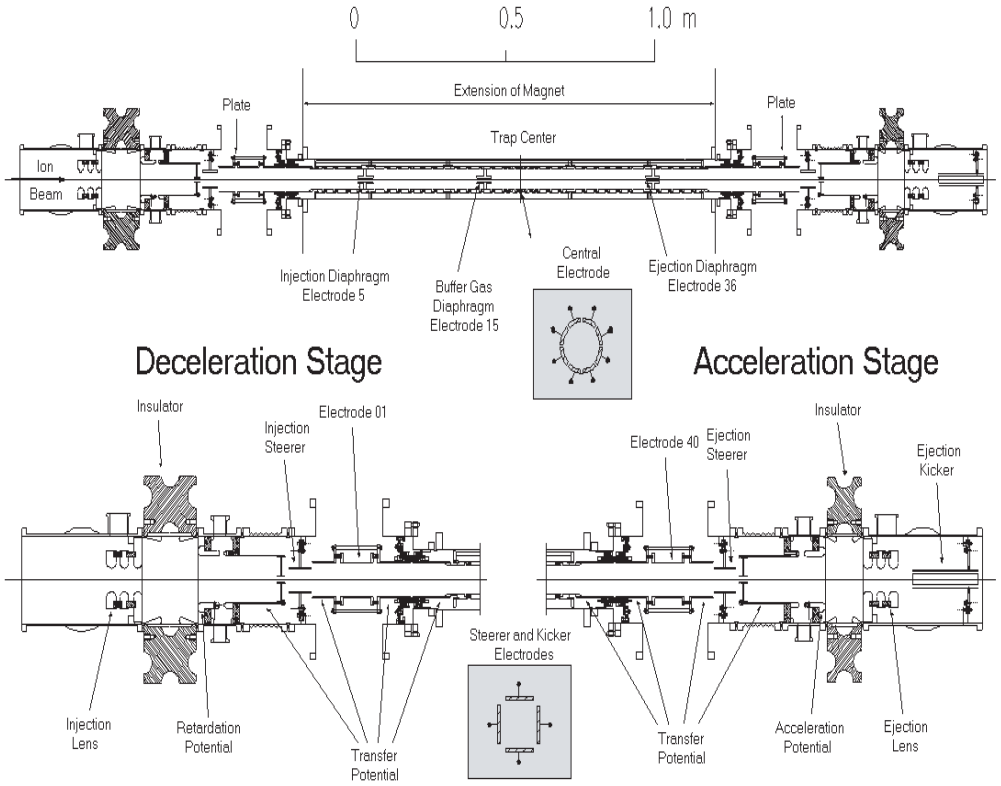

Fig. 4: REXTRAP deceleration, trapping, and acceleration stages

All materials used for the inner trap structure, including screws, washers, etc., have been specially selected and checked to ensure they are non-magnetic, as magnetic materials in this region could deform the magnetic field lines and thus influence the cooling or the size of the extracted ion cloud. The trap structure is situated in a vacuum tube residing inside the solenoid. The stainless steel of the tube has been selected for low magnetic susceptibility and lack of magnetic enclosures. The tube has been honed inside and the dimension of the trap structure has been adapted exactly to its inner diameter. Thus, alignment and straightness of the trap is guaranteed. Large MACOR discs are mounted on the outer parts of both sides of the trap. They contain sockets for electrical connections. Counterparts with plugs are fixed in the vacuum crosspieces on both sides. These also contain the electrodes for deceleration and acceleration. To allow alignment of the trap with respect to the magnetic field the entire tube is fixed to the cryostat of the magnet with an adjustable holder. The trap is aligned using an electron source installed in the centre of the tube and a position-sensitive detector on each side. The complete magnet with the trap inside can then be aligned with respect to the incoming beam axis.

The calculated pressure distribution within the trap structure is shown in the upper part of Fig. 5. The trap is divided into two sections. The first, with a high buffer gas pressure, provides the energy loss to capture the ions, whereas the second section, at the trap centre and at a pressure lower by about a factor of 10, ensures a better resolution for the mass selective cooling and avoids reheating of the ions by collisions during ejection. The distribution has been calculated using the conductance of the diaphragms, the holes in the electrodes, and the feedthroughs applying the pumping capacity on both sides. The central part of Fig. 5 shows the electrical potential distribution. By choosing to put the trap centre on the same potential as the high-voltage platform, the RF fields can be easily coupled in at this point.

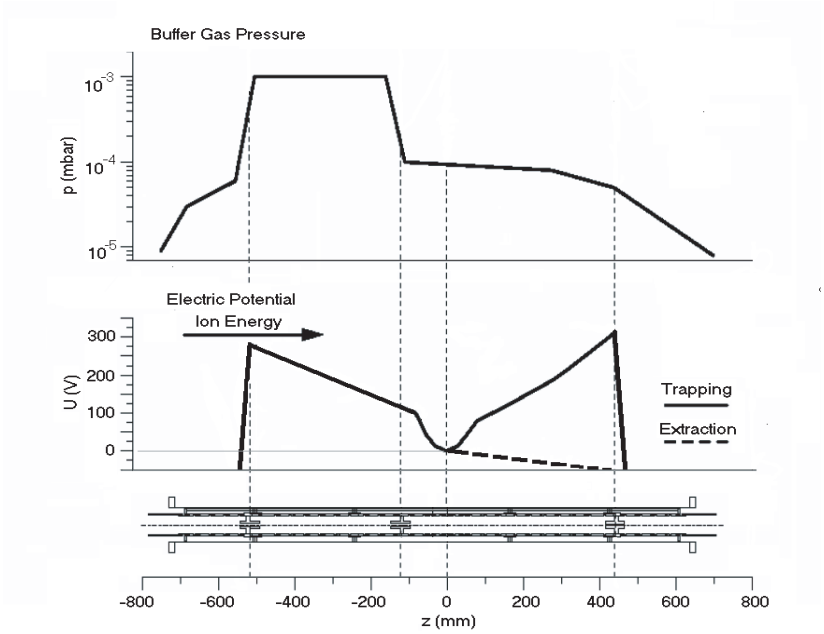

Fig. 5: The pressure distribution of the buffer gas and the electric potential in the inner structure of REXTRAP. The positions of the diaphragms are indicated in the lower part of the figure

2.1.4 Buffer gas handling and vacuum system

The buffer gas is fed into the high-pressure part of the trap via a 0.8 m long Teflon tube with an inner diameter of 2 mm. From the outlet the gas diffuses in both directions through 50 mm long differential pumping barriers of 10 mm diameter. Two additional differential pumping barriers, still within the high-voltage region, are also installed on both sides of the trap. A schematic of the gas flow is shown in Fig. 6. Two turbo pumps (Alcatel 400 l/s) maintain a buffer gas pressure below 5×10^{-7} mbar in the adjacent beam lines for some 10^{-3} mbar (Ne or Ar) in the high-pressure region. The buffer gas pressure is controlled by a Pirani gauge via a regulation valve for the gas inlet. The flow through the Teflon tube can be calculated using Knudsen's formula for a viscous flow. The relation of the pressures in the high-pressure region of the trap and the control voltage from the gauge can also be seen in Fig. 6.

Viton O-ring seals adhering to ISO standards are used throughout the vacuum installation, giving a background pressure of about 10^{-7} mbar. The installation can be baked to a temperature of 70°C via heating bands installed around the vacuum tube. The temperature is limited by the surrounding cryostat. Additionally, getter material can be installed along the trap electrodes to clean the buffer gas.

2.1.5 High-voltage platform and cage

The REXTRAP high-voltage platform consists of an aluminium frame covered with aluminium plates. It rests on 10 insulators made of Delrin. A second frame, with alignment devices that hold the superconducting magnet, is mounted on top of it. The second frame is placed on a rail system, which

allows the magnet to be moved perpendicularly to the beam line for easy access to the inner electrodes of the trap. Additionally, two electronic racks installed on the platform house power supplies and control equipment for the different trap devices. Electrical power on the platform is supplied by two 2 kVA insulation transformers. A cage, surrounding the platform at a shortest distance of 0.6 m, provides protection from the high voltage and the stray magnetic field. The size of the cage has been determined so that the magnetic field—with the exception of a small area around the beam axis where it reaches 5 mT—is 1 mT on the outside. The two entrance doors are equipped with an interlock system connected to the high voltage.

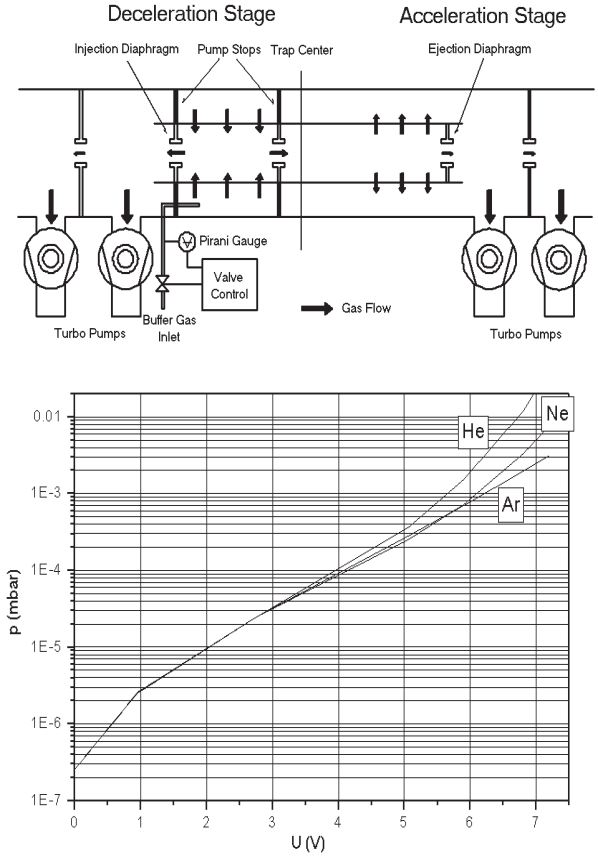

Fig. 6: Top: schematic drawing of the REXTRAP vacuum system; bottom: the relation between control voltage from the vacuum gauge and buffer gas pressure for different noble gases

2.1.6 Operation

The DeviceControl program and its initialization files are used for trap operation. All parameters, such as electrode potentials, frequencies, etc., are set using this interface. To facilitate the procedure, the values from previously saved sets of parameters can be recalled and downloaded to the hardware. Settings for the gas pressure and the high voltage are excluded from the automatic procedure for safety reasons—these parameters are instead set individually.

In a second step the RexControl program sets the time structure for the trapping cycle and also sets parameters for device scanning for data acquisition. The program also facilitates the basic starting and stopping functions of the trap cycle. Several diagnostic elements are included for the optimization of the set-up. A standard ISOLDE Faraday cup and scanner system is installed in front of the high-voltage cage. Furthermore, for current measurements, plates situated close to the entrance and exit points of the Penning trap magnet can be introduced and read out via picoammeters. As a result of the relatively high magnetic field at these points, and its combination with the surrounding electrodes,

additional secondary electron suppression is not necessary for correct current measurement. A Faraday cup and a Microchannel Plate (MCP) are installed close to the trap in the beam transport section leading to the EBIS (see Section 2.2). This allows for measurements of beam size and position or for recording of the ejected ions' Time-Of-Flight (TOF) spectra. A multichannel scaler can process the signal for this purpose if the count rate is sufficiently low. Alternatively, the signal is sent to and grabbed by a digital oscilloscope. Both systems can be read out using the control system.

2.1.7 Performance and measurement results

Several runs have been carried out with stable and radioactive ion beams (covering the entire mass range from helium to uranium) to test the performance of the trap, to find the best parameter settings, and to measure the emittance of the ion beam (see Fig. 7). For the most part, Ne and Ar have been used as buffer gases in these measurements. The majority of experimental runs have so far been performed with the trap at 30 kV, since the test ion source and the EBIS were not previously able to run at the normal ISOLDE voltage of 60 kV. However, to demonstrate the voltage stability of the trap some experiments have been performed with the ISOLDE beam and the Penning trap at 60 kV. A typical efficiency of 40% was reached in these tests.

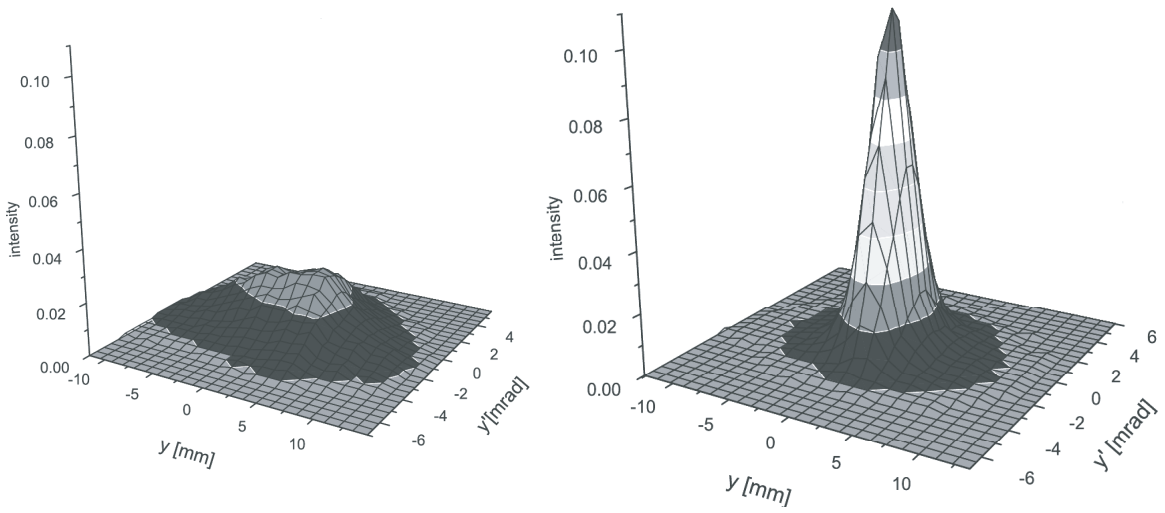

Fig. 7: The emittance in the yy′-place for a non-cooled (left) and a cooled beam (right) as measured by an electrostatic emittance meter

As mentioned above, the ions have to pass a diaphragm at the trap exit. If this diaphragm has a diameter smaller than the entrance diaphragm, then cooling or compression of the ion cloud can be detected by recording the number of ejected ions. Figure 8 shows this number as a function of the applied centring frequency, using the sideband technique for the case of ^{133}Cs. The Full Width at Half Maximum (FWHM) of this resonance curve corresponds to a mass resolution of $M/\Delta M = 300$. This value corresponds well to the theoretical value [2] for an excitation time of 20 ms and a gas pressure of ~10^{-4} mbar Ar in the trap centre. The mass resolution in the case of REXTRAP depends mainly on gas pressure.

Figure 8 also shows an example of a TOF spectrum for ions extracted from the trap after the injection of ^{29}Na ($T_{1/2}$ = 44.9 ms). Besides ^{29}Na, ions from the buffer gas or impurities can also be seen in the spectrum. At this point possible isobaric contamination of the ISOLDE beam, for example with ^{29}Al, cannot be distinguished.

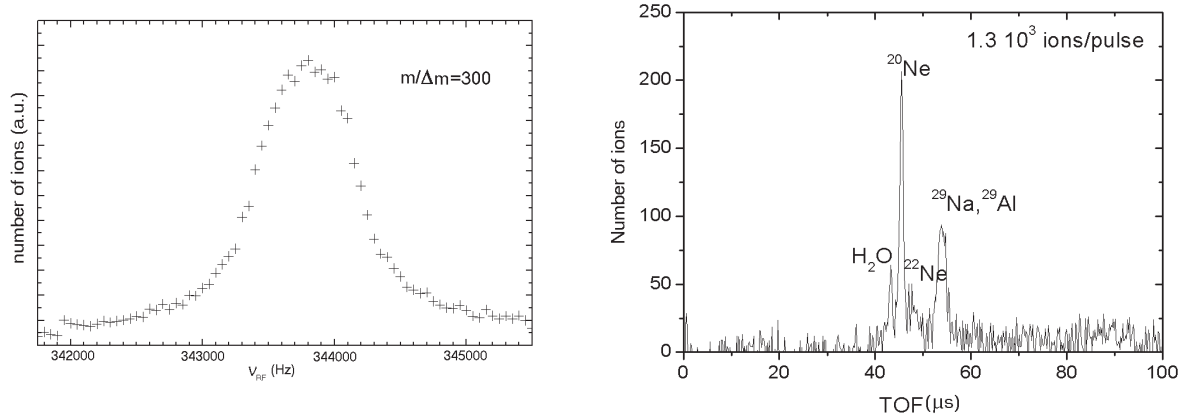

Fig. 8: Left: resonance curve with a mass resolution of 300; right: the TOF spectrum showing an extracted beam composed of background and injected Na ions

Space-charge effects have been observed if the number of simultaneously stored ions per bunch exceeds about 10^6 elementary charges. The effect is manifested as a shift in the centring frequency and, lastly, a decrease in efficiency. In most cases this is not a severe limitation, as the radioactive beams from ISOLDE are weak and a typical experiment runs with a secondary beam intensity of 10^4–10^6 ions/s. However, it can be a limitation if the accumulation time has to be increased to furnish a longer breeding time in the EBIS for high masses. Another challenge is if the incoming beam contains a high number of contaminating isobaric ions, reaching the space-charge limit, and a smaller number of the species of interest.

As indicated in Fig. 7, the emittance of the ejected ion beam is determined with an electrostatic emittance meter [6]. The apparatus is behind the forward-pointing outlet of the first bender of the beam transport system. A clear reduction in the emittance down to about 10 π·mm·mrad at 30 keV can be seen if sideband cooling is applied. The depicted measurement resulted from a run with about 4×10^4 ions per bunch. A clear increase in the emittance to more than 25 π·mm·mrad can be observed for 10^6 ions per bunch.

To overcome space-charge effects, rotating wall compression of the ion cloud has also been tested. So far most tests have utilized a rotating dipole field. As mentioned above, rotating wall compression of the ion cloud can be done rapidly if a coupling to plasma modes can be achieved. To identify such modes, the ion signal was measured as a function of the rotation frequency. The resonance observed on these measurements can most probably be attributed to the so-called 2,1 plasma mode. This is a coupled mode between longitudinal and transversal ion-cloud oscillations. An effect of the rotating field on the ion signal can only be observed if the number of stored ions is high enough to allow the ion cloud to be considered as a plasma. In the case of potassium this number is about 10^6 stored ions. Above 5×10^6 ions per spill the emittance obtained with a rotating dipole field becomes smaller than the emittance after sideband cooling. Additionally, at high ion numbers, rotating wall cooling seems to increase the possible storage time in the trap. This is demonstrated in Fig. 9, where, starting with the same number of injected potassium ions, the number of ejected ions is compared for three cases: rotating wall cooling, sideband cooling, and no cooling. It is clear that when no cooling is applied the number of ejected ions decreases quite fast due to their Coulomb repulsion; there is a smaller, though still clearly visible, decrease in ions with sideband cooling; whereas in the case of rotating wall cooling no decrease could be observed.

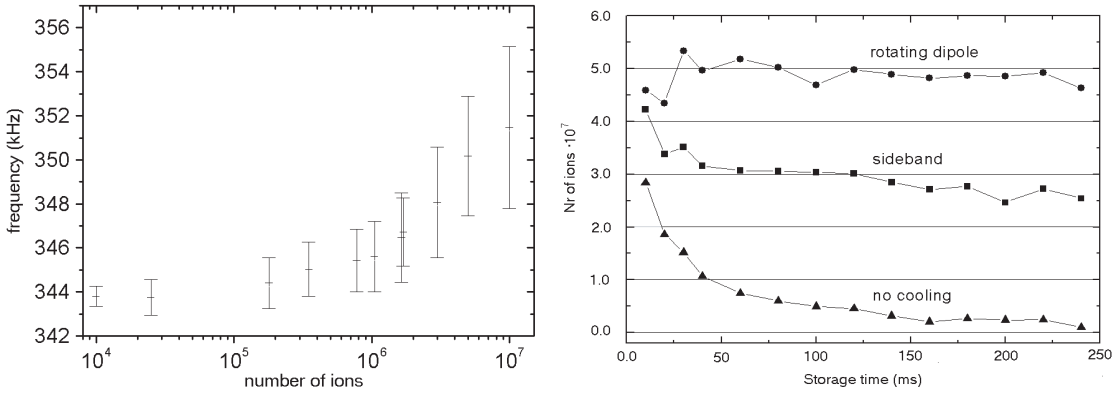

Fig. 9: Left: evolution of the resonance frequency as a function of the number of ions in the pulse; right: the time evolution of the number of extracted ions for a rotated dipole field, sideband cooling, and no applied cooling

2.2 The beam transport system between REXTRAP and EBIS

This part of the REX-ISOLDE system is designed to transfer the ion pulses from REXTRAP to REXEBIS with minimum intensity loss (Fig. 10). Additionally, it provides differential pumping to achieve good insulation of the buffer gas-filled trap and the EBIS, which operates at Ultra-High Vacuum (UHV). As the intensity of the beam pulses from REXTRAP is normally very low, special emphasis has been put on the beam diagnostics in this section.

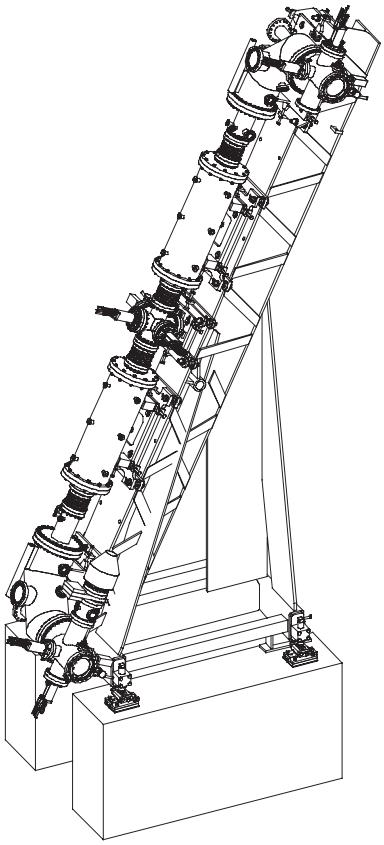

Fig. 10: The beam transport system between REXTRAP and REXEBIS

The EBIS is located on a platform above REXTRAP because of space restrictions in the ISOLDE hall. The transport line therefore consists of two 90° bends and an intermediate straight section. The beam axes of the Penning trap and the EBIS are shifted horizontally relative to one other, making the transport line tilt at an angle of 22° with respect to the vertical. The bending sections allow the beam to go straight through as well as to bend. This enables the connection of further beam diagnostic elements or additional experiments that make use of the small emittance beam in the bend at the trap exit [7]. The beam steering elements in front of the EBIS are switched between injection and extraction in order to bring the charge-bred ions through the mass separator. A combination of an 82.5° spherical electrostatic bender and a 7.5° kicker has been chosen for this part of the system. Two quadrupole triplet lenses have also been installed for focusing. To match the beam properties from REXTRAP to the Beam Transport System (BTS), an Einzel lens has been installed where the beam enters the system from the Penning trap.

2.2.1 Ion optics

The ions from REXTRAP are extracted from the trapping volume using a sloped electrical potential. This results in an energy spread that depends on the longitudinal size of the ion cloud. As an example, the energy spread can be up to several 10 eV for an ion cloud of about 10 cm in length. To compensate for this the layout of the BTS is achromatic. This is achieved by using a symmetric beam path and a focal plane in the centre of the straight section. Simulations of the beam trajectories have been performed using the GIOS and COSY codes. In the simulations (see Fig. 11) the ions started at the first focal plane, between the lower kicker and bender. The calculations were made with 30 or 60 keV beam energy and an energy spread of up to 100 eV. The transversal phase space emittance was assumed to be 10 π·mm·mrad, with an elliptical shape of axes ±2 mm and ±5 mrad. This is an upper limit when deducing the emittance from the measurements described above and back-tracing the beam to the entrance of the first bender.

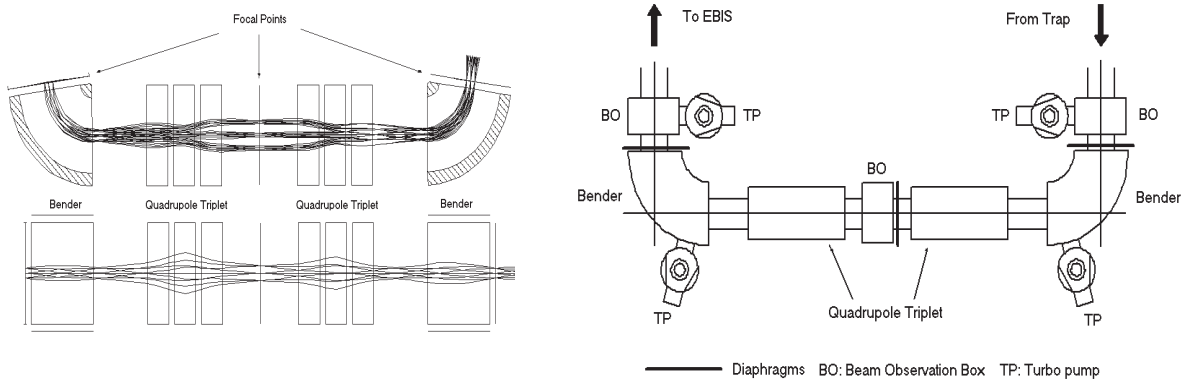

Fig. 11: Left: the result of beam transport calculations (see text for a more detailed discussion); right: the general layout of the BTS beam line, showing the positions of turbo pumps for differential pumping and beam diagnostic devices

2.2.2 Set-up

In order to facilitate the alignment of the system, all elements of the BTS have been installed on a reinforced steel bar. This allows the relative alignment of all parts while the steel bar is in a horizontal position. After relative alignment the system can be lifted into the upright position, put on two concrete blocks and aligned according to the beam axis of the trap and of the EBIS, respectively.

2.2.3 Vacuum

Special care has been taken in the layout of the beam transport section vacuum system because it has to separate the buffer gas-filled trap from the UHV of the EBIS. The maximum operating pressure at the end of the trap section, after the differential pumping diaphragm, is about 10^{-6} mbar when operating the trap with Ne as buffer gas. The partial pressure of Ne in the EBIS should be at least four to five orders of magnitude lower than this to avoid overcompensation by the electron beam and a too high output current. For this reason the entire BTS has been built using UHV technology. The system can be baked to about 200°C. It is separated into four parts by differential pumping diaphragms, and each is pumped with one turbo pump (Pfeiffer TMU 261). Simulations of the gas flow through the system result in a partial pressure of Ne of 7×10^{-11} mbar in the last section before the EBIS, when starting at 10^{-6} mbar in the first section. A schematic view of the vacuum system is shown in Fig. 11. With one baking session after initial installation, a residual gas pressure of about 5×10^{-9} mbar was achieved in the upper section.

2.2.4 REXTRAP beam diagnostics

The beam intensity in this section can vary over quite a large range, between ~1 nA for trap operation at the space charge limit and a few ions per pulse for radioactive ions with a low production yield. Therefore a combination of a Faraday cup and an MCP system has been chosen for the beam diagnostics. Unlike the system used for the rest of the accelerator set-up, the beam diagnostics is designed to be UHV compatible, therefore the collimator wheel (with its stepper motor), which is used in the rest of the machine, has been omitted. Four systems are installed: two between the two kicker–bender systems, one in the centre of the straight section, and one directly in front of the EBIS. The systems can all detect a beam from either direction. This enables the detection of a beam sent from the EBIS towards the trap to find the correct electrostatic steering for hitting the EBIS's electron beam with the RIB. Because of the limited space available, especially for the systems between the kickers and benders, the beam is sent directly onto the channel plates without additional secondary electron production on a foil. The disadvantage of this is that it increases the risk of accidentally destroying the plates by hitting them with an ion current that is too high, or of radioactive ions accumulating activity on the plates, thus increasing the background.

The set-up for one of the units between the kicker and bender is shown Fig. 12. A UHV cross piece houses the system. The Faraday cup and the microchannel plate are mounted on pressure-actuated mechanical feedthroughs. As both can be moved into the same position inside the chamber, special care has been taken to avoid accidental collisions. For this reason each pressure actuator is equipped with two pairs of position sensors. One pair acts as an input for the software control, and the other interrupts the power to the second actuator when the first is in (and vice versa). Additionally, the actuators are spring loaded to avoid collisions in case of a failure in the compressed air supply. The channel plate is tilted by 45° with respect to the beam axis and a camera views its phosphor screen. The camera is at a glass view port outside the vacuum chamber, perpendicular to the beam line. The control and readout is carried out using the same software as, and similar control boxes to, the rest of the accelerator's diagnostic system. The phosphor screens can also be used as an anode similar to that of electron multipliers. The signal can be amplified and fed to an oscilloscope for storage or to a multichannel analyser for pulse-shape analysis. Both devices can be read out from the REXTRAP control system. This control system makes it possible to distinguish ions with different mass due to their different TOF after ejection from the trap.

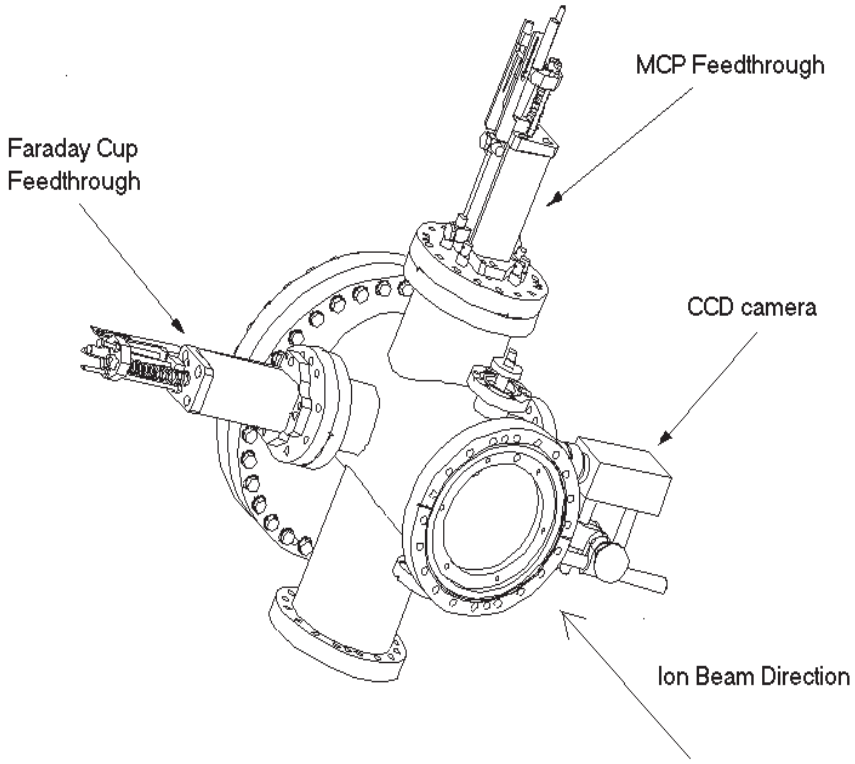

Fig. 12: View of a cross piece containing a beam diagnostic device in the BTS beam line

2.3 REXEBIS: The electron-beam ion source

The first feasibility tests for injection and extraction of an ion beam using an EBIS for the REX-ISOLDE project were carried out with the CRYogenic Stockholm Ion Source (CRYSIS) at the Manne-Siegbahn Laboratory (MSL) in Stockholm and at the Dione EBIS at CEA at Saclay in 1994 [8],[9]. The tests aimed to establish firm numbers for total injection efficiencies and charge-state distributions using an EBIS as charge multiplier. A pulsed, so-called fast injection mode was attempted, with a resulting total efficiency of 14% for an injected beam of N^+ ions. At CEA the tests were extended to higher mass and continuous injection was also tried (in a separate experiment). These rendered a total efficiency of 59% and 52% for N and Ar ions, respectively, using fast injection; the partial efficiencies of the main charge state were measured as 30% and 9.4%, respectively. The continuous injection mode, however, gave a very modest total efficiency of less than 0.1%. It should be noted that relatively straightforward modifications of the CEA set-up might lead to higher injection efficiencies for the continuous mode. Nevertheless, drawing on the experiences of the tests, the design and construction of the REX-ISOLDE EBIS (REXEBIS) were subsequently carried out at MSL in collaboration with Chalmers University of Technology in Gothenburg, and pulsed injection was the intended mode of operation.

2.3.1 Principle of operation

Like the buncher and cooler trap, the REXEBIS [10] (see Fig. 13) is positioned on a high-voltage platform. However, contrary to the Penning trap, the REXEBIS potential is switched between ion injection and extraction. The injection potential is set to decelerate the ions extracted from REXTRAP, and this is typically done at 30 kV or 60 kV. The extraction potential is adjusted to give the correct injection energy for the Radio Frequency Quadrupole (RFQ) accelerator. Therefore the platform potential provides a reference for the REXEBIS set-up that varies over time. Potential barriers, lenses, trapping tubes, and other devices of the REXEBIS all have their potentials set with respect to this reference.

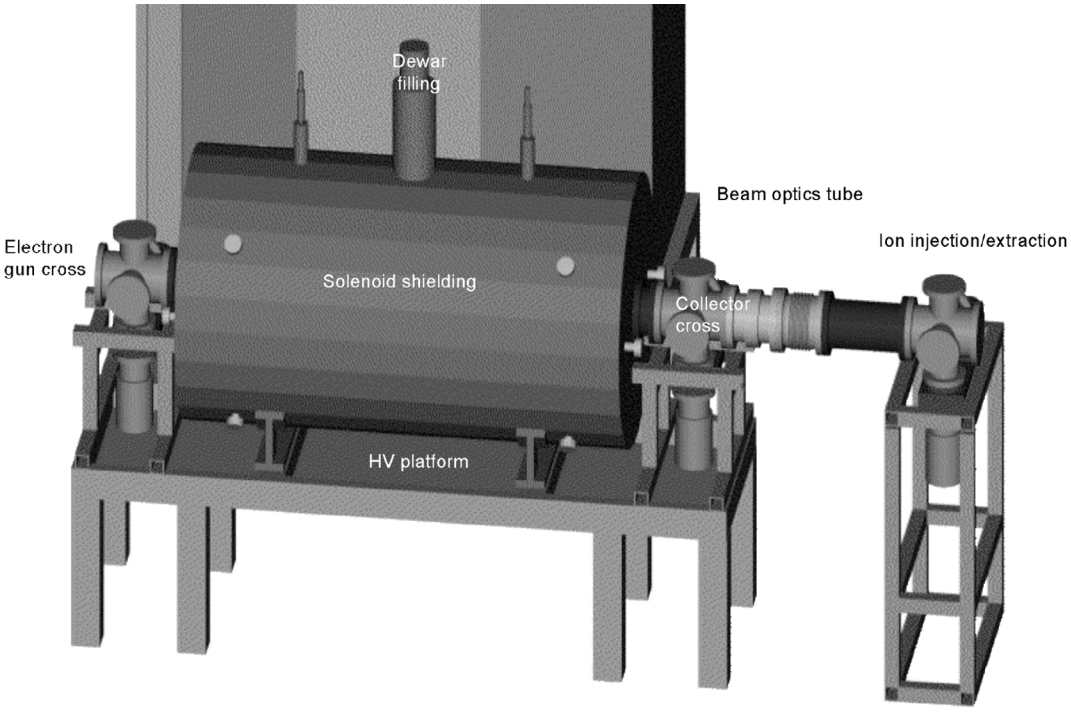

Fig. 13: The REXEBIS

An EBIS achieves charge multiplication via electron impact. An electron gun at one end of the device produces an e^- beam that is confined in a cylindrical volume over a distance of approximately 1 m by a magnetic solenoidal field. The axis of the magnetic field is parallel to the direction of propagation of the e^- beam. The beam fans out onto an open-ended collector at the opposite end of the device, while the charge-bred ions are extracted along a straight path. The inner structure of the EBIS comprises a set of cylindrical tubes whose potentials are varied during the charge-breeding process. This process can be time-ordered into an injection phase, when an outer potential barrier is lowered to let ions enter the device; a charge-breeding phase, when the barrier is raised to trap the ions; and a final phase, when the barrier is again lowered to extract the ions.

The main entity describing an EBIS is the product $j_e\tau$ of the electron-beam density and the breeding time. For example, to ionize an Ar atom to charge state 11^+ $j_e\tau$ has to be 3.3 As/cm^2. For the REX-ISOLDE accelerator a mass-to-charge state ratio of approximately 4.5 is required. The cooling time of the trap imposes the condition that this ratio should be reached within approximately 20 ms but the allowed confinement time is also determined by the short lifetime of the radioactive isotopes. A design utilizing a 5 keV electron beam with a maximum current of 0.5 A and a current density of up to 250 A/cm^2 has therefore been chosen. With these parameters the REXEBIS can hold up to 6×10^9 charges at an electron beam neutralization of 10%. This charge is more than one order of magnitude larger than that delivered by REXTRAP using the sideband cooling technique.

2.3.2 General magnet properties

The magnet makes up the largest part of the EBIS in terms of weight and cost. The purpose of the magnetic field is to compress the electron beam as it propagates from the gun cathode to the trap region. The solenoid, manufactured by Oxford Instruments, is superconducting and thus consumes less power than ordinary non-superconducting magnets. The shapes of the solenoid and iron shielding were calculated using the POISSON program [11] as described in Ref. [12]. In contrast to all existing high-performance EBIS, the REXEBIS has a warm bore, i.e. the inner cylinder containing the drift structure

is kept at room temperature by thermal decoupling of the cryostat from the ionization volume. Single-wire NbTi is used in the superconducting coil.

2.3.3 Solenoid construction and magnetic field

The solenoid is iron shielded for two reasons. It was initially intended to use a Pierce-type electron gun positioned in a low axial magnetic field, which requires an iron shield for field shaping. The other purpose of the shield is to reduce stray fields—to minimize the effects on personnel and nearby beam lines. The REXEBIS is therefore surrounded by a ring of passive iron bars of 25 mm thickness. Neither extra shims, nor cancellation coils, nor extra iron field clamps are added. Two identical solenoids have been constructed. One is used for the twin-ion source that has been installed as a test-bench at MSL.

The accuracy of the field straightness, and the homogeneity and stability of the field are three important specifications for the magnet. The field straightness specifies the maximal radial deviation from the geometrical axis of the central field line. This is of importance since the electron beam follows the field lines and a shift from the tube axis alters the potential distribution inside the tube. The straightness was deduced by measuring the magnetic field components in both horizontal and vertical directions with a Hall probe. The central field line was traced as shown in Fig. 14 by integrating the transverse field components along the z-axis. Twelve position knobs adjust the position of the solenoid within the iron shield. The field mapping procedure is similar to the method presented in Ref. [13].

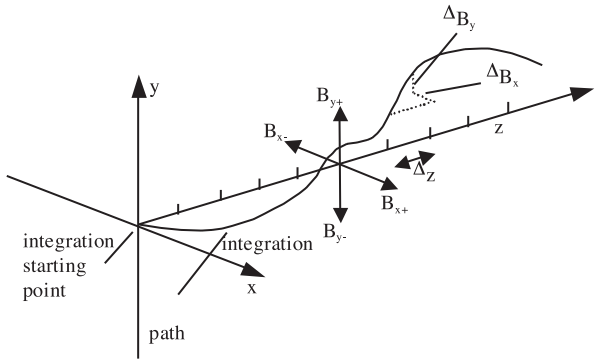

Fig. 14: Tracing of the central field line of the EBIS solenoid field.
(The method is described in the text.)

The cryostat was positioned inside the iron yoke while most of the iron bars covering the side were removed. Using the cryostat as a reference, the iron end flanges were adjusted to be parallel to the cryostat and to each other: this was ensured by attaching a mirror to the end flanges and using a telescope. The solenoid was then centred with respect to two 150 mm holes in the iron shield. The transverse field was mapped by mounting the Hall probe inside a brass tube that could be rotated around and moved along its axis. The applied method ensured cancellation of any deviations arising from possible bends in the tube itself.

The iron end flanges were finally measured to be parallel relative to each other within 0.75 ± 0.2 mrad. Furthermore, the solenoid was centred within ± 0.2 mm in the radial direction. The final result after a few iterations of adjustment is presented in Fig. 15. The sag is not compensated for and adds a convex shape to the y-curve. The traced central field line was found to be within a cylinder of 0.1 mm radius, concentric with the geometrical axis, over the range $-800 < z < 800$ mm. The specification required the central field line to be within a cylinder of radius 0.5 mm over $-825 < z < 825$ mm.

The second magnetic field parameter of importance is the field homogeneity, i.e. the variation of the longitudinal field strength. A field strength that fluctuates with the z-position leads to a varying beam radius, which in turn modulates the beam potential. The axial full field inside the REXEBIS is 2 T

with a specified field homogeneity of 0.3% over ±400 mm on axis. The measured homogeneity falls within 0.25% (see Fig. 16).

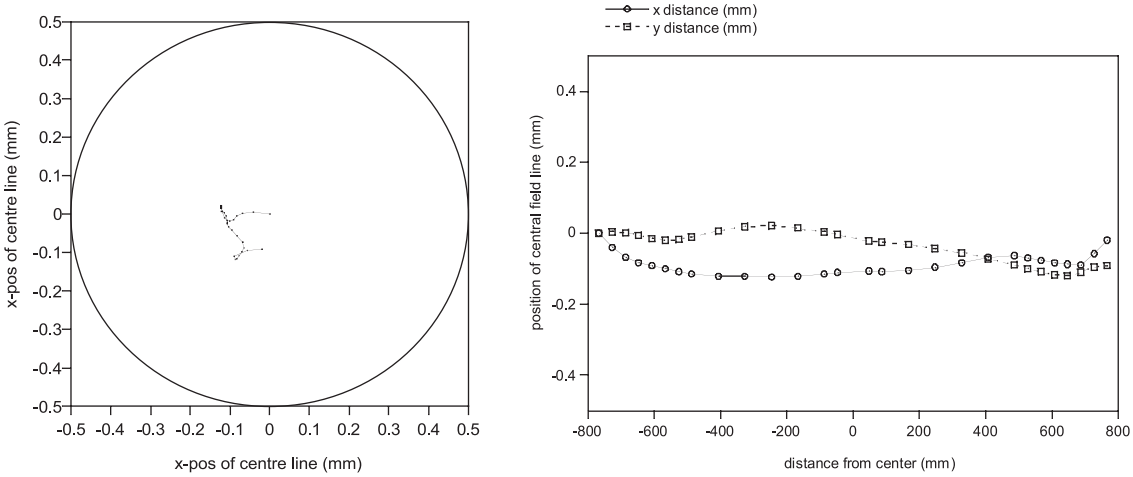

Fig. 15: The final result of the solenoid alignment. Left: the position of the central field line in the x–y plane; right: the position in the x and y directions along the field axis (z-direction)

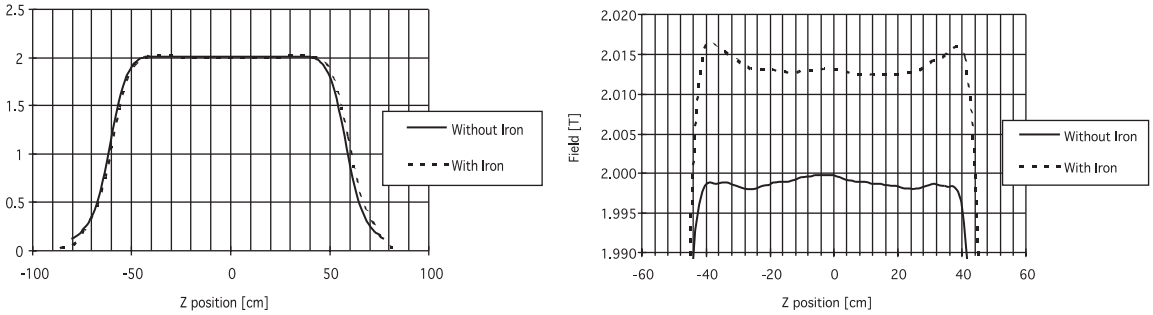

Fig. 16: Field homogeneity

The field also needs be stable over time, as a varying field changes the beam injection conditions. Even though the electron beam potential remains basically constant with a varying absolute magnetic field strength, both the cathode and the trap field decrease by the same factor and therefore the electron beam compression remains constant, and the magnetic part of the Lorentz force will vary with time. Oxford Instruments quoted a relative field stability of 5×10^{-6} h^{-1}, but the measured stability for the REXEBIS solenoid is $\sim 13 \times 10^{-6}$ h^{-1}. The measurement was performed with a Nuclear Magnetic Resonance (NMR) probe.

The current can run for one year without interference. However, the EBIS parameters will be affected because of the slow, but non-negligible, field decrease. The EBIS cryostat consists of an eccentric helium reservoir containing the magnet. It is surrounded by He-cooled radiation shields and super-insulation. The cryostat has an effective volume of 70–75 l. A 120 l LN_2 cryostat cools the outer parts of the magnet to 77 K. The hold times for LHe and LN_2 are approximately 14 and 10 days, respectively.

2.3.4 Electron gun

The electrons of the e^- beam are extracted from an electron gun and accelerated by an anode potential before being collected at the other end of the device. The REXEBIS has a semi-immersed gun with compression proportional to B^n (n~1). EGUN simulations of the extracted electron beam, with and without post-acceleration, are shown in Fig. 17. From the simulations it is concluded that post-acceleration results in less beam scalloping, as expected, but for $U_{\text{post anode}} < 10\,000$ V the effect is

small. At U_{anode} = 6500 V the electron beam is I_e = 0.46 A, rendering a perveance of 0.87 μA/V$^{3/2}$. The cathode surface is 738 mm from the magnet centre. The magnetic field in this position is B_z = 0.2 T. The cathode loading and a phase space plot at 722 mm from the centre in the direction of the gun side are shown in Fig. 18. The simulated beam profile r_{ebeam} is ~0.25 mm in full field. The beam current density at full field is higher than the specified 200 A/cm^2. Figures 19 and 20 contain photos and a commented drawing of the electron gun.

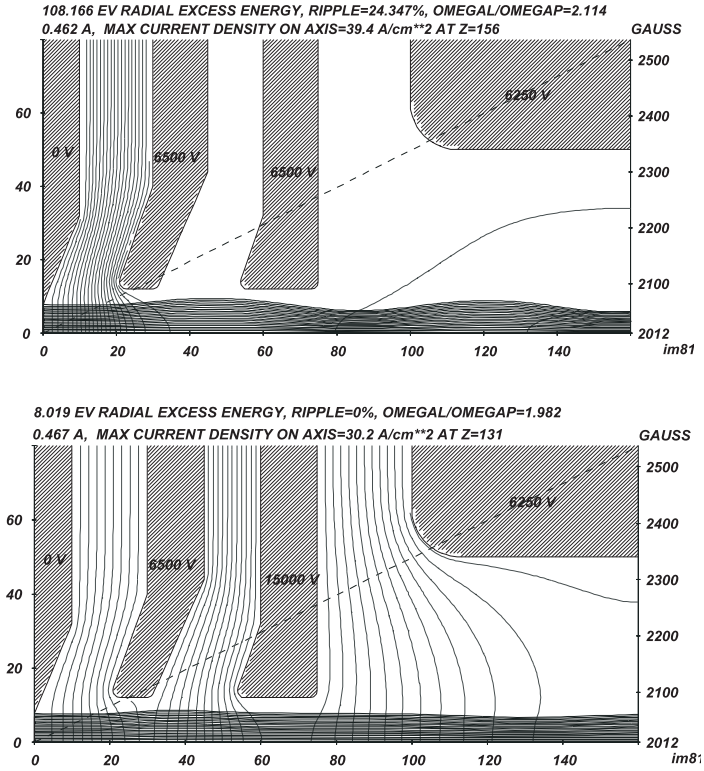

Fig. 17: Simulation of the electron gun geometry using the program EGUN. Top: a non post-accelerated electron beam; bottom: a post-accelerated beam

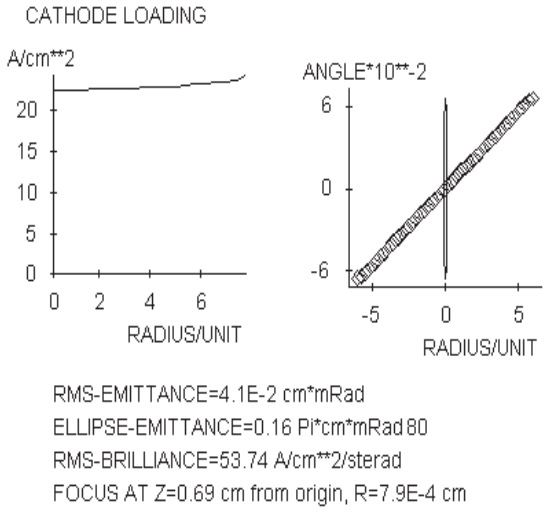

Fig. 18: Cathode loading and phase space

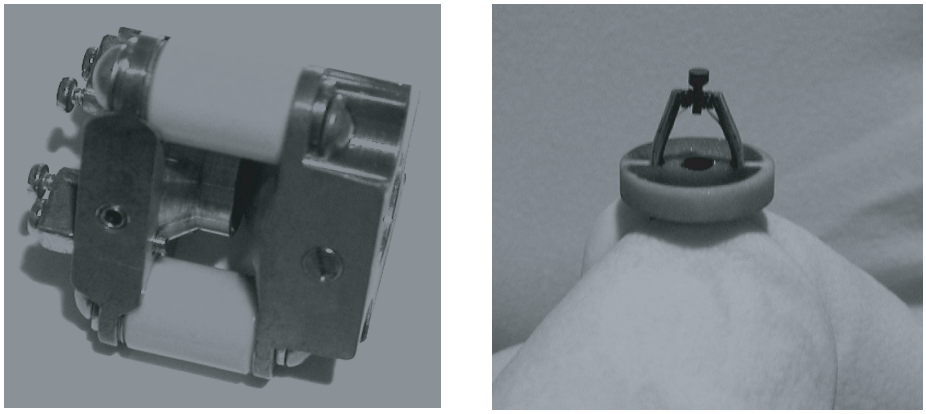

Fig. 19: The electron gun (left) and its cathode

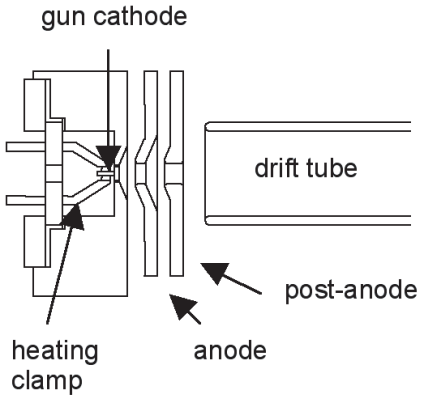

Fig. 20: Schematic drawing of the cathode in its mount, with the anode structure and the first drift tube

Lanthanum hexaboride (LaB_6), produced by FEI Co. [14], is used as cathode material. The work function in the 310-crystal direction is 2.41 eV. A cathode temperature of $T_c \sim 1750$ K is sufficient to yield a cathode current density jc, of 25 A/cm^2, which is necessary for this design. The lifetime at $T_c = 1750$ K is approximately one year if a surface degeneration of 100 μm is accepted over that period. The limiting factor for cathode lifetime has so far been the cathode clamping mechanism, which typically fails after a few months of operation.

The electron gun is mounted on a flange, which is connected to the flange of the inner structure. The cathode end surface must reside 400 mm from the flange face to reach a compression factor of 10. The cathode is powered via a current- and voltage-controlled power supply, and is also connected to a capacitive buffer to protect it from rapid current changes. The cathode can be biased to a maximum of –6.5 kV.

Successful injection of charged particles into a magnetic field sets limitations on the alignment of the source with respect to the magnetic field axis. The tolerances of the REXEBIS gun were estimated to be $\Delta r_c \leq 1$ mm and $\Delta(dr/dz) \leq 3$ mrad. The accepted axial displacement of the gun with respect to the magnetic field was estimated from the EGUN simulations to be at least $\Delta z = \pm 5$ mm. Such a variation would cause a change in electron current density at full field. In practice it was found that the transverse alignment of the gun in the magnetic field is critical. The position has to be accurate within one-tenth of a millimetre to avoid severe losses in electron current. As a consequence, after each bake-out the loss current must be minimized by moving the gun and the collector crosses in the magnetic field with the help of adjustment screws.

2.3.5 Inner structure

The inner structure includes the drift tubes, the support structure, and the non-evaporable getter (NEG) strips. All these elements are in UHV, and at low room temperature (warm bore ~15°C). The drift tubes can be categorized as transport, barrier, and trapping tubes. A certain trap length, L_{trap}, is required to capture the injected ion pulse. The REXEBIS has a trap length of 0.8 m, which can be shortened. The theoretical trapping capacity equals the electron space charge, and for nominal REXEBIS parameters it amounts to

$$N = \frac{\rho_l L_{trap}}{e} = \frac{I_e}{e\nu_e} L_{trap} = \frac{I_e}{e\sqrt{2\frac{e}{m_e}U_e}} L_{trap} = \frac{0.5}{e\sqrt{2\frac{e}{m_e}5000}} \times 0.8 = 6 \times 10^{10}$$

expressed in elementary charges. Passive extraction has been chosen, which means that the outer barrier is lowered to let the previously confined ions move out by their own kinetic energy. Typical extraction times are approximately 50 μs. Other types of extraction mode are illustrated in Fig. 21.

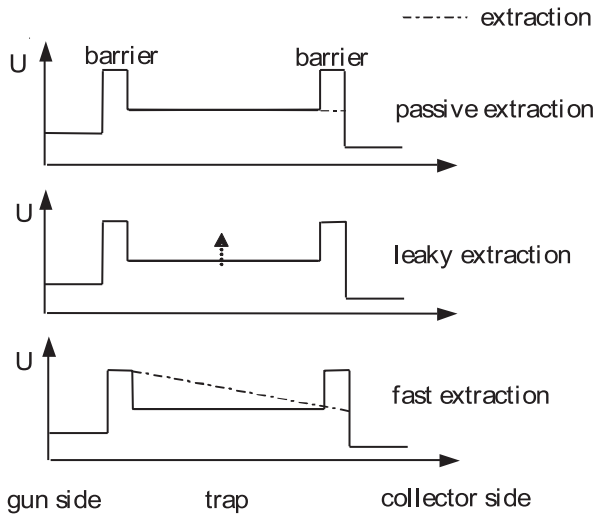

Fig. 21: The different types of extraction modes for an EBIS

The leaky mode gives a slower extraction but a more well-defined energy, while fast extraction achieves the opposite.

The potential along the axis is varied by applying different tube voltages. High potentials at the barrier tubes define the trap size and force the ions to be reflected longitudinally between the barriers. The potential of the trapping tubes relative to the gun cathode determines the electron beam energy E_e.

The trap and outer barrier tubes are pulsed. Approximate tube potentials for a complete cycle are given in Fig. 22. One should note that if the REXEBIS runs fully compensated then the barrier potentials must be $\Delta U \times [1 + 2 \times \ln(r_t/r_{ebeam})] \approx 750$ V higher than the trapping potential. After extraction there is a cleaning phase. This involves applying a potential slope to the tubes to make sure that the trap is clean of ions. Lanthanum and boron from the cathode, ionized in the anode tube, are reflected at the inner barrier back to the cathode, keeping most of the ions out of the extracted ion beam. For a 20 ms breeding time La^{20+} is reduced from about 2 to 0.05 pA by proper setting of the inner barrier tube.

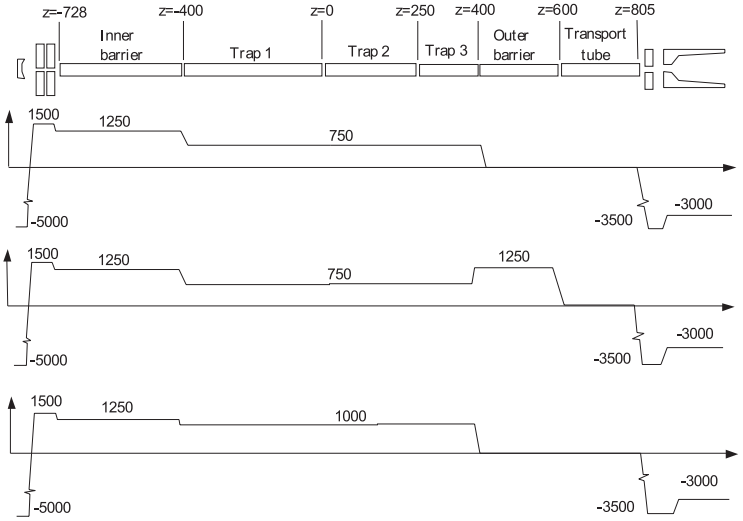

Fig. 22: The approximate potential distribution for the trapping tubes during injection (top), breeding (middle) and extraction (bottom)

The inner structure is about 2 m long and mounted on a flange at the gun cross. The structure is inserted in a 50 mm radius vacuum tube. The drift tubes have an inner and an outer radius of 5 and 6 mm respectively, and are made of titanium. The choice of titanium is due to the sublimating properties of the material. Its moderate electrical conductivity (2.4×10^6 S/m) should also reduce the probability of electron beam resonance phenomena in the structure. The tubes are of varying length. The anode tube is 278 mm, the inner barrier 46 mm, the three trap tubes 396, 196, and 196 mm, the outer barrier 46 mm, and the transport tube 358 mm. The trap tubes are situated in full magnetic field. NEG strips are placed in an octagonal shape around the inner structure and provide high pumping speed. The drift-tubes are perforated by approximately two thousand 2 mm holes for better pumping conductance. There are no RF coupling/damping sleeves at the end of the drift tubes for pumping reasons, only a 2 mm insulation distance between the flat front faces of the tubes. The tube ends can be adjusted sideways, in pairs, by three insulating supports, which are mounted on the support plates. The support plates are in turn fixed to the vacuum tube by three titanium support tubes. With only two supports at the end the maximal vertical deflection of the structure is ~0.15 mm. The two drawings in Fig. 23 show the side and end views of the inner structure.

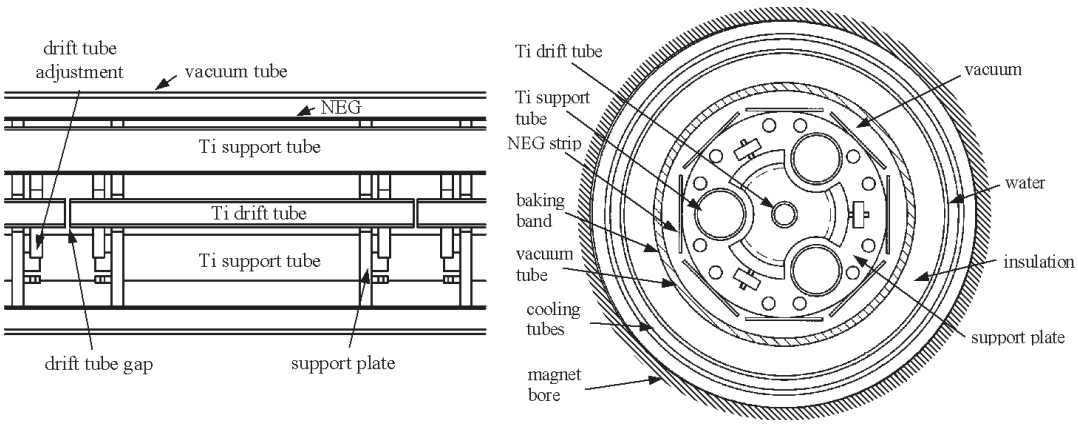

Fig. 23: Side and end views of the inner structure

2.3.6 Electron beam collector

The electron beam is separated from the extracted ions in the collector. Important properties of collector design are a high electron collecting efficiency, a small ion-beam influence, and a low out-gassing rate. In our design we use a collector with a cylindrical instead of conical shape in the absorbing region (see Fig. 24). Usually, the residual axial magnetic field keeps the electron beam together and prevents it from diverging to the absorbing collector surfaces. To counteract this, we reduce the magnetic field inside the collector by putting a cylindrical iron screen around it. Thus the electron beam has the opportunity to expand by space-charge. The REXEBIS collector has been designed with an open end. With this large extraction hole, we expect to minimize ion-beam aberrations. As a secondary effect the pumping conductance increases.

A cylindrical extractor at a voltage of –17 000 V relative to the drift tube is positioned at the end of the collector to extract the ions. The extractor tube has a radius of 14 mm. The large radius ensures that aberrations are small. From SIMION simulations it has been concluded that the ion beam fills less than one-fifth of the extractor diameter. The simulations also indicate a non-distorted phase space. The extractor acts as a strong lens, because of the electrical field, and creates a focus inside the collector.

Figure 24 shows an EGUN simulation of the absorbed electron beam. The dashed line visible to the left indicates the magnetic field strength. One unit of length corresponds to 0.25 mm. Each trajectory, of a total of 210, carries approximately the same current, ~2.5 mA. The trajectories have a thermal starting energy of 0.1 eV at the cathode. The electron beam is dissipated over an area of ~65 cm^2, i.e. the average current load is < 8 mA/cm^2.

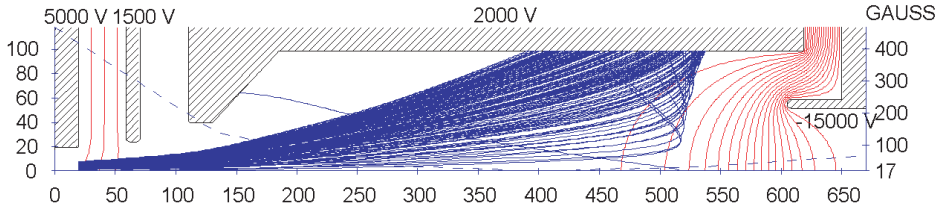

Fig. 24: Simulation of the electron collector

A cross section of the collector is shown in Fig. 25. The water-cooled collector is made of Oxygen-Free High-Conductive (OFHC) copper and mounted to a flange with a Helicoflex metal seal. The flange is connected to the collector cross via an HV insulator. The whole collector structure is bakeable to 350°C. A two-way spiralling water canal for cooling is housed between the two cylinders. The total length of the water canal is 1.6 m. With a 5 mm cylindrical screen of Armco iron (μ_{rm} = 250) surrounding the collector, the magnetic field inside the collector is reduced to < 0.02 T.

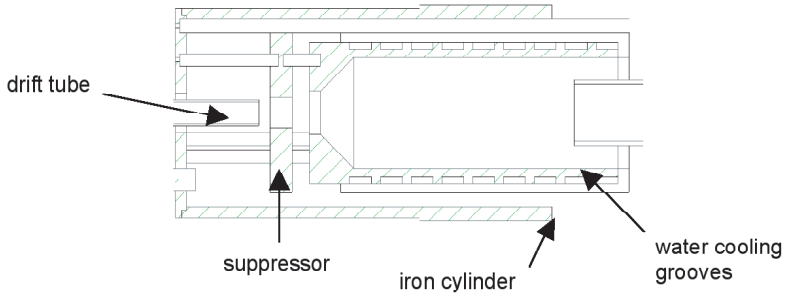

Fig. 25: Cross section of the electron collector

2.3.7 Beam optics

2.3.7.1 Optical elements

Two larger cylinders are mounted behind the extractor tube. These comprise a second extractor and a spare lens. Both have 80 mm internal diameters and are normally electrically connected. Two pairs of vertical and horizontal deflectors follow at the ground potential side. The so-called inner Einzel lens is positioned between these. The outer Einzel lens follows downstream of the outer deflector elements. Both lenses are connected to pulsed power supplies at ground potential. The lenses are pulsed by the different injection and extraction voltages and provide phase space matching for ion injection into the EBIS. Typical voltage settings are given in Fig. 26. An MCP at the entrance of the EBIS beam enables observation of either incoming or outgoing beam.

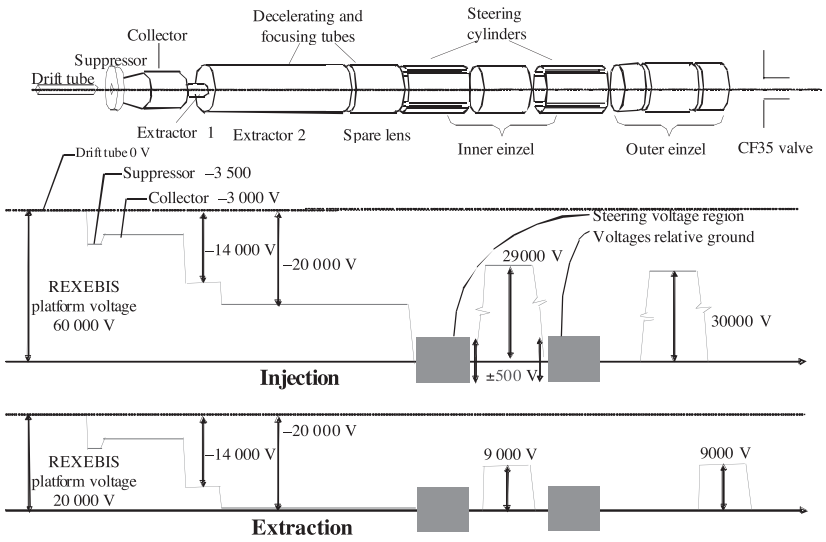

Fig. 26: Typical voltage settings

The REXEBIS beam optics system is connected to the transfer line with a bellow. The beam transfer point between REXEBIS and the transfer line is at an intermediate focal point at the end of the beam transport system. The beam is delivered to the mass separator at the same longitudinal position, but shifted slightly since the second kicker is inactive at extraction. A set of miniature horizontal–vertical deflectors is placed between the upper kicker and the optical elements of the EBIS.

In summary, the REXEBIS optics consists of four main sections:

(i) The gun and the inner structure, mounted on a CF160 flange on the gun cross.

(ii) The collector and extractor, located in the collector cross, which also hosts a spare lens usually connected to the second extractor.

(iii) The inner steering elements, the inner lens, and the outer steering elements in the ground cross.

(iv) The outer lens and the beam diagnostics mounted on the long cross.

2.3.7.2 Acceptance and emittance

REXTRAP delivers a 60 keV ion bunch with an emittance of ~10 π·mm·mrad (80%) at the second bender. The simulated maximum acceptance of the EBIS is approximately 11 π·mm·mrad (100%) at 60 keV. To obtain a Q/A resolution of 150, the ions emitted at 20 kV extraction voltage through the mass separator must fit in a phase-space ellipse of 40 π·mm·mrad at the 4σ level. The emittance of the extracted and non-separated beam has been measured at an extraction voltage of 20 kV using an

emittance meter of the slit-grid type. The device was positioned directly behind REXEBIS. The relatively weak average current of ~150 nA extracted from the EBIS resulted in a modest signal-to-noise ratio in the emittance meter. The first measurement was limited to a non-synchronous measurement, meaning that the emittance meter was not gated with the extraction pulse. The effect of the breeding time on emittance was investigated in this test. With an increased breeding time, the geometrical emittance increased from 10 to over 60 π·mm·mrad. The electron beam was gradually compensated with longer breeding times. The first measurements were carried out under poor vacuum conditions. The pressure was $2–5 \times 10^{-9}$ mbar. Compensation of the electron beam generates a large emittance as it forces the ions to move inside the trapping region with larger radii. As a result of the high beam intensity required for these measurements, they were performed with residual gas ions. It is not expected that a different result would be reached for injected ions. It should be noted, however, that lower ion currents should result in an even smaller emittance.

The calculated geometrical emittance for low-charged (1^+ or 2^+) rest-gas ions is 19 π·mm·mrad. This is in good agreement with the measured value. The horizontal phase space for a breeding time of 1 ms is shown in Fig. 27. At the current improved vacuum conditions this would correspond to a breeding time of 100 ms.

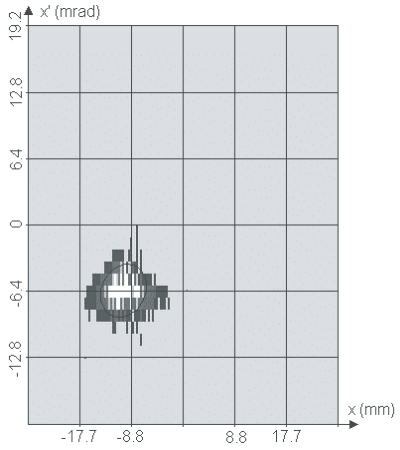

Fig. 27: Horizontal phase space for a breeding time of 1 ms

2.3.8 Vacuum system

A good vacuum is vital to an EBIS, since residual gas ions may compensate the trap and cause a large beam radius with an increased emittance. Poor vacuum conditions also result in the deposit of contaminants on the cathode surface. Finally, the low number of injected ions can be outnumbered by the residual gas ions by several orders of magnitude, even at very good UHV. The last issue is the most critical from the experimental viewpoint. The main cause of ionic background in the EBIS itself is desorption occurring at the filament of the electron gun, in the drift-tubes, and at the electron collector. This desorption is caused by elevated temperature and electron impact on the metal surfaces. An important external source of residual gas ions is the diffusion of neutral cooling gas from REXTRAP into REXEBIS. This effect is reduced by the introduction of several differential pumping stages.

All high-performance EBISs to date have been designed with a cold bore, and therefore have a cryogenic pumping mechanism in the drift structure. The REXEBIS, however, has a warm bore, which calls for other pumping techniques. The pumping system relies on two 180 l/s and one 260 l/s turbo molecular drag pumps from Balzers. The two 180 l/s pumps are positioned at the HV platform on each side of the EBIS, and the 260 l/s pump at ground potential near the second bender in the transport system. These three pumps are backed by a small turbo at ground potential, providing a fore vacuum better than 10^{-5} mbar. Around the inner structure, NEG strips with an area of 6000 cm^2 are mounted in an octagonal geometry. These NEGs, SAES St707, provide additional pumping in the ionization region.

Optionally, the drift tubes can be internally coated with a special NEG coating. The getter material has a pumping speed of 1 l/cm^2·s for H_2 [15] while O_2, N_2, and CO are pumped at 65%, 15%, and 40% of that speed. The hydrocarbon sorption efficiency is very low, and inert gases are not pumped. To further enhance the pumping capacity of the system, the drift and supporting tubes are made of titanium, which has gettering properties and forms pseudo-hydrides with hydrogen. The pumping speed for H_2 is of the order of 1 l/cm^2·s. A fast-closing gate valve has been installed between the EBIS and the beam transfer line to protect the EBIS from air in-rush in case of lost vacuum in other components. A manual precision gas leak valve is mounted on the gun cross, enabling the addition of gases to the system. The complete vacuum system and the internal parts have been vacuum-fired, the stainless steel parts at 950°C and the titanium at 700°C, to reduce the out-gassing of hydrogen. After venting to atmosphere, the system is baked out to between 200 and 350°C for at least 24 hours. The heating also activates the NEG pumps. Heat jackets and wound heating bands provide the heating. The temperature is surveyed by a microprocessor-controlled system. The system is vented with argon.

After bake-out and a week of pumping, the pressure is in the low 10^{-11} mbar range inside the EBIS even when the electron beam is switched on. The pressure inside the drift-tubes was estimated from the extracted current of residual gas ions and found to be in the region of 2×10^{10} mbar. The perforation of the drift-tubes with more than 2000 holes has lowered the rest gas background by more than one order of magnitude. This improved vacuum results in an increased compensation time for the electron beam. In fact, the vacuum is so good that full compensation is not obtained. This allows for operation with long breeding times, which is necessary for breeding heavier elements to $A/q < 4.5$.

2.3.9 Auxiliary systems

The complete REXEBIS apparatus is placed on a mechanical platform diagonally above REXTRAP and at approximately 3.5 m above floor level. The reason for this position is space restriction in the experimental hall. The REXEBIS HV platform is positioned on this platform and houses the EBIS and three electronics racks. It is insulated by 300 mm insulators from Siemens. These are made of epoxy and allow the REXEBIS platform to be switched between 20 and 60 kV.

The power needed on the REXEBIS platform is delivered by a motor–generator arrangement. A transformer would be a simpler solution, but the higher capacitance of such a device makes switching more problematic. The motor is positioned on the mechanical platform and grounded, while the generator is electrically insulated and impelled by an insulating rod. The generator is physically separated from the REXEBIS platform, but is electrically connected to it. During the breeding period, the potential is decreased to between 15 and 22.5 kV, depending on the A/q value. Figure 28 illustrates the platform potential function. The custom FuG supply for the REXEBIS platform ramping (60 kV, 100 mA) is controlled to 16-bit precision.

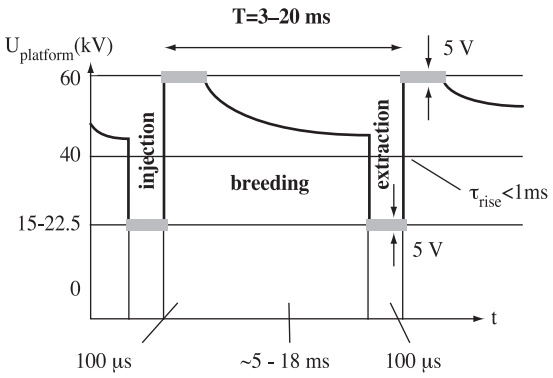

Fig. 28: Variation in platform potential as a function of time

Most of the electronics is physically situated in the racks on the HV platform. One of the racks, containing the electron gun, the suppressor, and the collector supplies, is on approximately –5 kV relative to the REXEBIS platform. The electronics are arranged by insulating the inner shelves from the rack cabinet, so the rack can be placed directly on the platform without electrical insulation. The power to the rack is delivered by a 5 kVA transformer. The other two racks, containing the magnet supply, vacuum controls, power supplies, etc., are at REXEBIS potential. At ground potential there are two further racks for control and beam optics supplies. For security reasons the entire apparatus is surrounded by a high-voltage cage, which is semi-transparent to allow supervision of the instruments in the racks.

Water interlocks on the platform ensure that the turbo pumps are not overheated, the electron beam is not running without collector cooling, and that bake-out is not performed without bore cooling. Vacuum interlocks protect the different HV supplies and inhibit cathode heating in case of poor vacuum. The rest of the vacuum interlocks are handled by the Simatics system for the vacuum.

2.3.10 Performance measurements

2.3.10.1 Electron beam results

A maximum electron beam current of 375 mA has been reached. It is limited by the loss current, i.e. the current going to the anode or to the EBIS ground potential instead of to the suppressor and the collector. For a moderate current of 200 mA the loss is < 0.5%, but at higher electron current the loss increases exponentially. The gun supply limits the loss currents to 2.5 mA. The major part of the loss current goes to the outer drift tube, close to the suppressor. The loss current is very sensitive to small movements of the EBIS structure. A translation of less than 1 mm at one end of the structure can occasionally increase losses by as much as 50%. Given that the REXEBIS is a warm-bore machine, the current losses are not critical, except for very high losses of > 5 mA, when out-gassing becomes critical. With the LaB_6 cathode a current density in the trap of 100–150 A/cm^2 has been achieved.

The experimental gun perveance value P_{gun}, was found to vary between 1 and 2 μP between different gun mountings, which exceeds the value of 0.9 μP given by the EGUN simulation. A perveance that exceeds the design value may in fact be favourable, since it allows for a lower electron beam current and energy while maintaining a short breeding time.

Abrupt cuts in the cathode heating current change the perveance in steps of 0.1 down to 0.2 μP. This can most probably be attributed to an axial movement backwards of the cathode in its support clamps. The problem has been eliminated by the insertion of a damping Resistor–Capacitor (RC) circuit in the cathode heating line. To limit the cathode heating, the gun is in most cases operated in emission, rather than space-charge limited mode. During operation a decrease in the electron beam of a few per cent during a beam time of several days' duration has been observed. By readjusting and keeping the heating power constant the current can stay constant. An alternative gun design, based on a 3.2 mm diameter dispenser cathode, has been tested. As the dispenser cathode uses a four times larger emitting surface and has a lower current density (of 10 mA/cm^2 compared to the 25 mA/cm^2 for the LaB_6 cathode), the compression of the beam has to be increased. A compression of 40 would give the same electron current density, but at such high compression instabilities are likely to occur, and therefore a compression of 20 was instead chosen. Over several weeks of operation, no decrease in the current from the dispenser cathode was noticed. The mechanical stability and precision of the cathode base were excellent. With the dispenser cathode the current was limited to 200 mA by electron beam losses. The lower current density (of about 45 A/cm^2) results in a maximum charge lower by one unit charge compared with the LaB_6 cathode for lighter elements (lighter than Ar).

2.3.10.2 Extracted ion beam results

The pulse extracted from REXEBIS is a few tens of microseconds long. The pulse shape has been measured both directly after the EBIS with a Faraday cup and after the linac. Figure 29 shows a non-separated beam. The pulse measured from scattered ions striking a target after acceleration in the linac is shown in Fig. 30. After a short rise-time the pulse decays with a fall time of less than 100 μs. The shoulder on the decay curve in both figures may be due to irregularities in the potential switching of the trapping tubes inside the EBIS during these measurements. The pulses observed on the oscilloscope are normally completely smooth. By applying a ramping voltage of 300 V to the trapping tubes during extraction, the extraction time can be reduced to almost half the length mentioned above. With the improved vacuum situation less than 50 pC of charge is normally extracted in each pulse. With gas inlet a maximum ion charge of 3.7 nC per pulse has been extracted. This corresponds to an electron beam compensation of 68%. High currents of several nA of He^+ ions have also been extracted and were used for studies of the beam dynamics of the accelerator structures.

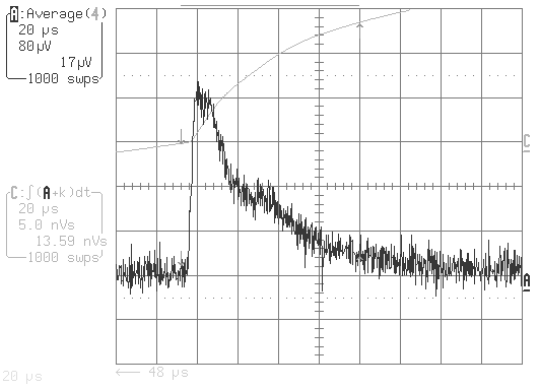

Fig. 29: The non-separated ion beam measured in a Faraday cup after the EBIS

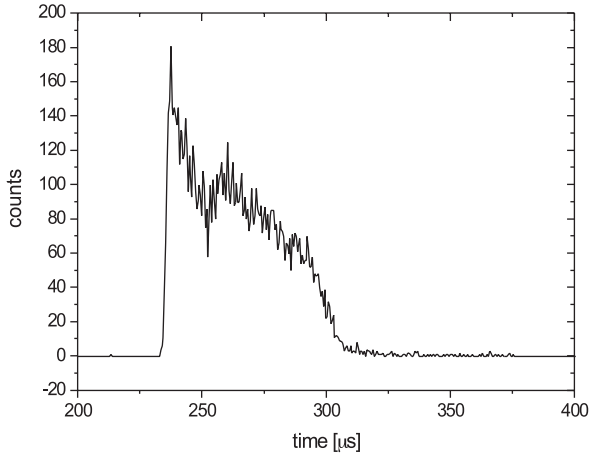

Fig. 30: The scattered beam measured by a Si detector in the target chamber after post-acceleration

A typical residual-gas spectrum analysed in the REX-ISOLDE mass separator is shown in Fig. 31. The presence of oxygen and carbon, and also of some nitrogen, is evident. The neon peaks seen in most spectra are due to cooling gas effusion from the trap to the EBIS, but in this particular case the valve to the trap was closed. For most isotopes, except for very light ones, an A/q ratio within the range accepted by the accelerator can be found without background from ionized residual gas. An ion spectrum showing high currents of charge-bred stable ^{23}Na, injected as singly charged ions from the trap, is presented in Fig. 32. The Na^{7+} current exceeded 70 pA or 6×10^7 p/s. To reach the $A/q < 4.5$ required by the linac for heavier masses, longer breeding times have to be applied. As an example,

the spectrum of the charge states of ^{133}Cs after 158 ms breeding is shown in Fig. 33. $^{133}Cs^{32+}$ with an A/q = 4.15 was successfully accelerated in this test.

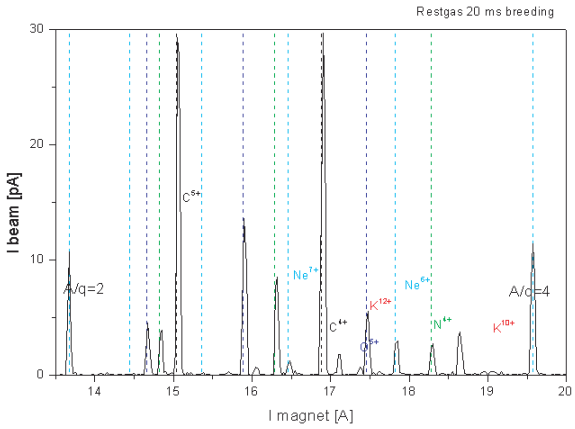

Fig. 31: Residual gas spectrum measured with the mass separator after REXEBIS

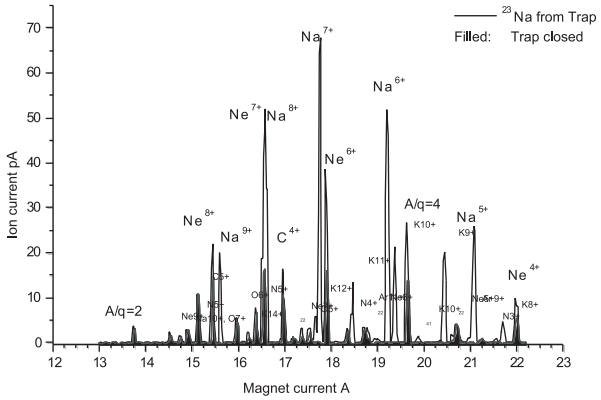

Fig. 32: Mass spectrum for injected stable ^{23}Na

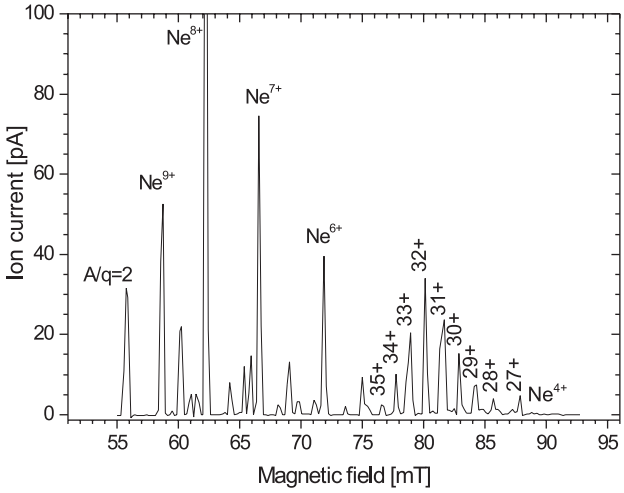

Fig. 33: Mass spectrum for injected stable ^{133}Cs

A mass spectrum after 18 ms charge breeding of radioactive ^{26}Na can be seen in Fig. 34. Despite the current associated with ionized residual gas or the buffer gas from the trap, the peaks of ^{26}Na can be readily identified. The maximum in the charge state distribution for this case is $^{26}Na^{7+}$. An example of

a longer breeding time for radioactive ions can be seen in Fig. 35. In this case unstable $^{153}Sm^{1+}$ was injected and charge-bred for 30 ms and $^{153}Sm^{28+}$ post-accelerated with the RFQ accelerator and implanted into semiconductor samples at an energy of 300 keV/u for a solid-state physics experiment. The peaks between the different samarium charge states belong to ionized lanthanum, which is outgassing from the cathode. The lanthanum and boron ionized in the first drift tube can be effectively suppressed by optimizing the setting of the inner barrier tube.

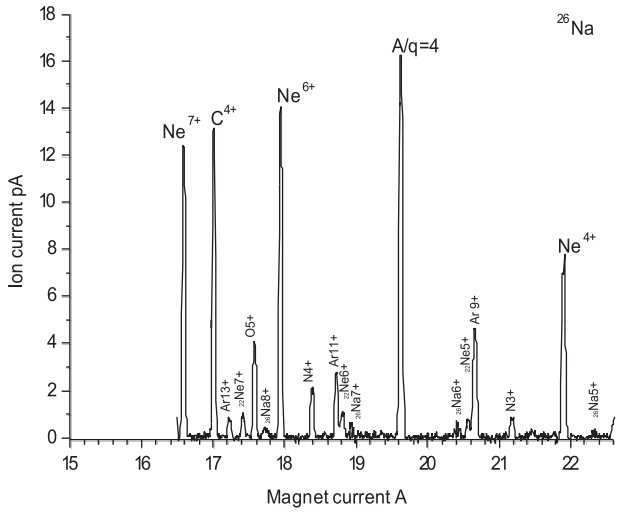

Fig. 34: Mass spectrum after 18 ms of charge breeding of radioactive ^{26}Na

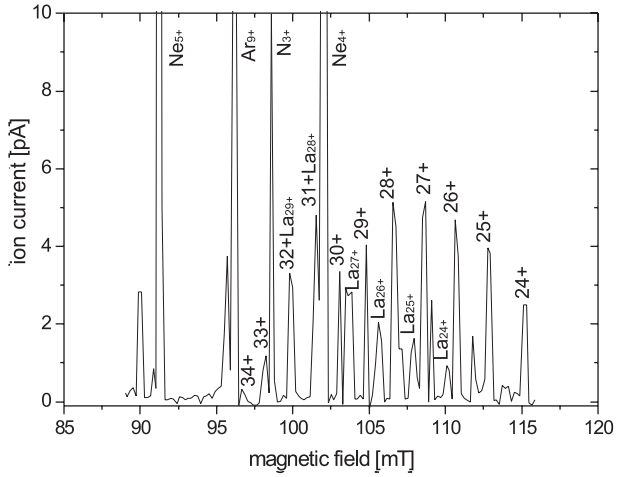

Fig. 35: Extracted charge states for ^{153}Sm after 30 ms breeding

So far the EBIS has run for more than two beam-time periods at ISOLDE. Radioactive ions ranging from ^{9}Li to ^{156}Eu have been charge-bred for several experiments. In most cases the total efficiency (i.e. the ratio of ions ejected from the trap to the sum of all charge states coming out of the EBIS) is over 30%. This includes transportation from trap to the EBIS, EBIS injection and extraction losses, and mass separation. For a single charge state the efficiency can be as high as 10%. Table 1 gives the efficiency for the selected charge state for several isotopes. The injected average current for all measurements was below 10 pA, corresponding to 1.2×10^6 ions per pulse at a pulse repetition frequency of 50 Hz. Efficiency decreases at higher injection currents as the ion bunches' emittance from the trap increases. As the intensity of radioactive ions delivered by ISOLDE is normally considerably smaller this does not restrict operations significantly. K^+ was also injected with the dispenser cathode and a gun current of 200 mA, and similar amounts of 9^+ and 10^+ charge states were obtained.

The efficiency depends strongly on the injected current. For 50 pA it is 5%, for 15 pA 8.8%, and for 2.5 pA 11.5% in one charge state after the analysing magnet. In the case of Na and K ions a total efficiency (from the ISOLDE mass separator exit to the end of the REX-ISOLDE accelerator) of up to 4% has been reached. This includes bunching efficiency in the trap of about 45%, charge-breeding efficiency of about 10%, and accelerator transmission of approximately 90%.

Table 1: Efficiency (ratio of injected current to the extracted current in one charge state) for charge breeding of several elements

Element	Charge state	Efficiency (%)
^{7}Li	2+	9.0
^{24}Na	7+	9.5
^{25}Na	7+	9.5
^{26}Na	7+	10.7
^{27}Al	7+	8.0
^{39}K	10+	10.0
^{133}Cs	23+	8.7
^{133}Cs	32+	7.3
^{153}Sm	28+	3.0

2.4 The REX-ISOLDE mass separator

As indicated above, it is necessary to mass-separate the ion beam extracted from REXEBIS although the EBIS itself is a UHV system. As an example, the yield of neutron-rich Na, Mg, K, and Ca isotopes from ISOLDE can be up to 1000 times lower than the amount of residual gas ions in the EBIS beam. This residual gas consists mainly of C, N, O, and Ar or Ne ions emitted from the atmosphere or the buffer gas of the Penning trap.

The energy spread of the ion beam from the EBIS is approximately $\Delta E/E$ of $\sim 5 \times 10^{-3}$. A simple magnetic separator with two 90° dipoles is therefore insufficient for separation since it would result in a deterioration of the $\Delta(q/A)/(q/A)$ resolution. For this reason a Nier-type separator [16] has been introduced. It was concluded from the predicted residual gas spectrum of the EBIS that an A/q resolution of about 100 would be sufficient to separate highly charged, rare radioactive ions from rest-gas contaminants. This assumption has been verified in commissioning experiments. The separator beam line also matches the beam from the mass slit to the acceptance of the RFQ. Moreover, it is possible to transfer the 60 keV·q beam back to the ISOLDE main beam line in order to deliver highly charged ions to other experiments. The transfer point is envisaged to be in front of the RFQ (see Fig. 1).

2.4.1 Beam line geometry

The separator (see Fig. 36), which is achromatic, consists of an electrostatic and a magnetic bender. The electrostatic bender compensates the energy dispersion of the magnet. In order to reduce the energy dispersion at the mass slit to zero, the second-order aberrations are corrected by appropriate magnet pole curvatures. Third-order aberrations are reduced by an electrostatic octupole, which is placed at the front of the system because of space restrictions [17]. The resolving power of the system depends on the emittance of the injected beam. In order to provide a resolving power of 100 the EBIS emittance has to be lower than 16 π·mm·mrad at 20 kV extraction potential.

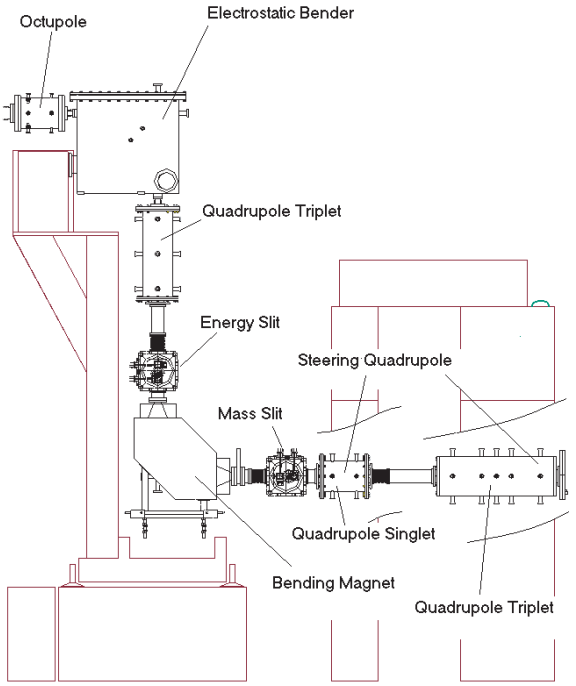

Fig. 36: The REX-ISOLDE mass separator

The beam line calculations start from the delivery point inside the electrostatic bender, BTS.BE130, situated 0.75 m upstream of the octupole, SEP.OP10. The names of and the distances between the beam line elements are given in Fig. 37. In the first stage of the separator the beam is bent by the electrostatic deflector, SEP.BE30, with a bending radius of R = 0.6 m. Ions extracted from the EBIS at the same potential are bent with the same radius, irrespective of their mass. This general feature of an electrostatically extracted ion beam is given by the relation between the bending radius and the two potentials that are relevant for determining the flight path:

$$U_{bender}[V] = \frac{2d}{R} U_o \ .$$

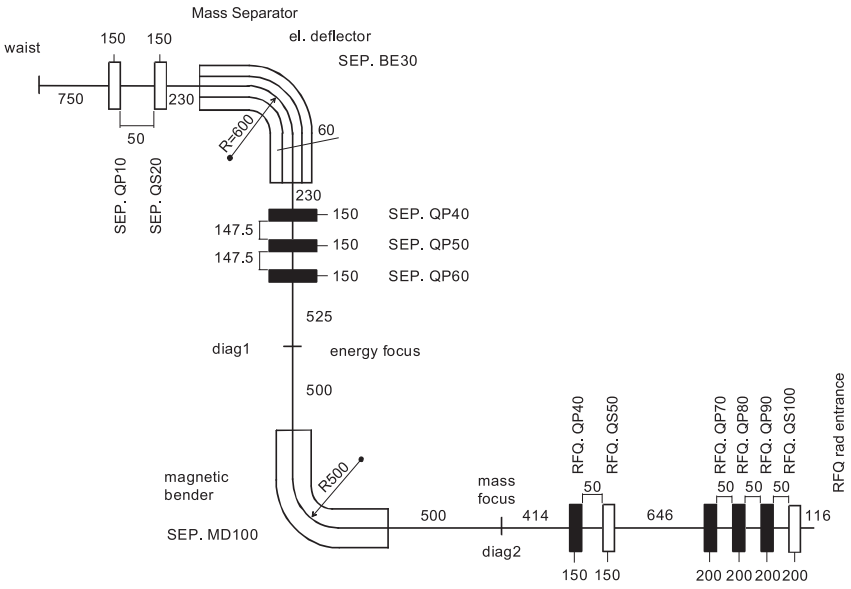

Fig. 37: Elements of REX-ISOLDE and the distances between them (mm)

Here U_o is the starting potential of the ions within the EBIS and the distance between the bender electrodes is given by: d = 60 mm. The term U_{bender} is the potential on the bender electrodes. As a result of the geometry, the potential of the bender electrodes is optimum at $0.1 \cdot U_o$. The energy focus is located inside the bender and the following quadrupole triplet projects the focus into the diagnostic box in the vertical beam line. In that focal point the energy spread can be restricted to a specific value by apertures. This focal point, 0.5 m in front of the bending magnet, is also the starting point for the mass separation section. The mass slit is positioned 0.5 m behind the magnet exit. The beam size can be measured at the energy focus as well as at the mass slit. The specification of the mass separator bending magnet, SEP.MD100, is given in Table 2 and that of the lenses can be found in Table 3.

Table 2: Specification of the magnet MD1 (SEP.MD100)

Gap size (mm)	50
Deflector angle	90^o
Bending radius (mm):	500
Curvature at pole entrance and exit (m):	–7.3, –1.16
Maximum field strength	0.2 T
I and U for B_{max}	50 A, 74 V
Field homogeneity	5×10^{-4}

Table 3: Specification of the electrostatic quadrupole lenses of the REX mass separator

Lens	**Aperture (mm)**	**Effective length (mm)**	**Separation (mm)**	**Polarity [in x (vertical), + is focusing]**
SEP.OP10	100	150	50	–
SEP.QS20				–
SEP.BE30	60	600 bending radius	–	+ upper electrode
SEP.QP40	100	150	147.5	+
SEP.QP50				–
SEP.QS60				+
RFQ.QP40	100	150	50	+
RFQ.QS50				–
RFQ.QP70	120	200	50	–
RFQ.QP80				+
RFQ.QP90				+
RFQ.QS100				–

The curvature at the entrance and exit of the magnet for higher-order optical corrections is established using iron fingers. These are attached to the mirror plates that limit the field extension at the pole shoe ends. The magnet should provide a magnetic field given by:

$$B \cdot \rho[T \cdot m] = 0.144 \cdot \frac{A}{q} \sqrt{E[(MeV)/u]} \ .$$

If a maximum A/q of 4.5 and an injection energy into the RFQ of 5 keV/u is assumed, then for a bending radius of 0.5 m, the equation above renders a required magnetic field of 0.091 T.

Besides the specification of the focusing elements, the length of the beam line section is important for particle dynamics calculations. Shunt plates have been introduced to define the field length of the electrostatic lenses and the two benders according to the calculations given in Ref. [18]. For the lenses in the mass separator, the distance of the shunt plates is $0.23 \cdot R_o$, where R_o is the radius of

the quadrupole apertures, which also corresponds to the half-distance of the bender plates. The radius of the quadrupole electrodes is $1.147 \cdot R_o$. The radius of the shunt plates is $R = 0.8 \cdot R_o$.

The resolving power of the mass separator is defined via

$$R = \frac{\langle x|\delta_m \rangle}{2x_f} ,$$

where $\langle x|\delta_m \rangle$ is the first-order mass dispersion matrix element and $2x_f$ is the final beam spot at the mass slit in the dispersive plane. The value of x_f is derived from the beam emittance. The above equation gives a first approximation since for higher order calculations the dispersion matrix element cannot be replaced by a combination of higher order matrix elements. A more realistic value for the resolving power is given in Ref. [17] according to the method discussed in Ref. [19].

In the next section we present the results of the calculations and a possible set of lens settings for an optimum mass resolution and injection of the beam into the RFQ.

2.4.2 Particle dynamics simulations

The calculations of the voltage settings of the lenses, the beam profiles, the emittances, and the energy dispersion at the mass slit have, as a starting point, the focal point of the EBIS optics. This point is located 750 mm in front of the electrostatic octupole lens. The Twiss parameter, and the beam emittance of the beam from REXEBIS according to emittance measurements are given in Table 4. The settings in Table 5 give optimal energy dispersion, transmission as well as beam profiles that fit through the slits. The COSY calculations give a third-order resolution of 105 for the injected beam described above. The results of the calculations are shown in Appendix G.

Table 4: Beam parameter of a beam with 0.66 π·mm·mrad normalized at the end of the RFQ rods

Parameter	**x**	**y**
α	0	0
β (mm/mrad)	0.4	0.4
γ (mrad/mm)	2.5	2.5
ε (π·mm·mrad)	10	10

Table 5: Settings for the electrostatic quadrupole lenses of the mass separator

Lens	**Voltage (V)**
SEP.OP10	–1240
SEP.QS20	–430
SEP.BE30	2001
SEP.QP40	1503
SEP.QP50	–1535
SEP.QS60	+1378

Using the calculated settings a residual gas spectrum from the EBIS was measured at 19.6 kV platform potential. The drift-tube potential was 700 V in these measurements. The potential depression is about 300 V. Figure 38 shows the rest-gas spectrum that was used to derive the resolution. The minimum current difference that is required to separate two peaks at ~ 4σ is 0.1 A. The current through

the magnet is proportional to the square root of the mass-to-charge ratio of the ions. Thus the resolution can be estimated via

$$R = \frac{\sqrt{A/q}}{2 \cdot \min(\Delta(A/q))} \ .$$

As mentioned above, the minimum Δ(A/q) results from a current of 0.1 required for proper separation of the peaks. Thus for the C^{5+} peak a resolution of about 78 and for the A/q = 4 peak a resolution of about 100 is reached.

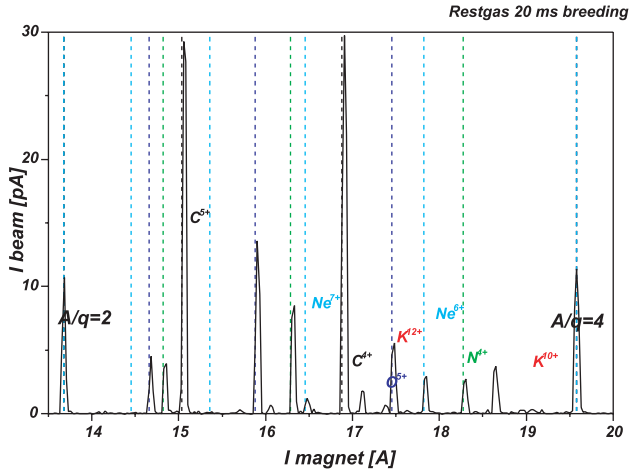

Fig. 38: EBIS rest-gas spectrum for a breeding time of 20 ms

2.4.3 Simulation of RFQ injection

Two electrostatic quadrupole lenses match the mass-separated beam for injection into the RFQ. The application of the lens settings given in Table 6 has resulted in a high injection efficiency with a minimum steering. See Appendix G for the matched beam emittances inside the acceptance of the RFQ. The beam emittance fits very well into the acceptance. The Twiss parameters of the RFQ acceptance are given in Table 7.

Table 6: Settings for the electrostatic quadrupole lenses for optimum injection into the RFQ

	Voltage (V)
RFQ.QP40	1128
RFQ.QS50	–670
RFQ.QP70	–925
RFQ.QP80	1564
RFQ.QP90	–1367
RFQ.QS100	1319

Table 7: Twiss parameter of the RFQ acceptance. Injection energy is 5 keV/u

Parameter	**x**	**y**
α	0.650	0.650
β (mm/mrad)	2.780	2.780
γ (mrad/mm)	0.512	0.512
ε (π·mm·mrad)	187.500	187.500

3 The REX-ISOLDE linear accelerator

3.1 Introduction

The REX-ISOLDE linac [20] (see Fig. 39) consists of a Radio Frequency Quadrupole (RFQ) accelerator [21], an Interdigital H-type (IH) structure [22] and three seven-gap resonators [23]. The first two structures accelerate the ion beam to 0.3 MeV/u and 1.1–1.2 MeV/u, respectively. The three seven-gap resonators allow a variation of the final beam energy between 0.8 and 2.3 MeV/u. A split-ring rebuncher [24] matches the beam from the RFQ to the acceptance of the IH structure. In addition to this set-up, a 202.56 MHz nine-gap IH structure was installed in 2003/2004 to increase the final energy to 3.0 MeV/u. Commissioning and testing of this structure is in progress. The resonance frequency of the original linac is 101.28 MHz. This is one half of the frequency of CERN Linac II. The maximum duty cycle is 10% and the highest repetition frequency 50 Hz. The largest mass-to-charge ratio of the ions is 4.5 with the exception that a beam energy of 3.0 MeV/u can be reached only for A/q ≤ 3.5.

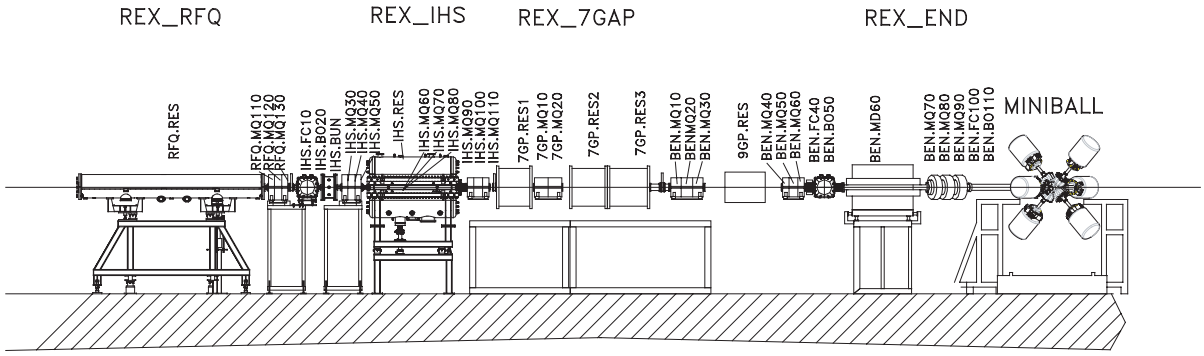

Fig. 39: Overview the REX-ISOLDE linac and names of beam line elements

The accelerators and a full specification of all beam line elements and geometries are presented in this section. For specific design parameters see Table 8. The codes PARMTEQ [25], LORASR [26], and LINAC [27] were used for the design of the linac components. The beam transport was mainly calculated with the codes MIRKO [28] and COSY Infinity [29]. The current section starts with a technical description of the accelerator and is followed by simulations of the beam transport and the beam optics. Results for beams with energies from 0.3 MeV/u (RFQ energy) to 3 MeV/u (maximum energy) are given. The beam transport towards the diagnostic boxes and the target chambers in the MINIBALL beam line has also been calculated. The idea is to produce a complete table of lens settings and different transport modes for the users who will work at REX in the future. Machine upgrades [30] to reach higher beam energies are discussed at the end. The upgrades are planned in two steps: a first step to 3.0 MeV/u and a second step to > 4.0 MeV/u.

3.2 The RFQ

The REX RFQ (see Fig. 40) and the IH structure were constructed and tested at the Physics Department of the Ludwig Maximilian University (LMU) in Munich. The REX RFQ is designed to accelerate radioactive ions, with A/q < 4.5, from the REX-ISOLDE mass-separator, from an energy of 5 keV/u to an energy of 300 keV/u. The electrode voltage is 42 kV for ions with A/q = 4.5 which requires an RF power of about 36 kW. The tank has a total length of 3 m. The RFQ is of the four-rod type and includes 18 stems. It operates at a resonance frequency of 101.28 MHz.

The transmission has been optimized with PARMTEQ calculations to be > 98% whereas an experimental transmission of > 90% has been reached for all isotopes at REX. The phase spread behind the RFQ is ±15° at an energy spread of ±1.5%. The characteristic parameters of the RFQ are listed in Table 9.

Table 8: Design parameters of the REX-ISOLDE linac. The entrance emittances shown are the limits for 95% transmission

Parameter	**RFQ**	**Buncher**	**IH structure**	**7-gap resonators**
E_{inject} [MeV/u]	0.005	0.3	0.3	1.1–1.2
β_{inject}	0.0033	0.0254	0.0254	0.049–0.051
E_{exit} [MeV/u]	0.3	0.3	1.1–1.2	0.85–2.2
β_{exit}	0.0254	0.0254	0.049–0.051	0.043–0.069
$\varepsilon_{xx'}$, ε^n [π·mm·mrad]	200, (0.66)	–	25.3, (0.643)	21, (1.03)
$\varepsilon_{yy'}$, ε^n [π·mm·mrad]	200, (0.66)	–	25, (0.636)	52, (2.55)
Q	4050	3700	8500	5370
R_p, Z_{max}	146 kΩm	35 MΩ/m	330 MΩ/m	60 MΩ/m
Voltage A/q = 4.5 (MV)	0.0933 × A/q	0.1667 × A/q	1.15 × A/q	0.389 × A/q
Rf power A/q = 4.5 (kW)	36.3	1.5	48.5	64.5

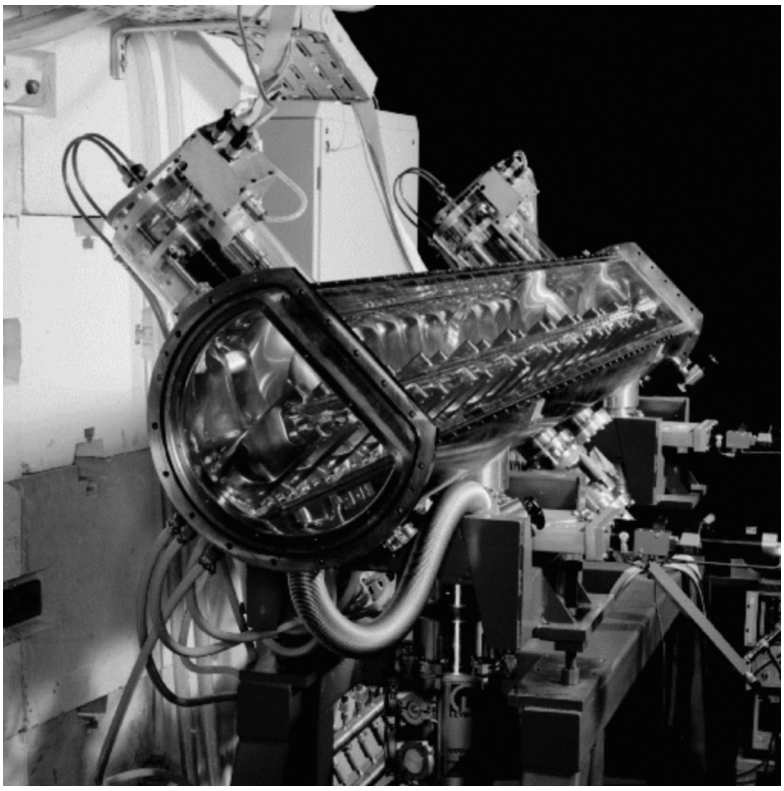

Fig. 40: The REX RFQ

The RFQ can also be used to accelerate heavier ions with a correspondingly higher A/q. For example, $^{153}Sm^{28+}$ (A/q = 5.46) was accelerated to 300 keV/u for solid-state physics experiments in the second beam line, while the other accelerators were switched off [31]. This is possible because, at the higher energies, the restriction to a maximum A/q of 4.5 is given by the drift-tube section (in particular by the inner tank triplet of the IH structure, which at A/q = 4.5 is at its limit) and by the beam transport.

Table 9: Basic parameters of the REX RFQ

Frequency	101.28 MHz
Input energy	5 keV/u
Final energy	300 keV/u
Duty cycle	10%
A/q	1/3–1/4.5
Rad. acceptance ε_{norm}	0.66 π·mm·mrad
Synchr. phase	–90° to –13°
Electrode voltage	9.33 × A/q
Rel. field deviation	< 1%
Quality factor Q_0	4050
R_p value	146 kΩm
Accelerator cells	232
Electrode length	2920 mm
Tank length	3000 mm
Tank diameter	320 mm
Stem height	189 mm
Number of stems	18
Output phase spread	±15°
Output energy spread	±1.5%
Transmission	> 90%
Vacuum during operation	3×10^{-7} mbar

3.2.1 Mechanical properties

A new stem design (see Fig. 41) was chosen for the water supply of the REX-RFQ rods. The cooling water channels were drilled inside the stems. This enables a simplified production method and provides an overall plain surface. The electrodes are so-called mini-vanes and have a hollow profile for internal cooling channels. The new design allows for efficient cooling of the electrodes and avoids having small tubes on the outside of the stems, a construction that turned out to be sensitive to corrosion and mechanical resonances.

Figure 42 shows the cooling system of the RFQ. It consists of seven, separately adjustable circuits, starting from one main distribution manifold. Circuits 1 and 2 supply the electrodes via the stems (see Fig. 41). Circuits 3 and 4 are used for the serial cooling of the standard stems. The piston tuners are supplied from circuits 5, 6 and 7. Only two tuners are built in. Circuit 6 is connected to a cooled ground plate in the low-energy part of the resonator. Circuit 8 is for the coupling loop.

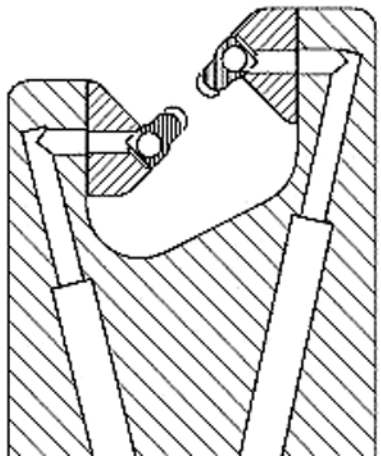

Fig. 41: Cross section of RFQ stem with mounted mini-vane electrodes

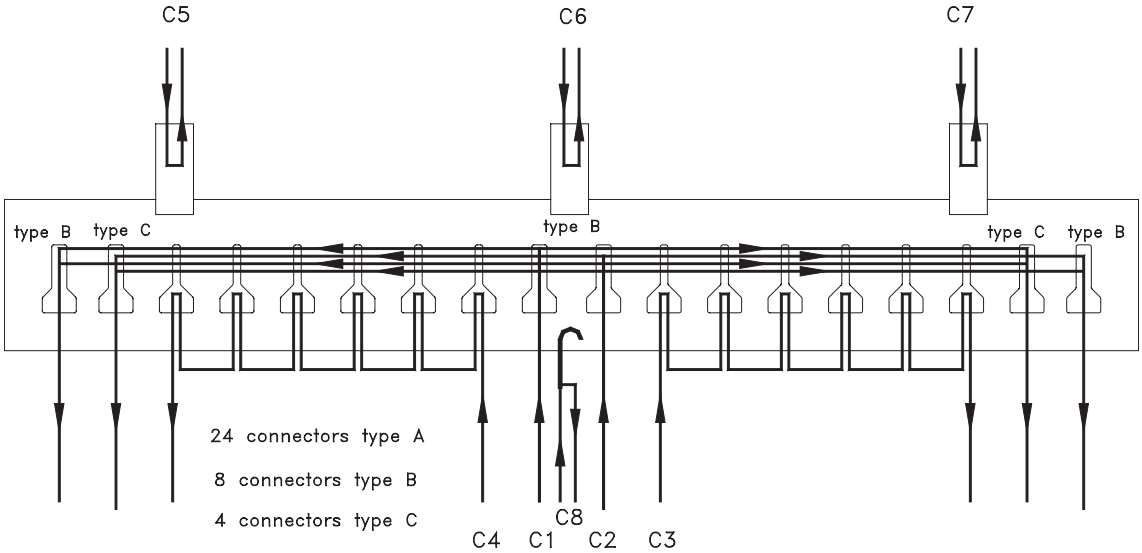

Fig. 42: Cooling system of the REX RFQ

Target holders, placed on the tank bottom (accuracy 2/100 mm), were used for adjusting the position of the targets on the end flanges. The axis, defined in this manner, was then used to align the stems and electrodes. For a picture of the targets refer to Fig. 43.

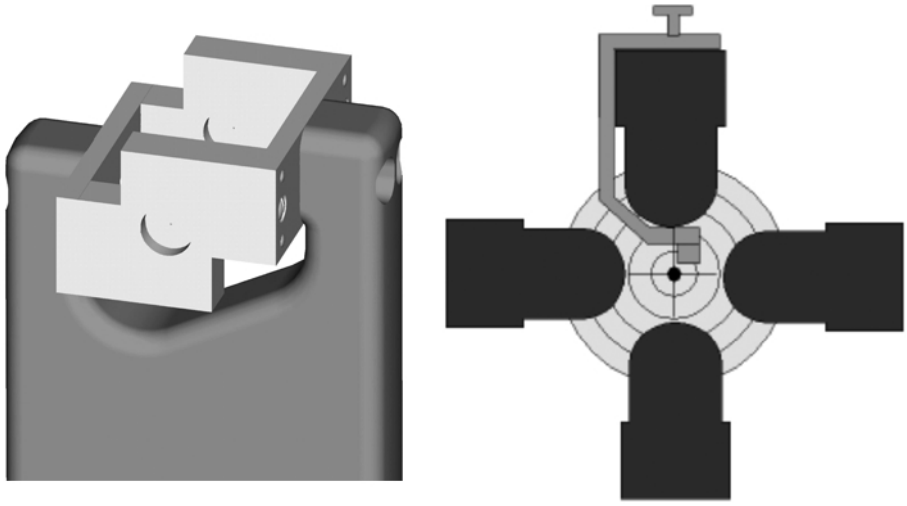

Fig. 43: RFQ stem and quadrupole electrodes with alignment targets

3.2.2 RF properties

The adjustment of the field distribution was done by introducing single plates between the stems. The plates were connected electrically to the stems by silver-plated contact springs (see Fig. 44). A cooled ground plate was installed in the first half of the tank. This solution was not suitable for the second half as it resulted in a resonance frequency that was too high. The lower part of this section was cooled via the stems which is sufficient at the power levels at REX. A mechanical solution for the second ground plate has been worked out at LMU, Munich, but has yet to be installed.

The RFQ has four pick-ups for measurement of the tank voltage. Two of these are used and two are spares. Table 10 shows the attenuation of the pick-ups from the low-energy end (No. 1) to the high energy end (No. 4).

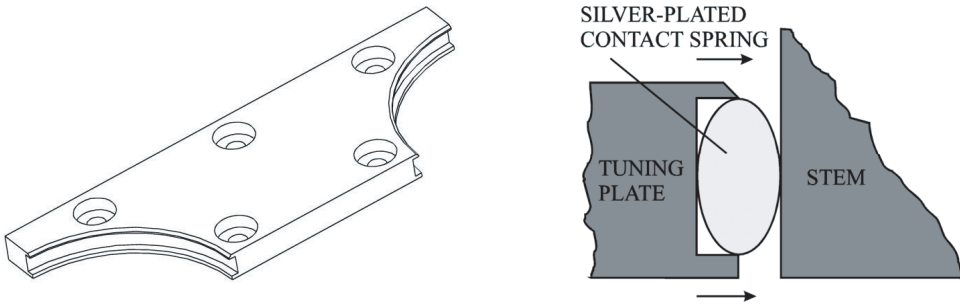

Fig. 44: Tuning plate and method to realize RF contact

Table 10: Attenuation of the RFQ pickup signals

Pickup no.	Attenuation (dB)
1	43.1
2	46.1
3	48.7
4	46.6

The coupling loop has a reflection factor of $P_{back}/P_{forw} = -35$ dB. It is mounted on a rotatable flange for adjustment, if necessary. Figure 45 shows the coupling loop mounted in the tank.

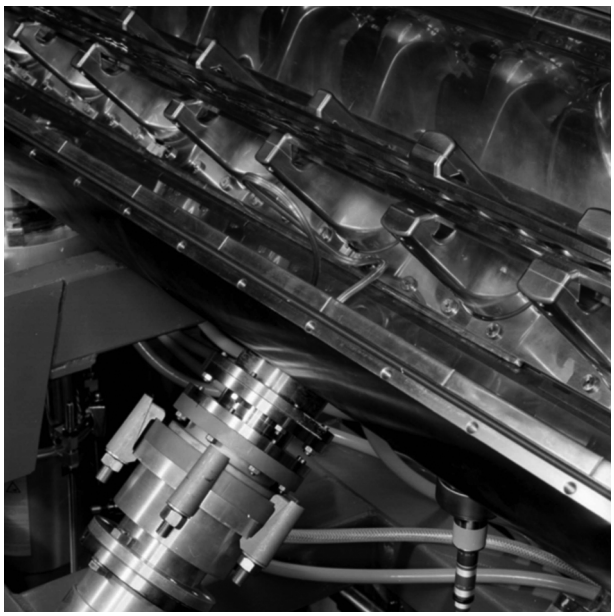

Fig. 45: Coupling loop fixed with rotatable flange

3.2.3 Particle dynamics

Figure 46 shows the electrode design of the RFQ. It is a modification of the classical Los Alamos design with constant focusing strength [32]. It was developed mainly at the University of Frankfurt [33]. Shorter structure lengths have been obtained. The drastic change of the synchronous phase (ϕ_s), the modulation (m), and the aperture (a) in the last 10 cm indicates the matching-out section, which has been introduced to avoid beam losses during the transport through the matching section.

Figure 47 shows the comparison with RFQ output emittances with and without the matching-out section.

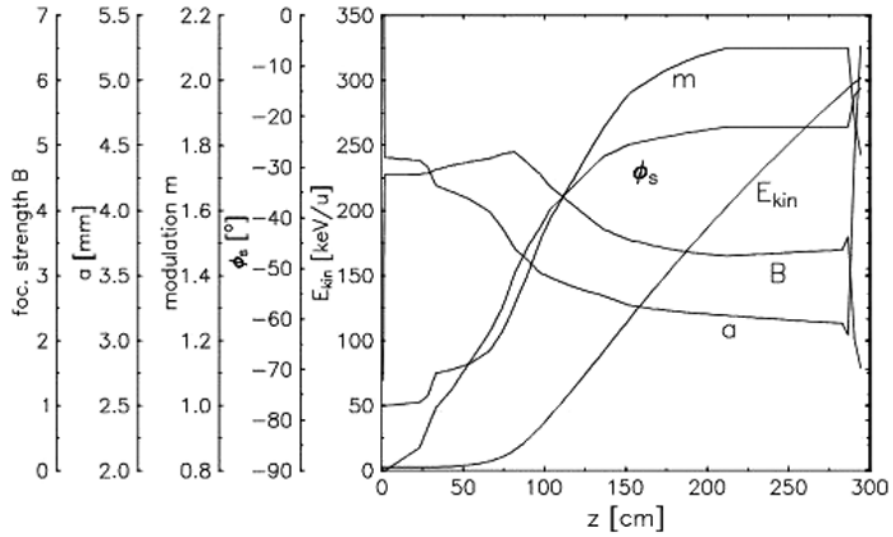

Fig. 46: Electrode design of the REX RFQ

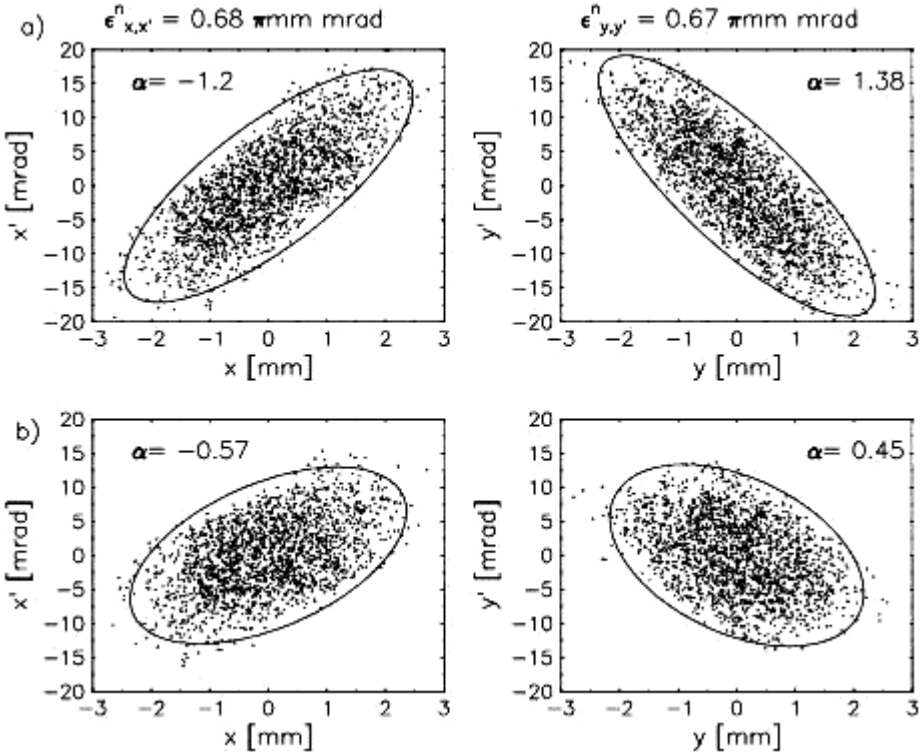

Fig. 47: RFQ output emittances without (above) and with (below) matching-out section

The measurements of the energy spread of the RFQ were in remarkably good agreement with the PARMTEQ design calculations. Figure 48 shows a measured energy spectrum and a calculated spectrum folded with the resolution of the energy spectrometer.

Consequently, the RFQ beam was used to calibrate the bending magnet at the end of the beam line. This magnet can thus be used as an energy spectrometer for the other resonators. As a result of this extrapolation over a wide energy range, the accuracy of the absolute value for energy measurements at the IH structure and seven-gap resonators is no better than 1%. A new calibration of the magnet will be carried out using nuclear (p,γ) reactions at energies in the range 2–3 MeV/u.

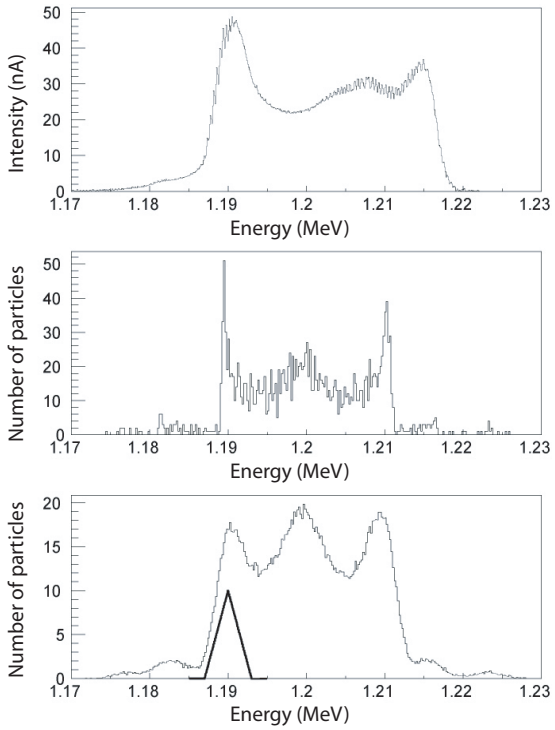

Fig. 48: Energy distribution of the REX RFQ. Top: Measured spectrum at 28.35 kW (A/q = 4). Middle: Spectrum calculated with PARMTEQ. Bottom: PARMTEQ spectrum folded with triangular curve where the FWHM corresponds to the energy resolution of the spectrometer

3.3 The rebuncher section

A small phase spread of the beam, as well as a beam convergent in both transverse planes, is required at the entrance of the REX IH-DTL on account of its special particle dynamics design. A matching section is used at REX for this purpose. It consists of a split-ring rebuncher, two magnetic quadrupole triplet lenses, and a diagnostic box. The length of the section is ~1.7 m. Figure 49 shows a picture of the rebuncher with open tank. The characteristic values of the buncher can be found in Table 11.

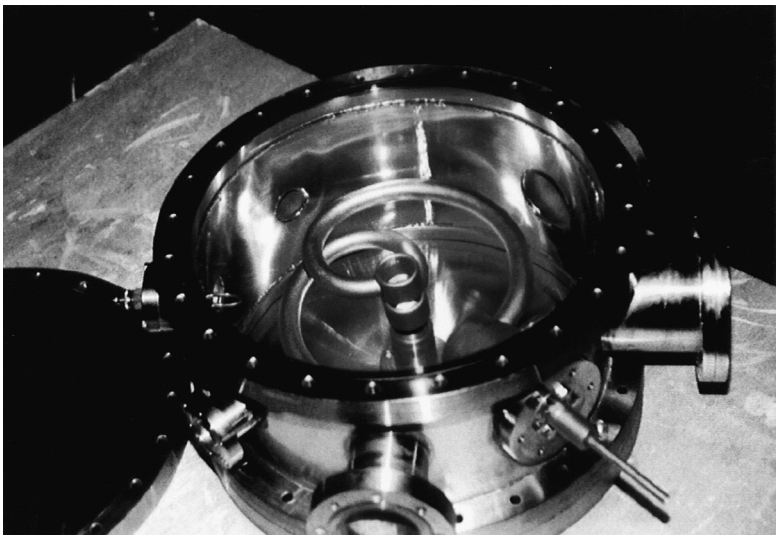

Fig. 49: The rebuncher

Table 11: Parameters of the rebuncher

Frequency	101.28 MHz
RF coupling	–27 dB
Quality factor Q_0	4000
Transit time factor (β = 2.5%)	0.672
Effective shunt impedance	20.0 MΩ/m
$U_{eff, int}$ for A/q = 4	79 kV
RF power consumption (A/q = 4)	1.56 kW
Tank length	200 mm
Tank diameter	350 mm
Aperture	30 mm
Gap length	8 mm
Drift tube length	28 mm
Spiral length	475 mm

3.3.1 Particle dynamics

The beam dynamics concept of the IH structure requires a convergent beam in the transverse and longitudinal directions. The first triplet lens produces a waist in front of the rebuncher. The second triplet matches the beam to the IH structure acceptance. Figure 50 shows the beam envelope in the section together with the drift towards the emittance scanner during the test measurements. In addition, the emittances expected at the position of the emittance meter are shown in comparison to the measurement results. The settings of the lenses have been derived from simulations with TRANSPORT [34] for a matched beam at the entrance of the IH structure. The measurement results in Fig. 50 show that the matching of the transverse phase spaces can be easily achieved using the two lenses. For the emittance measurements the buncher was driven with 1.56 kW RF power at a phase of –90°.

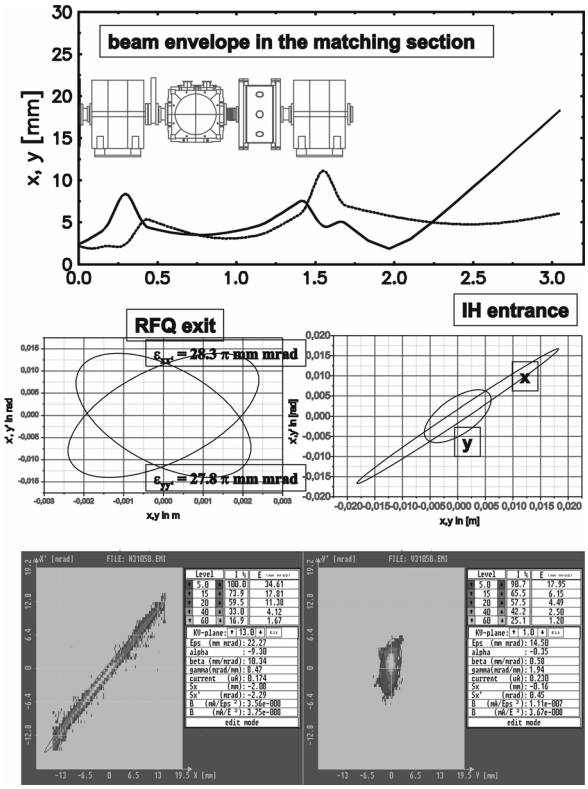

Fig. 50: Calculated beam envelope in the matching section and towards the emittance meter and resulting emittances in comparison with measurements

The measurement of the longitudinal beam parameters as a function of the buncher phase was effected by analysing the energy distribution. TRANSPORT calculations resulted in a required effective buncher voltage of 79 kV (integrated voltage), for an A/q = 4 beam, in order to reduce the phase spread at the IH entrance from ±35° to the required ±10°. With a shunt impedance of 20.0 MΩ/m, this corresponds to an RF power in the buncher of 1.56 kW. The calculations give an energy spread (resulting from the time focusing of the buncher) of ±2.8%. Figure 51 shows the energy spectra of beams from the buncher at the four relevant buncher phases. The measured energy spread at the bunching phase (270°) is ±3.2% slightly larger than the calculated value and shows that an RF power of ~1.5 kW would be sufficient for the IH injection. The test measurements shown were verified during the optimization of the injection into the IH structure.

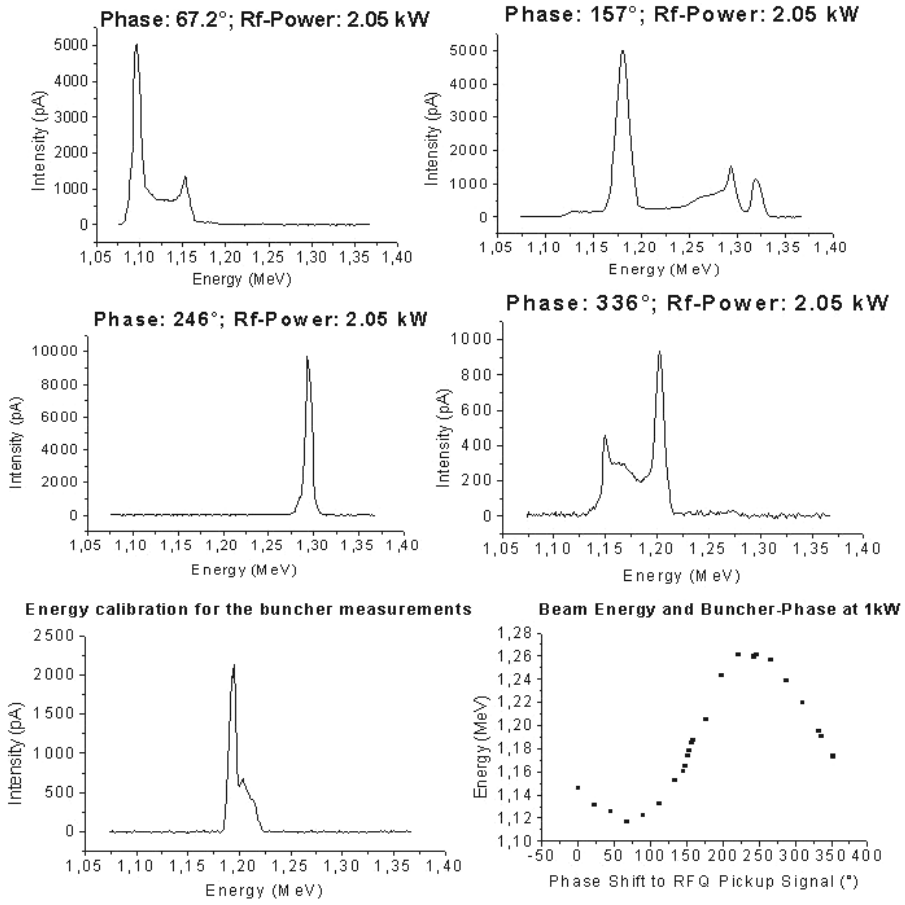

Fig. 51: Energy spectra of the rebuncher (A/q = 4) at different phases together with the RFQ peak as a reference and the beam energy depending on the buncher phase at 1 kW

3.4 The REX IH DTL

The design of the REX-ISOLDE IH accelerator is based on experiences drawn from the development of the IH structures for the GSI Hochladungsinjektor (HLI) [35] and CERN LINAC3 [36]. The REX IH structure is similar to these accelerators in many ways. As mentioned above, the frequency of the 1.5 m long structure is 101.28 MHz and the maximum duty cycle is 10%. The resonator accelerates heavy ions with a maximum A/q of 4.5 from 300 keV/u to a final energy which can be continuously variable between 1.1 and 1.2 MeV/u. The basic parameters of the accelerator are given in Table 12. Figure 52 shows a photo of the drift-tube arrangement and the magnetic inner tank triplet.

Table 12: Parameters of the REX-ISOLDE IH accelerator

Frequency	101.28 MHz
Duty cycle	10%
Tank length (outside)	1.50 m
Rad. acceptance ε_{norm}	0.6 π·mm·mrad
Number of gaps	20
Inner diameter of drift-tubes	18 to 20 mm
Maximum A/q	4.5
Input energy	300 keV/u
Final energy	1.1 MeV/u–1.2 MeV/u
Effective voltage at 1.1 MeV/u	3.75 MV
Effective voltage at 1.2 MeV/u	4.16 MV
Quality factor Q_0	13 000
Shunt impedance	330 MΩ/m

3.4.1 Mechanical properties

For increased thermal conductivity, the tank of the IH structure is made of black steel and not stainless steel. For the same reason the drift tubes and the holders are made of massive copper. The eighth drift tube, counted from the low-energy end, is a water-cooled, copper-plated magnetic quadrupole triplet lens that provides the radial focusing inside the tank. The coupling is, like for all other REX resonators, inductive via a water-cooled coupling loop. The tuning of the cavity is done via two capacitive plungers, which are also used to modify the gap voltage for energy variation between 1.1 and 1.2 MeV/u (see below).

Figure 52 shows the IH structure with the upper half-shell dismounted. The black steel has been copper-plated in the areas where RF currents occur during operation. The sealing between the three parts has been done with a 1.8 mm silver wire, which provides good vacuum sealing and good electrical conductivity. It is for this reason located quite close to the inner wall of the tank.

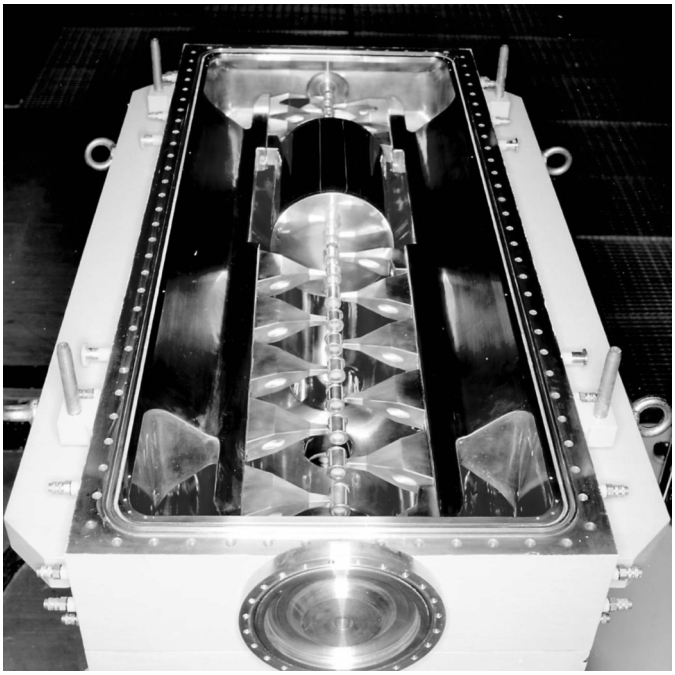

Fig. 52: View from the high-energy end inside the IH resonator. The upper half-shell is removed, the large drift tube houses the magnetic triplet lens

The cooling water channels are drilled inside the black steel central frame, while the half-shells have double walls and are completely filled with water. Figure 53 shows the triplet housing and the support structure.

Fig. 53: The RF incoupling loop (left) and the pick-up loops (right). The fastener of the incoupling is rotatable for optimization of the coupling. The loop itself consists of two parallel soldered copper tubes with 4 mm inner diameter for water cooling

The incoupling loop for RF power is also mounted on the lower half-shell and rests on a flange in the middle of the tank. From the mechanical point of view, with the exception of the cross-sectional area, it is nearly identical to the one used in the REX-RFQ.

The distributor for the vacuum system is fixed to a large flange on the lower half-shell. Three small flanges are used for the RF pick-ups. The pick-ups are small coupling loops for measurement of the field inside the tank. They have a rotatable slit copper-cap for adjustable attenuation.

The central frame is, in mechanical terms, an extremely rigid body that protects the IH structure from deformation under vacuum conditions. Two girders, which carry the 18 drift-tubes, are fixed on the inner side of the structure. The highest currents occur on these girders. For this reason special attention has been paid to ensure that they are efficiently cooled.

The upper half-shell has two small flanges for vacuum gauges, mass spectrometers, etc. Two other flanges are used for the piston tuners (capacitive plungers) and their stepping-motor-driven, vacuum-sealed, actuator. The piston tuner is shown in Figs. 54 and 55.

The plunger positions are calculated from the encoder values using Eqs. (1) and (2). HE stands for the high-energy piston tuner and LE for the low-energy piston tuner. The right panel of Fig. 56 also indicates from where the distance d is measured. Limit switches fix the maximum range for the tuners at 338 mm. The closest possible distance to the beam axis is 47.4 mm (HE tuner) and 48.2 mm (LE tuner), respectively. Resonant excitation of the piston tuners must be avoided since the water cooling is insufficient if the full RF power is dissipated on them. The encoder positions which are strictly forbidden during high power operation are: 1420 ± 20 (LE tuner) and 2400 ± 20 (HE tuner).

The IH can be operated at power levels up to 100 kW, which, at 10% duty cycle, means that 10 kW have to be dissipated via the cooling water. As mentioned above the cavity is made of black steel because it has higher thermal conductivity than stainless steel and better mechanical stability than copper. The disadvantage of black steel is its susceptibility to corrosion. For this reason the cooling of the IH is accomplished with two separate circuits. The primary circuit, which cools the cavity, is closed. This prevents further inflow of oxygen and allows for the addition of chemical compounds. The cooling liquid is anti-corrosive. A biocide has been added to prevent the growth of bacteria and the generation of gas and algae. The cooling liquid has to be checked every year. The closed circuit is connected to the

ISOLDE circuit via a stainless-steel heat exchanger. Drawings of the cooling water circuit are shown in Appendix E.

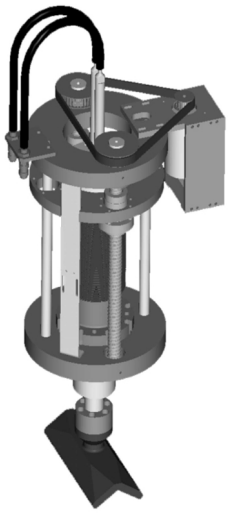

Fig. 54: Model of the piston tuner and its actuator. The position of the piston tuner is detected with a digital encoder

Fig. 55: High-energy (HE) piston tuner inside the tank

$$d_{HE} = \left(79,2 + \frac{Z_{HE} - 500}{11,2}\right)[mm] \quad (1)$$

$$d_{LE} = \left(79,3 + \frac{Z_{NE} - 500}{11,2}\right)[mm] \quad (2)$$

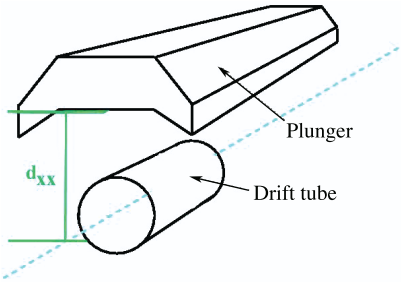

Fig. 56: Calibration of the encoder values (left) and measurement of the tuners' distance from the beam axis (right)

3.4.2 RF properties

Figure 57 shows a comparison between the gap-voltage distributions calculated with the MAFIA code [37] and those measured with the perturbation method. The calculated distribution has been used for the LORASR particle dynamics calculations. After adjustment of the frequency (see below) the remaining deviations were found to be negligible for the particle dynamics.

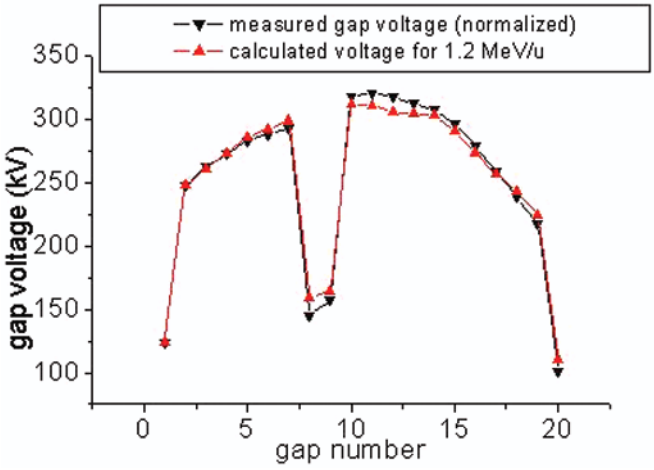

Fig. 57: Comparison of measured and calculated gap voltage in the IH structure

During the low-level measurements the resonance frequency of the IH structure was approximately 1 MHz too low when the tuners were adjusted for the desired voltage distribution. To solve this problem and to produce the right gap voltage distribution at the right frequency, the height of the undercuts had to be modified mechanically. Figure 58 shows the copper plates that were added to each end of the tank. The plates can only be cooled passively via the girders and the tank, although they are at the tank's highest current-density position. However, no evidence of overheating or thermal damage was observed after high-power tests.

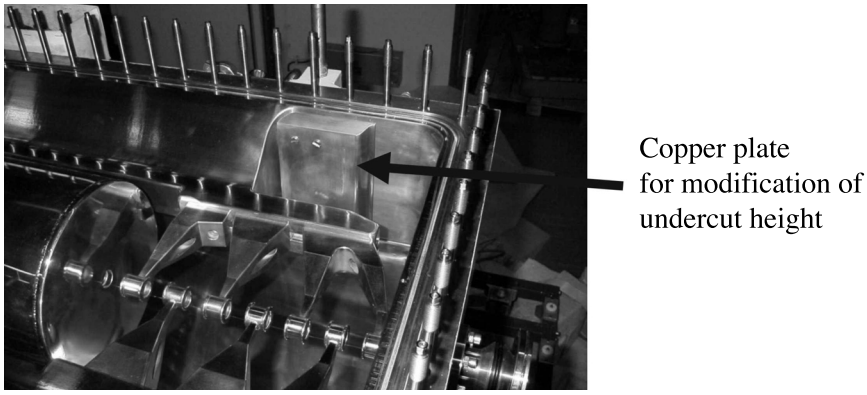

Fig. 58: Modification of the undercut height to increase the frequency

An important issue for the operation of the IH structure in the ISOLDE hall was the bremsstrahlung produced by secondary electrons in the acceleration gaps. Without a lead shielding, the dose rate at the entrance, the exit, and the coupling loop was in the range of several mSv/h at 60 kW and 10% duty cycle. CERN regulations required these values be reduced to <10 μSv/h at a distance of 1 m from the tank. So the IH structure was encased in a lead housing. The housing consists of a steel frame that carries stainless-steel plates to which 6 mm lead plates are mounted. Flexible lead mats were fixed around the tank's large flanges. Figure 59 shows the accelerator inside the lead shielding. After installation of the shielding and the mats, the dose rate fell to <30 μSv/h at the tank and was negligible

at a distance of 1 m. Nonetheless, an additional shielding was installed in parallel to the beam line to protect the sensitive MINIBALL detector.

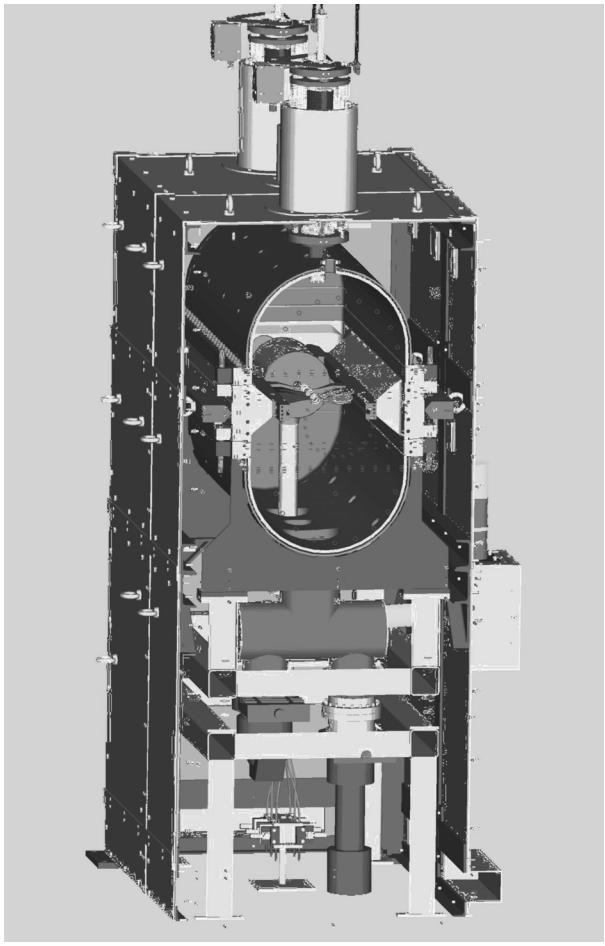

Fig. 59: Cross section showing the IH tank inside the lead shielding

3.4.3 Particle dynamics

The particle dynamics design of the IH structure is based on LORASR [26] and MAFIA code calculations and low-level measurements that provided the required gap-voltage distributions. The Kombinierte Null Grad Sollteilchen Struktur (KONUS) particle dynamics [38] allows for very efficient use of the gap-fields by switching between 0° sections and rebunching sections. The REX IH structure consists of three such sections, which are displayed with the mechanical dimensions of the structure in Fig. 60. The beam is injected with a slight delay relative to the synchronous particle in order to reduce the longitudinal defocusing in the 0° sections.

Figure 61 shows the phase differences between the synchronous particle and the test particle along the z-axis of the IH structure. It shows how the beam is injected with a positive phase into sections I and III (0° sections), while in the rebunching (section II) the particles are injected exactly at the synchronous phase.

A new feature of the REX-ISOLDE IH structure, compared to its progenitors in the GSI and CERN linacs, is the option of continuously switching the final energy between 1.1 MeV/u and 1.2 MeV/u. This variation can be achieved by adjusting the position of the piston tuners and by adapting the RF power.

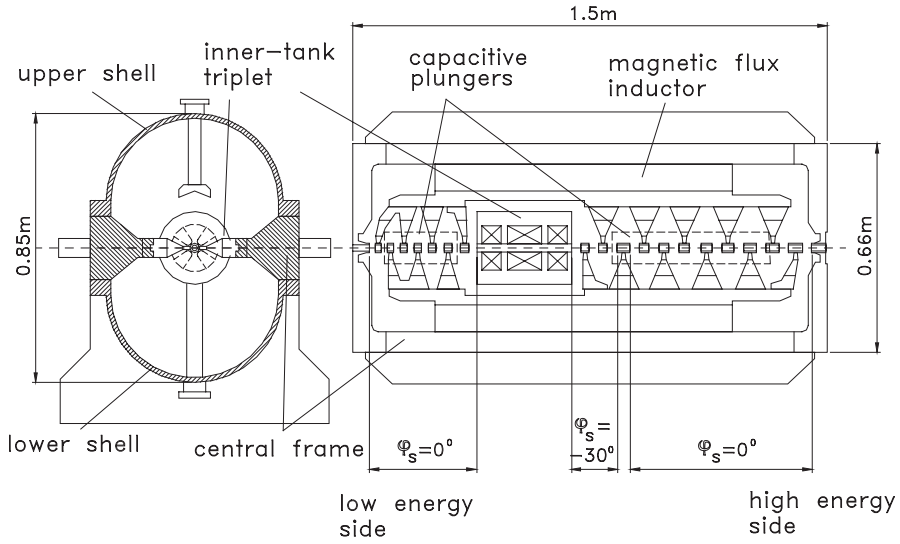

Fig. 60: KONUS sections of the REX IH and schematic mechanical layout

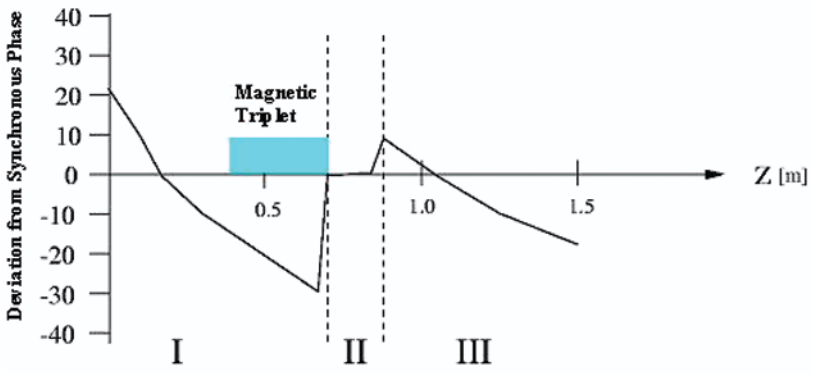

Fig. 61: Injection phase in the IH sections along the z-axis

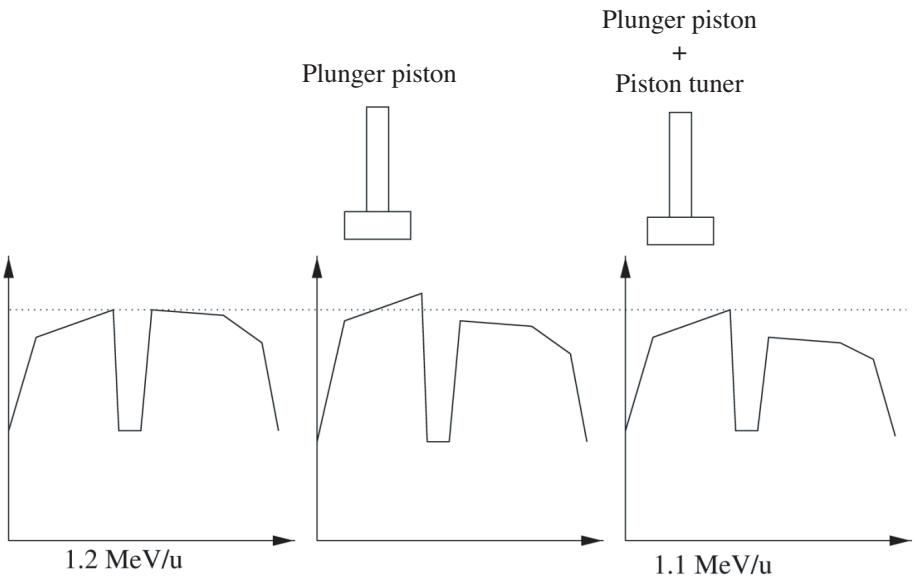

Fig. 62: Principle of energy variation in the REX IH

Figure 62 shows how this works: starting from the design distribution at 1.2 MeV/u in the left panel, the capacitive effect of the piston tuner increases the gap voltage in the low-energy section as shown in the central panel. At the same time the RF power is lowered until the overall voltage in this section is the same as it was previously. The beam experiences lower acceleration in the high-energy section and reaches 1.1 MeV/u (for a detailed description see Ref. [22]). When this report is published this principle will still not have been tested because, as mentioned above, copper-plated drift tubes produce a start frequency that is too low. A new set of drift tubes has been produced to make the energy variation possible. Figures 63 and 64 show the results of the corresponding LORASR calculations in order to give an impression of the beam quality in the two different modes. To date, only the 1.2 MeV/u calculations have been verified by measurement.

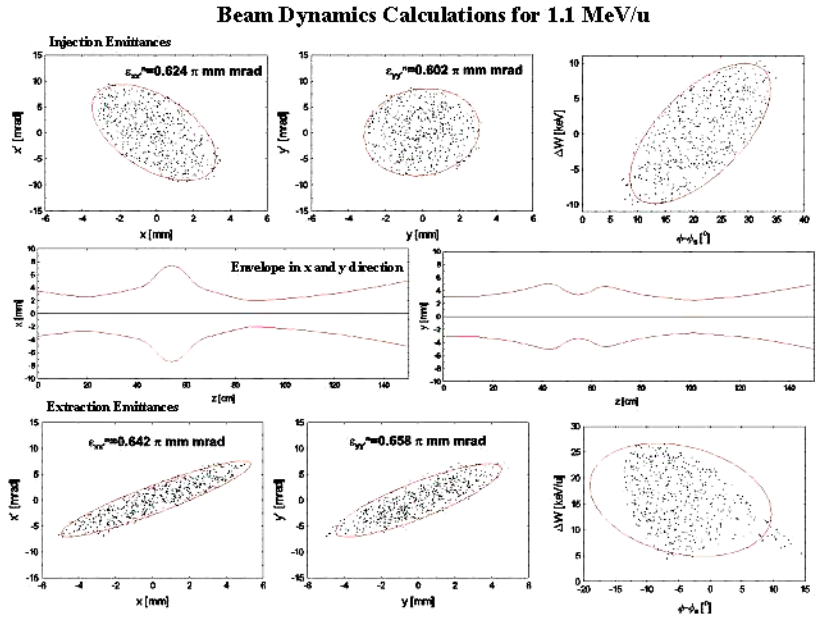

Fig. 63: Design calculation for a final energy of 1.1 MeV/u

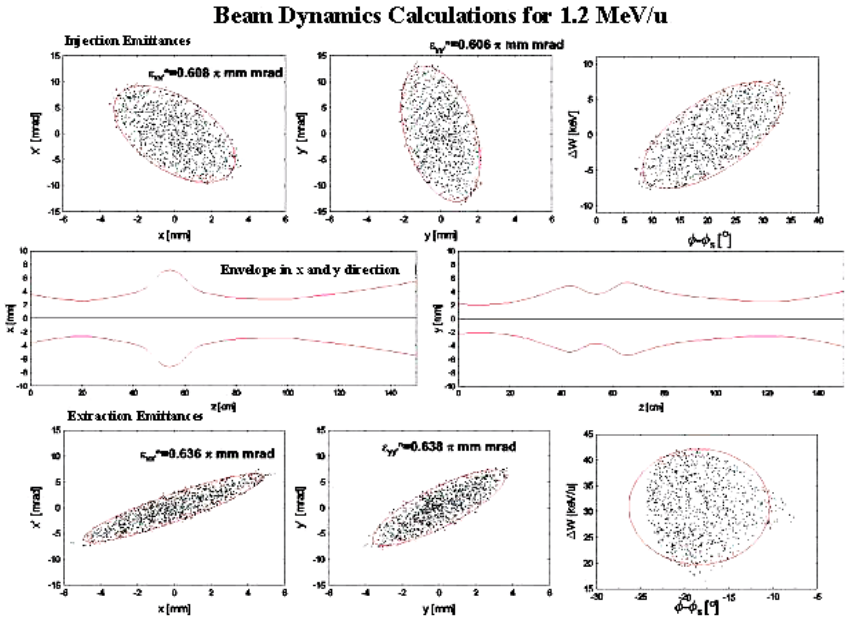

Fig. 64: Design calculation for 1.2 MeV/u

Energy and emittance measurements have been performed at REX to verify the calculations shown above. Figure 65 shows an energy spectrum taken at an RF power of 43 kW for an A/q = 4 beam. The resolution of the spectrometer was 0.6% and the error in energy ~1%. With an absolute energy of 1.21 MeV/u and an energy spread of 1.5%, the measurement fits nicely with the calculated values.

The emittance behind the IH structure is shown in Fig. 66. The injected normalized emittance was 0.26 mm·mrad and 0.2 mm·mrad and the normalized emittance from the IH structure was 0.29 and 0.21 mm·mrad in the x and y directions, respectively. Thus, an emittance growth of about 10% occurs in the IH cavity. Very low beam intensity of about 1 nA, which is the limit of the emittance meter is a challenge for emittance measurements at REX. In addition the angular resolution of 0.5 mrad results in an error of approximately 20% which is in the same range as the emittance growth.

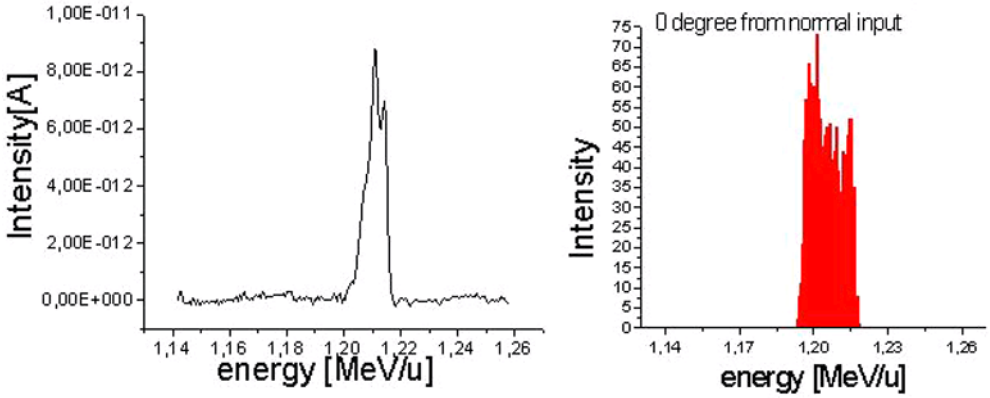

Fig. 65: Measured and calculated energy spectrum of an A/q = 4 beam from the IH structure

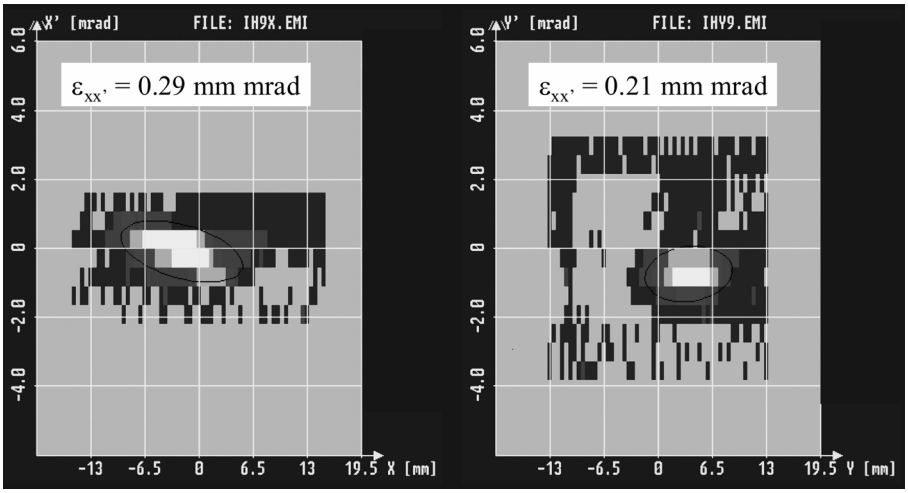

Fig. 66: Normalized emittances from the IH structure. A 1 nA He^+ beam has been used for the measurements

3.5 The seven-gap resonators

The high-energy section of the REX-ISOLDE linac consists of three seven-gap resonators similar to those developed for the High-Current Injector at the Max Planck Institute for Nuclear Physics in Heidelberg [39]. The seven-gap section was introduced to provide a variable energy for the experiments. As a small number of gaps is required for energy variation, seven gaps were chosen as a compromise between high variability (a 'broad' transit time factor) and high accelerating voltage per tank.

Figure 67 shows the transit time factor for different numbers of gaps as a function of the particle velocity. The design velocity in the example shown is β = 6.0%. The gap length of 20 mm is yet another compromise in order to get the highest possible transit time factor and still guarantee a safe operation and avoid sparking and breakdown of the RF voltage.

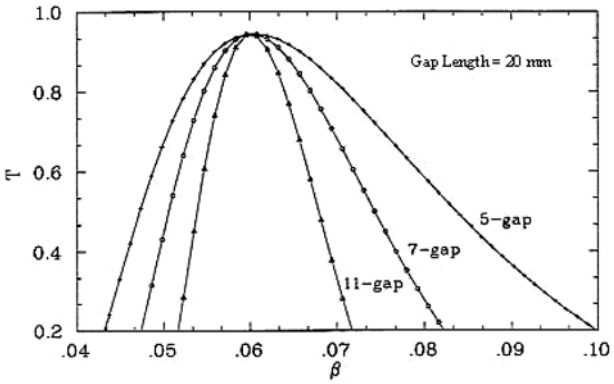

Fig. 67: Transit time factor as a function of the ion velocity for a 5-, 7-, and 11-gap resonator, with a design velocity of β = 6.0% and the gap length used in the REX seven-gap resonators

The seven-gap resonators are designed to accelerate the ion beam from 1.2 MeV/u to final energies of 1.55, 1.88 and 2.2 MeV/u at a synchronous phase of –20°. They have been called 5.4%, 6.0%, and 6.6% resonators referring to the particle velocity in the middle gap. The synchronous phase is defined by the particles' phase in this gap. The energy can be varied continuously from the injection value by increasing the voltage and switching on the next resonator. The scenario of continuously decelerating a 1.1 MeV/u beam from the IH structure down to 0.8 MeV/u would employ the first seven-gap resonator only. This has not yet been tested.

Figure 68 gives a view into an open seven-gap resonator. The resonator is similar to the split-ring type. Six drift tubes are connected to spirals arms (λ/4 lines) that end in a half-shell. The total resonator voltage is about 1.7–1.8 MV at a typical power of 90 kW.

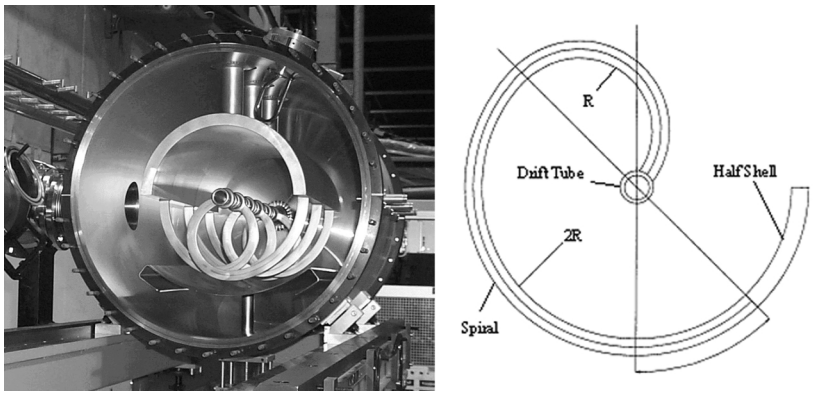

Fig. 68: View into a seven-gap resonator and the geometry of the spirals

3.5.1 Mechanical properties

The tanks of the seven-gap resonators are made of massive copper. The major components of the resonator are water cooled. There is separate cooling for the tank walls, the half-shells, the spirals (in series) up to the drift tubes, the coupling loops and for the piston tuners.

The resonance frequency and the field distribution are tuned via the length of the spirals, which can be inserted into the half-shell to a variable depth. The spirals have a special geometry, which keeps the drift tube on axis while the spiral length is varied (Fig. 68).

Figure 69 presents a schematic drawing of the seven-gap resonator. Table 13 presents the geometrical parameters.

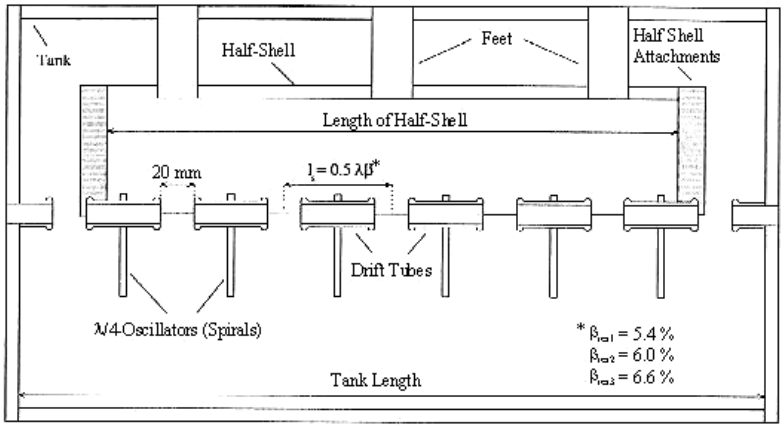

Fig. 69: Schematic of a seven-gap resonator

Table 13: Geometrical parameters of the seven-gap resonators

Parameter	**5.4%**	**6.0%**	**6.6%**
Tank			
Inner diameter [mm]	500	500	500
Outer diameter [mm]	530	530	530
Tank length [mm]	558.32	611.60	664.88
Half-shell			
Inner diameter [mm]	254	254	254
Outer diameter [mm]	298	298	298
Half-shell length [mm]	429.6	474.0	518.4
Gap [mm]	20	20	20
Gap distances [mm]	79.92	88.80	97.68
Drift tube			
Inner diameter [mm]	20	20	20
Radius [mm]	3	3	3
Length [mm]	59.92	68.80	77.68
Tuning plate length [mm]	435	435	435

3.5.2 RF properties

After tuning the eigenfrequency to the operation frequency of the amplifiers (101.28 MHz) the qualtity factors were determined at 5560 (5.4%), 5280 (6.0%) and 5030 (6.6%), respectively. During the low-level measurements, the shunt impedances were derived to 71 MΩ/m, 68 MΩ/m and 67 MΩ/m. The field distributions could be adjusted via the spiral length to a homogeneous flat distribution as shown in Fig. 70.

A high-power-level measurement of the resonators' shunt impedance was carried out at the Tandem accelerator beam line of the Max Planck Institute in Heidelberg. The d.c. beam from the Tandem experiences a momentum modulation inside the resonator. The modulation is then measured with an energy spectrometer. The resonator voltages and the shunt impedances were calculated from the energy gain measured with a 90° magnet at different power levels. Figure 71 shows the results of the measurements.

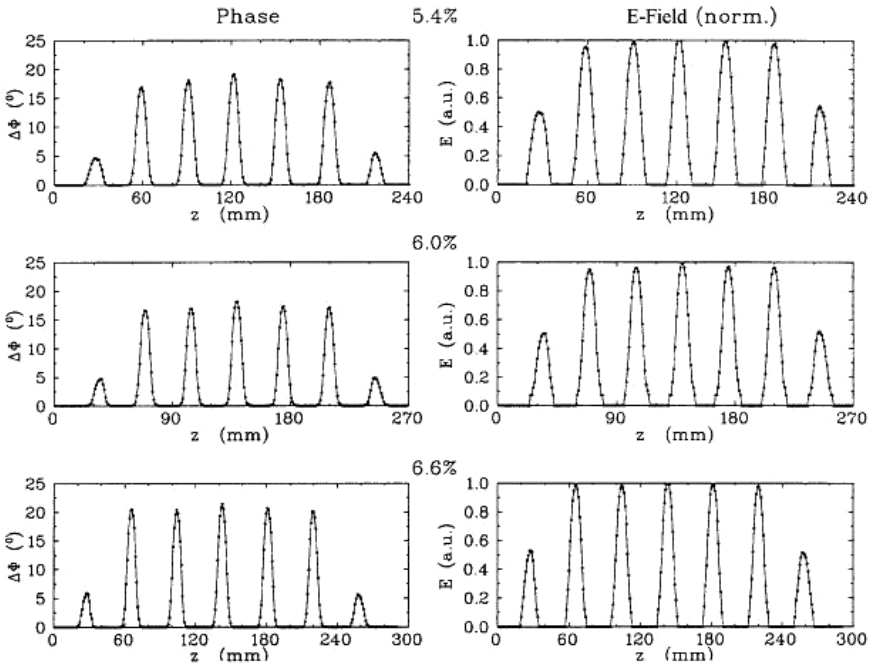

Fig. 70: Optimized field distribution of the three seven-gap resonators in π mode. Left: phase displacement along the z-axis from bead pull measurements. Right: Electrical field strength normalized to one along the z-axis

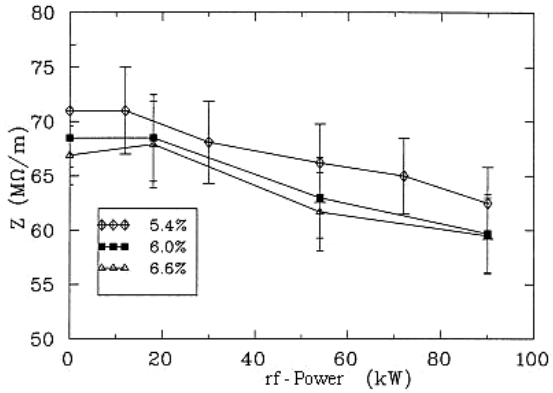

Fig. 71: Measured shunt impedance of the three resonators as a function of the RF power. The values at 0 kW correspond to the low-level measurements

Table 14 summarizes the measured parameters of the three resonators. The resonator voltages (see Table 15), determined in beam tests, are between 1.77 and 1.88 MV. This is slightly lower than the values expected from the low-level measurements. The difference is explained by the temperature dependence of the surface resistance. In spite of this, all three resonators exceed their design voltage of 1.74 MV (absolute voltage).

At 90 kW RF power and a pulse length of 1 ms the radiation level on the outer surface of the copper tank was in the range 10–100 μSv/h. During the setting-up at ISOLDE, all resonators were shielded with lead to reduce the X-ray radiation below 10 μSv/h at a distance of 1 m.

When switching between different isotopes the scaling of the Linac settings with A/q turned out to be very efficient: by maintaining the settings of the phases and by scaling the amplitudes and the settings of the lenses, the same transmission was reached for the new A/q. Since there were problems which we do not yet fully understand when reproducing the calibration of the amplitudes of the three

seven-gap resonators, the amplitudes were adjusted with the input power. To set the required synchronous phase we determined the 0° phase from the maximum acceleration at a given amplitude. Relative to the 0° the required absolute phase could be set.

Table 14: Voltage and shunt impedance determined by measurement

Resonator	Parameter	Low-level test	Beam test
5.4%	Voltage [MV]	1.88 ± 0.08	1.77 ± 0.05
	Z [MΩ/m]	71 ± 6	62.5 ± 4.0
6.0%	Voltage [MV]	1.94 ± 0.04	1.81 ± 0.05
	Z [MΩ/m]	68.5 ± 2.7	59.7 ± 3.6
6.6%	Voltage [MV]	2.00 ± 0.04	1.88 ± 0.05
	Z [MΩ/m]	66.9 ± 2.7	59.5 ± 3.5

Table 15: Resonator voltage versus incoupled power. The design voltage for A/q = 4 is 1.74 MV

	P [kW]	U_0
7-gap 1	90	1.77
	72	1.61
	54	1.4
	30	1.075
	12	0.687
7-gap 2	90	1.81
	54	1.44
	18	0.87
7-gap 3	90	1.88
	54	1.49
	18	0.90

3.5.3 Particle dynamics

Figure 72 presents the transverse beam optics from the IH structure to the seven-gap section. A triplet focuses the beam into the acceptance (as shown in Fig. 73) of the high-energy part of the linac. The gradients of the lenses are given below in Section 3.8. The asymmetry in the acceptance of the seven-gap section results from the beam transport between the first and second seven-gap resonator where a magnetic doublet lens is installed (see Fig. 39).

Figure 74 shows the transverse and longitudinal shape of a beam with A/q = 4.5. The exit energy, calculated for $^{36}Mg^{8+}$, is 2.19 MeV/u. The design energy is 2.2 MeV/u. It is possible to reach 2.3 MeV/u using a –20° phase in the fourth gap of each resonator but the beam's phase spread and the size in both transverse planes increase.

To achieve an energy of 2.3 MeV/u all synchronous phases of the seven-gap resonators have to be set to 0°. With this setting, the beam envelope is worse than for the design case of 2.2 MeV/u. The emittance grows by a factor of 4 in the x-direction as compared with the emittance of the designed synchronous phase of –20°. Moreover, the longitudinal beam shape changes to a much longer bunch length. Nevertheless, a sufficiently small beam spot of less than 10 mm diameter was produced on the target.

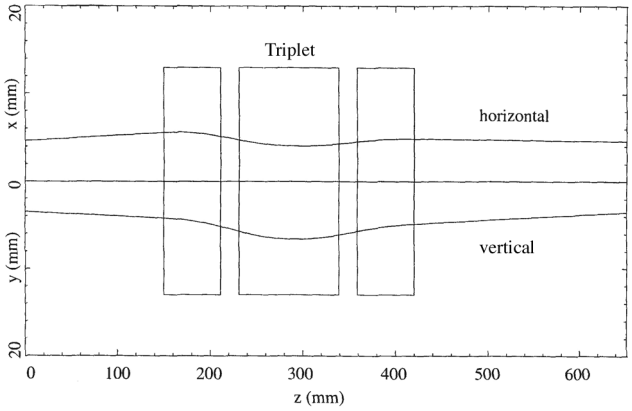

Fig. 72: Beam envelope from the IH to the seven-gap resonators focused via lens MQT3

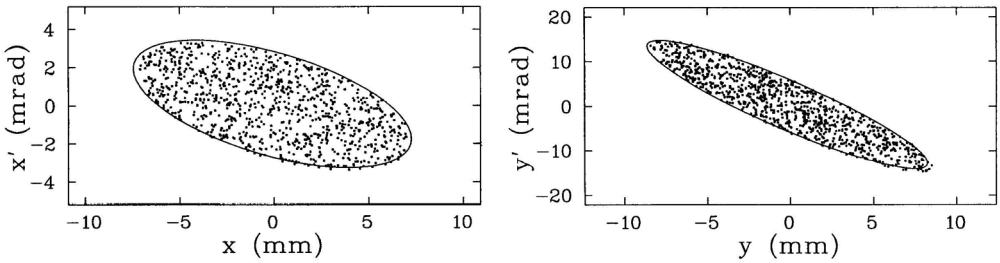

Fig. 73: Transversal acceptance of the seven-gap section. The beam has to be injected convergent in both planes

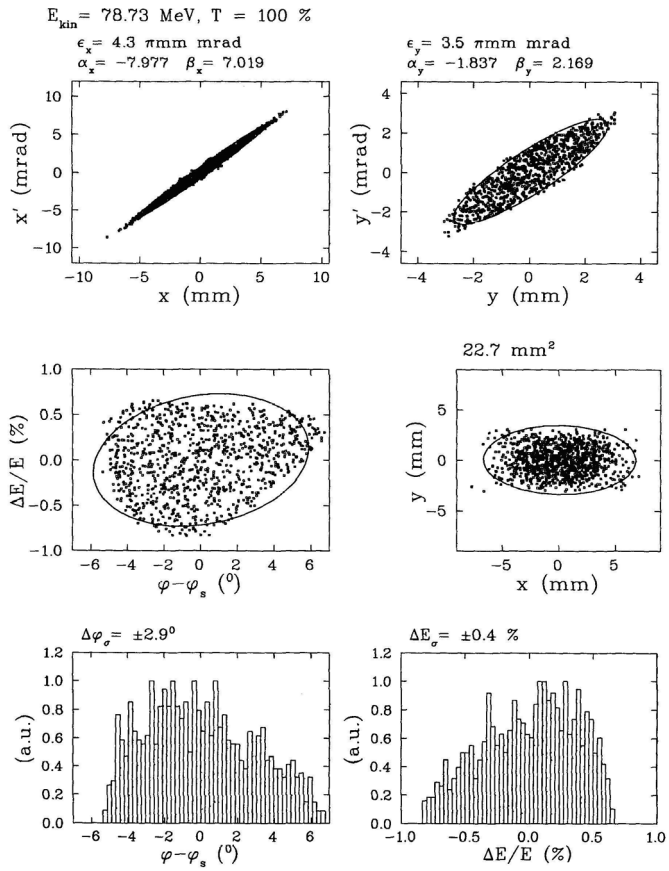

Fig. 74: Longitudinal and transverse emittances directly behind the third seven-gap resonator

The energy spread of the beam from the three seven-gap cavities is summarized in Table 16 for the 2.2 MeV/u setting of the accelerator. An example of the energy measurement is shown in Fig. 75 for the first seven-gap resonator at 1.55 MeV/u beam energy.

Table 16: Measured and calculated energy spread of the seven-gap resonators. The phases are adjusted for a 2.2 MeV/u final energy

	Phase	**E spread calculated [%]**	**E spread measured [%]**
7-gap 1	–20°	±1.1	±0.75
7-gap 2	–20°	±0.8	±0.7
7-gap 3	–20°	±0.7	±0.65

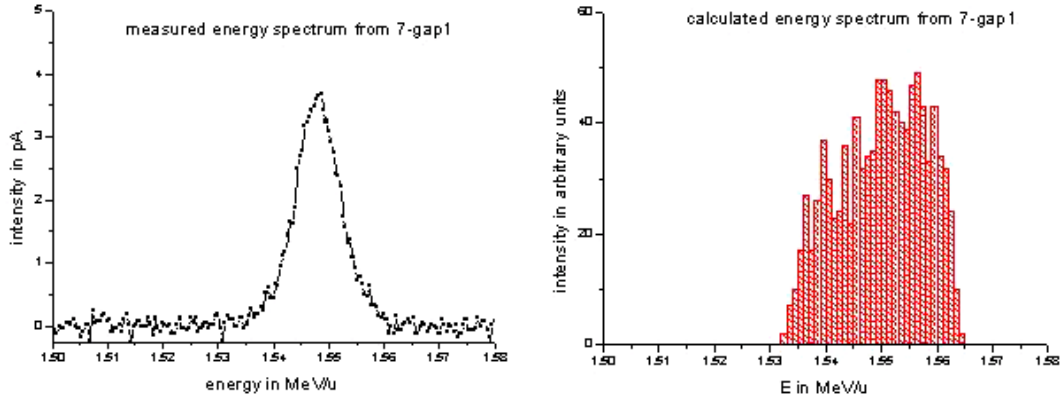

Fig. 75: Comparison of the measured and calculated energy spectra of the first seven-gap resonator

3.6 REX-ISOLDE energy upgrade

Higher beam energies than those described above are required at REX in order to use the full range of isotopes from ISOLDE for nuclear physics experiments using Coulomb excitation and transfer reactions.

An energy increase to approximately 3 MeV/u allows studies of nuclear reactions up to mass A = 85 on deuterium targets. A beam energy of 4.2 MeV/u would be suitable up to mass A = 145. An energy upgrade of the REX-ISOLDE linac has therefore been started. We expect to be able to raise the beam energy to approximately 4.2 MeV/u in two steps while maintaining the beam quality [30].

The structure of the REX-ISOLDE linac for the two energy upgrade scenarios is shown in Fig. 76. In order to reach 3.0 MeV/u the simplest solution is to include a nine-gap IH cavity operating at 202.56 MHz resonance frequency. As a result of the delay of the final permission to run FRM II [40], the prototype for the Munich Accelerator for Fission Fragments (MAFF) [41], the IH seven-gap resonator was modified to an IH nine-gap cavity [42]. During the preparation of this report, this resonator was installed in the REX beam line. It was successfully conditioned to a power level of 90 kW and accelerated the first beams with A/q = 3.5 to 3.0 MeV/u.

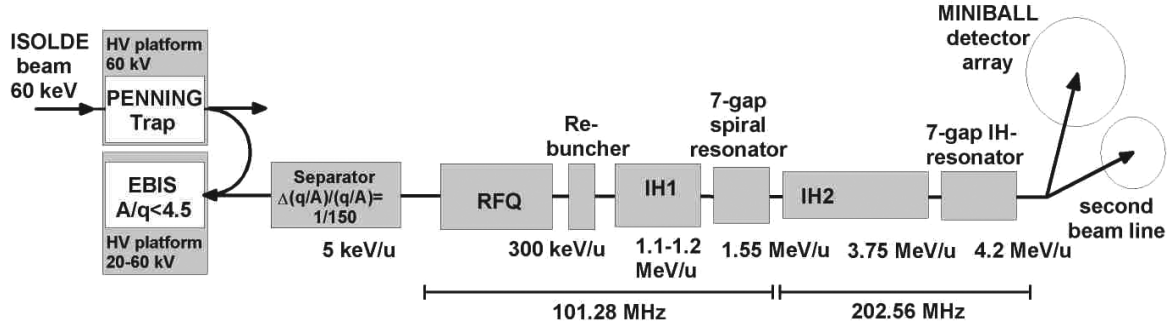

Fig. 76: Upgrade of the REX-ISOLDE linac to 3 MeV/u

A major change of the linac structure will be necessary to reach energies of approximately 4.2 MeV/u. Thus two of the seven-gap spiral resonators with 101.28 MHz resonance frequency have to be replaced by a 1.5 m IH cavity with 202.56 MHz resonance frequency to boost the energy to the required region of 3.75 MeV/u. A seven-gap IH resonator of the MAFF type cavity can then be used to accelerate to final energies above 4 MeV/u.

3.6.1 The IH nine-gap resonator

The MAFF-LINAC [43] at the Munich High Flux Reactor FRMII requires a more efficient seven-gap structure, than the split-ring resonators of REX-ISOLDE for energy variation. Hence the seven-gap structure for MAFF has been designed as an IH structure. As a result of the higher shunt impedance of IH structures, a higher resonator voltage, and a very compact design can be achieved with the same RF power as for split-ring resonators. Since the resonator is used for both acceleration and deceleration, the cell length is kept constant. A cell length of 74 mm was chosen since the beam energy at MAFF will be varied between 3.7 MeV/u and 5.9 MeV/u. This corresponds to a design velocity of $\beta = 0.1$ and results in a total length of 518 mm for the seven cells. The inner tank is therefore 520 mm long and the overall outside length is 646 mm.

The first design for the REX 3.0 MeV/u upgrade changed the MAFF resonator from a seven-gap to a nine-gap resonator while keeping a constant cell length corresponding to 2.5 MeV/u synchronous particle energy. Nine gaps were necessary to match the reduced cell length to the lower injection energy of 2.2 MeV/u (instead of the 3.7 MeV/u that was planned at MAFF). Low-level measurements have been carried out to determine Q values and shunt impedance (Table 17) of both the seven- and nine-gap set-ups.

Table 17: Specifications of the seven- and nine-gap IH cavity

	7-gap	**9-gap**
Cell length [mm]	74	55
Gap length [mm]	24	22–26
Drift-tube length [mm]	50	32
Drift-tube diameter [mm]	20/26	16/22
Max. A/q	6.3	4.5
Synchronous particle β	0.1	0.073
Shunt impedance [MΩ/m] (low level measurements)	129	218
Q (measured)	9800	10 100

Before installation at REX, the resonator was tested with the beam from the Munich tandem accelerator. A test bench for high-power and beam measurements was installed on a high-energy beam line of MLL. Momentum spectra of a d.c. beam at different amplifier power and spectra for beam pulses at different phases, using a 70° bending magnet positioned behind the resonator tank were

obtained. The spectra taken with a d.c. beam from the tandem were used to determine the effective shunt impedance.

A O^{5+} beam at 2.2, 2.25 and 2.3 MeV/u was used to test the ability of the nine-gap IH structure to post-accelerate at power levels from 5 to 70 kW. An energy spectrum is shown for 70 kW RF power in Fig. 77. The tandem peak was used for energy calibration. The drift-tube structure was adjusted to a constant cell length of 55 mm at that point.

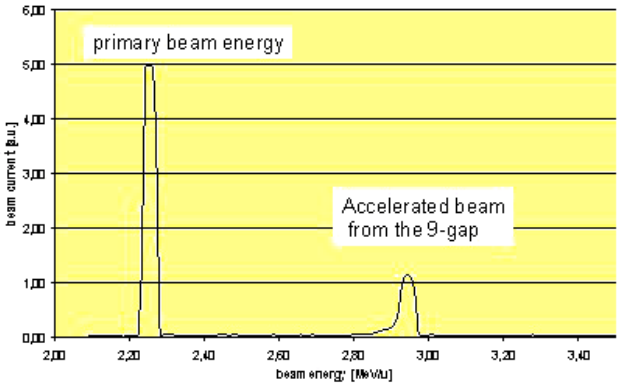

Fig. 77: Accelerated beam from the nine-gap resonator with equidistant gaps

The measured effective shunt impedance (see Fig. 78) shows variations with the RF power level, which corresponds to small values of the TTF (below 0.8). This is a result of the constant cell length, which was designed for 2.5 MeV/u synchronous particle energy. An increase in injection energy led to a higher effective shunt impedance as shown in Section 3.6.2, Fig. 81. However, the curves definitely show saturation at values around 140 MΩ/m, which corresponds to a TTF ≤ 0.8. This meant that the drift-tube structure had to be installed according to the velocity profile, otherwise the energy gain required for REX-ISOLDE would have been impossible to attain.

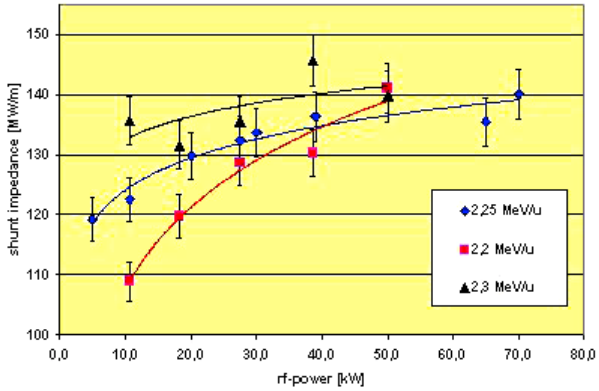

Fig. 78: Effective shunt impedance of the nine-gap resonator for different injection energies

The gap voltage distribution has been calculated for constant cell length and the adjusted velocity profile using MAFIA. Taking the distribution shown in Fig. 79 into account, beam dynamic calculations delivered a TTF of 0.87 and an effective shunt impedance of 165 MΩ/m. This is sufficient to reach 3.0 MeV/u at REX-ISOLDE at 90 kW power for a beam with A/q = 3.5.

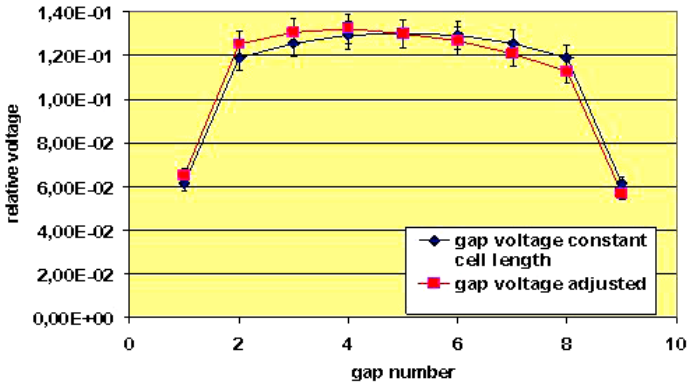

Fig. 79: Adjustment of the gap voltage distribution

Table 18 shows the final geometry of the nine-gap resonator after changing to a $\beta\lambda/2$ structure with a fixed velocity profile. Figure 80 shows the power resonator during the installation in the REX-ISOLDE beam line.

Table 18: Specifications of the final version of the nine-gap IH cavity

	IH 9-gap
Frequency [MHz]	202.56
Outer tank length [mm]	676
Inner tank length [mm]	520
Half-shell radius [mm]	145
Cell length [mm]	38.5–58.5
Gap length [mm]	19–27
Drift-tube length [mm]	32
Drift-tube diameter inner/outer [mm]	16/22
Maximum RF power [kW]	100
Duty cycle [%]	10
Kilpatrick	1.5
Shunt impedance (pert.) [MΩ/m]	218
Q_0	10 100

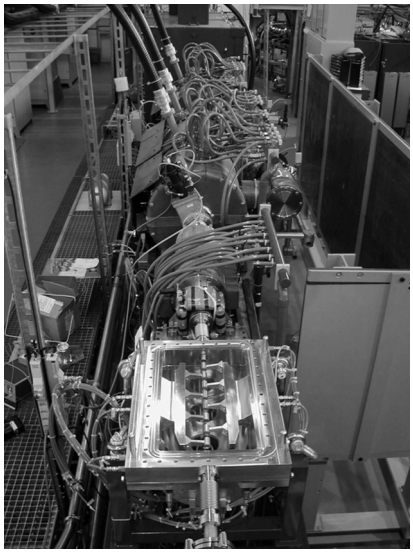

Fig. 80: The (open) 202.56 MHz IH nine-gap resonator installed at REX

3.6.2 Particle dynamics

A magnetic triplet lens, MQT5b, was added to the bender section to compensate for the RF defocusing in the nine-gap accelerator. In the REX naming scheme, the lens is called BEN.MQ40 (x-foc.), BEN.MQ50 (y-foc.), BENMQ60 (x-foc.). It is between the resonator and diagnostic box 4. The gradients, apertures, etc. are identical to the those of the triplet (IHS.MQ90, IHS.MQ100, IHS.MQ110) behind the IH structure. The geometry of the new bender section is schematically shown in Section 3.8.2, Fig. 90.

The input for the LORASR simulations comes from the original linac design calculations for the seven-gap resonators. These calculations were verified in detail during the commissioning phase of REX-ISOLDE. The main goal of the calculations, after having fixed the drift-tube geometry, was to find out to what extent the structure was still energy-variable despite having been designed for a fixed input and output energy. As a result of the short length and the small number of gaps, as well as the relatively high injection energy, one can expect that beam quality and transmission, after the nine-gap resonator, are much less sensitive to changes in the accelerating voltage than is the case for long IH structures at lower energies.

The design injection energy produced by the seven-gap resonators is 2.25 MeV/u at a phase spread of ±15° (after 1.3 m drift) and at an energy spread of ±0.45%. The beam is injected with a transverse emittance of $\varepsilon_{n,x,y}$ = 1.4 π·mm·mrad and is convergent in both planes. Slightly converging beams lead to the best transmission. Figure 81 shows the input and output emittances derived from the calculations. Although the inner diameter of the drift tube is decreased to 16 mm, the acceptance is still two times larger than the emittance of a beam that fills the full RFQ acceptance.

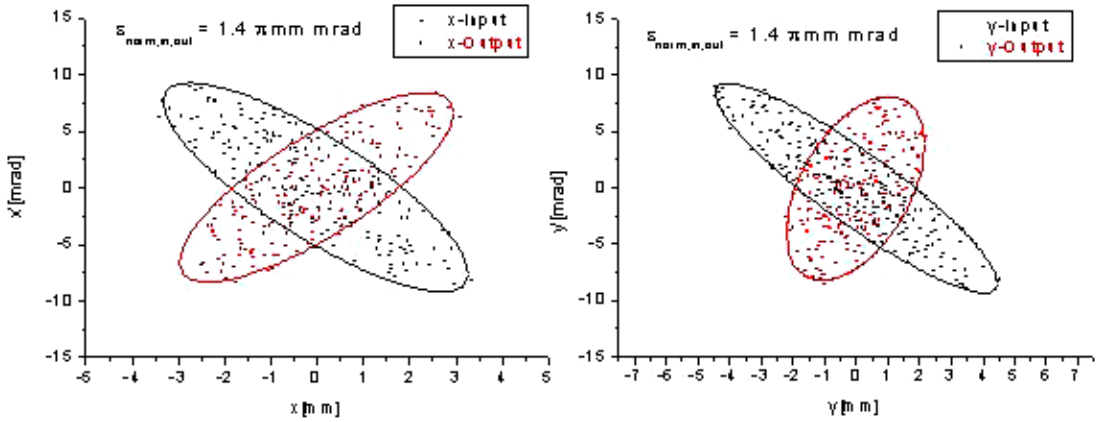

Fig. 81: Transverse emittances of the nine-gap resonator from LORASR

The resonator voltage was changed in steps according to the measurements at different RF power levels in order to test the energy variation.

The spectra in Fig. 82 show that the transmission, as well as the energy spread, stay within a reasonable range down to an output energy of 2.55 MeV/u. With this result, which can be verified in the measurements shown below, the REX accelerator becomes continuously energy variable over a range from 0.8 MeV/u to 3 MeV/u.

The calculated transit-time factors in the fifth gap remain always between 0.855 and 0.865. The accelerator's flexibility in output energy makes a wider range of mass-to-charge ratios available at energies around 3.0 MeV/u. The only limit is the maximum available RF power. With an RF power level limited to 90 kW, the maximum A/q at 3.0 MeV/u is 3.5. During the first runs with radioactive ions compromises were found, such as accelerating $^{76}Zn^{20+}$ ions (A/q = 3.8) at 90 kW to ~2.9 MeV/u. Table 19 shows the calculated parameters of the nine-gap resonator for regular operation at 3.0 MeV/u and for the variable energy.

An effective shunt impedance of 163 MΩ/m was expected for the IH structure from the low-level measurements and LORASR calculations. An energy gain of 0.75 MeV/u requires an effective acceleration voltage of 2.63 MV for ions with A/q = 3.5. This corresponds, at the given shunt impedance and structure length, to an RF power of 85 kW. We therefore performed tests with a N^{4+} residual gas beam from REXEBIS. The injected current was approximately 50 pA initially and fell to ~10 pA because of the slits in front of the energy spectrometer. The slits were used to reduce the emittance influence on the energy spectra. Figure 83 shows the measured spectra [44].

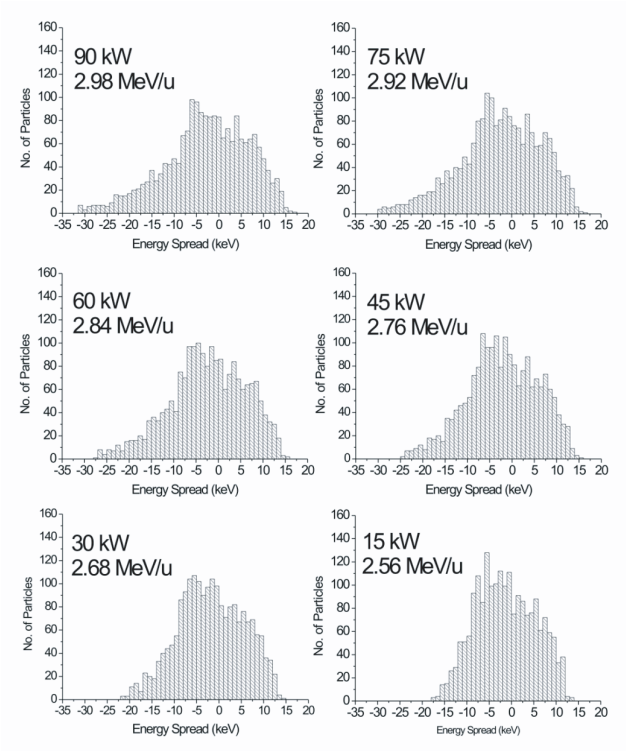

Fig. 82: Energy spectra at different acceleration voltages

Table 19: Design parameters of the nine-gap IH cavity

	IH 9-gap
Input energy [MeV/u]	2.2
Output energy [MeV/u]	2.55–3.0
Energy spread [%]	1.0–1.6
Phase spread [°]	25
Transmission [%]	100
TTF on axis in gap No. 5 (2.55–3.0 MeV/u)	0.855–0.866
Maximum A/q (90 kW)	3.5
Radial acceptance $\alpha_{x,y,norm}$ [π·mm·mrad]	1.4

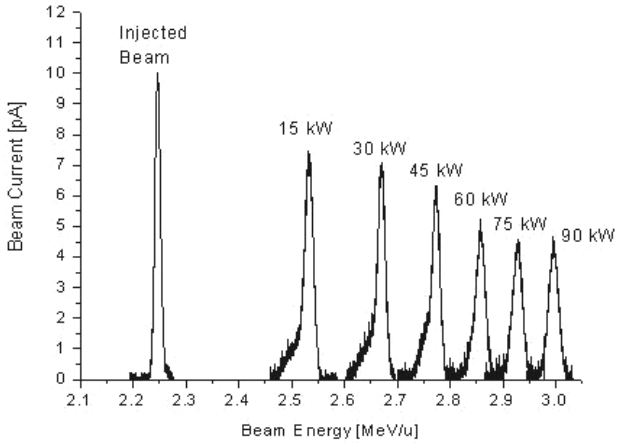

Fig. 83: Energy spectra measured with a A/q = 3.5 beam

The final energies measured were in good agreement with the calculations. The decrease in the beam current at higher energies occurred because the beam transport was optimized for a parallel 2.25 MeV/u beam through the spectrometer rather than a convergent injection into the nine-gap resonator. With optimized injection and beam transport scaled to the different energies, the transmission was close to 100%.

The energy peaks at lower power levels show a tail towards the low-energy side. This might be the result of a slightly erroneous injection phase. However, the FWHM of the peaks corresponds remarkably well to the design calculations.

Calculating the effective shunt impedance for an effective acceleration voltage of 2.63 MV at 90 kW gives a value of η_{eff} = 154 MΩ/m. With an average transit time factor of 0.865 we derive a shunt impedance of η = 205 MΩ/m. If the decrease of the shunt impedance at higher power levels caused by heating of the resonator is taken into account, this value fits nicely to the η = 218 MΩ/m given by perturbation measurements.

3.7 The RF system

Five 101.28 MHz RF amplifiers of the type Bertronix KB/SVS-101/100-P were installed for the RF power supply of the REX-ISOLDE accelerators. A 202.56 MHz amplifier of the type Bertronix KB/SVS-202/100-P was added later for the first stage of the energy upgrade. The amplifiers give a maximum output power of 100 kW at a duty cycle of 10%. The maximum possible operation frequency is 50 Hz and the lowest frequency is 0.5 Hz. Continuous-wave operation is possible up to 9 kW. The amplifiers have a bandwidth of 1.5 MHz.

The 101.28 MHz amplifiers have enough reserve (10%) for regulation, tube ageing, etc. at A/q = 4.5 operation. However, the maximum output power of the 202.56 MHz amplifier limits the final energy of 3.0 MeV/u to beams with an A/q ≤ 3.6. Since the majority of REX experiments require the highest possible energy, the 202.56 MHz amplifier is operated at its upper limit most of the time.

Figure 84 shows how the amplifiers are arranged in the amplifier room. A detailed description of both amplifier types can be found in Refs. [45], [46]. A solid-state amplifier with a maximum output power of 2.5 kW, at 10% duty cycle, is used for the rebuncher cavity. It is similar to the 2.5 kW preamplifier of the Bertronix amplifiers.

A low-level system, very similar to the systems used in CERN Linac2 and Linac3, is used for the closed-loop operation of the amplifiers. It was planned that the REX low-level modules be identical to the CERN modules to facilitate maintenance work and to make it possible to have a common spare-

parts pool. For this reason no new developments were required and largely identical copies of the modules were produced at LMU. The main functions of the control loop are:

1. Exact regulation of phase and amplitude of each resonator using the actual amplitude in the resonator. The amplitude is measured with the ‘tank loop’; an inductive pick-up inside each cavity.
2. Fine-tuning of phase and amplitude and measurement of these two parameters; allowing remote control of the system via Simatic.
3. Regulation of the piston tuners that keep the resonant frequency of the cavities constant. Avoidance of critical tuner positions.

Figure 85 shows the complete layout of the system. The modules are described briefly below.

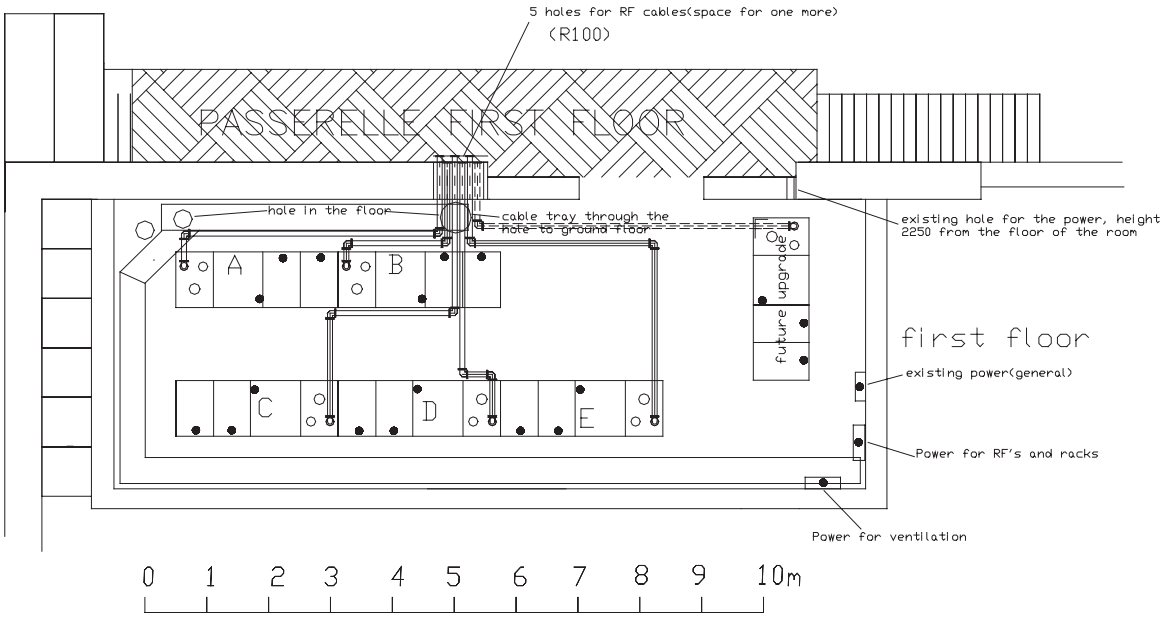

Fig. 84: Arrangement of the amplifiers in the amplifier room

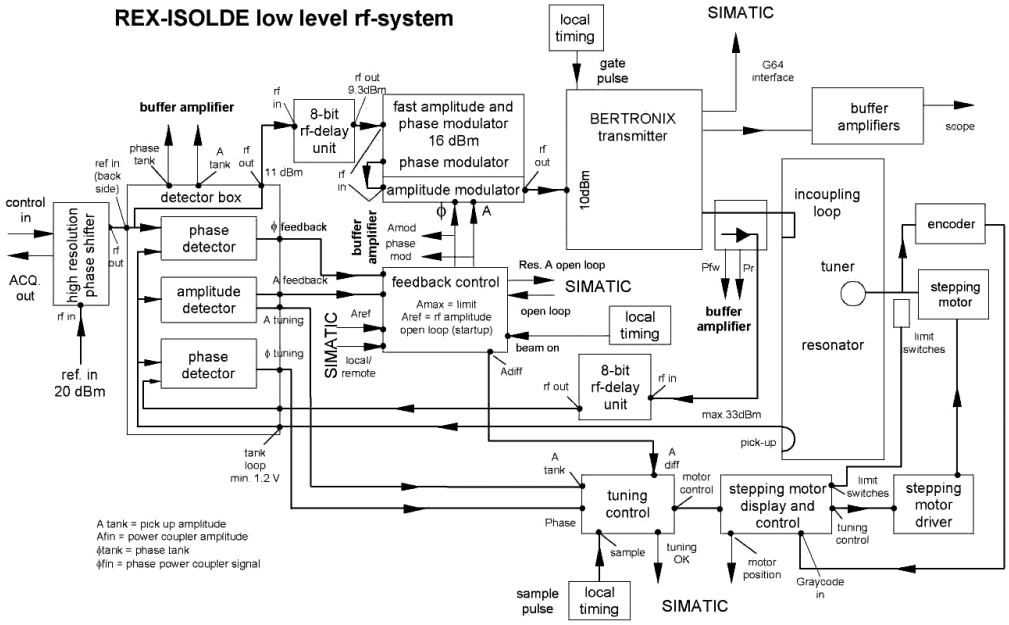

Fig. 85: REX low-level RF control system

3.7.1 Detector box

The detector box is mainly responsible for the measurement within the system. It compares the pick-up signal from the resonator with the forward signal from the directional coupler of the amplifier and with the signal from the master oscillator. For example, the phase relation between amplifier and pick-up (which has to be adjusted with a RF delay unit) changes if the resonance frequency of the amplifier increases significantly (e.g. due to heating). Then the detector box gives a voltage signal PH_{fin}, proportional to this phase difference, to the tuning control module. The change of the amplitude of PH_{fin} is ~100 mV at 1° phase difference. At the same time the detector box compares amplitude and phase of the pick-up signal with the master oscillator (phase difference: $\Delta\varphi$). Analogous to the frequency tuning, the module gives d.c. levels, A_{tank} and PH_{tank} to the feedback control module.

The signal from the master oscillator is attenuated by the detector box. It goes from the high-resolution phase shifter to the fast amplitude and phase modulator. Another delay unit is used in between to shift the signal into the limited adjustment range of the fast amplitude and phase modulator.

To control the loop operation, a number of connectors on the front side of the detector box enable the different d.c. levels to be checked.

3.7.2 RF delay unit

This module is used to shift the phase of the RF signals. It simply consists of a number of shielded pieces of transmission line of different lengths that are connected with a relay switch. During the switching process, it is important that the relay closes the new connection before it opens the old one. Otherwise the RF signal is interrupted and the loop is not closed, something which normally leads to a breakdown of the system.

3.7.3 Tuning control

The tuning control regulates the piston tuners (frequency tuning of the cavities). As mentioned above it gets the PH_{fin} signal from the detector box. Depending on the polarity of the incoming signal it decides if the tuner moves in or out. The sensitivity and the tolerated phase difference are adjustable. The sensitivity is also dependent on the repetition rate of the signals from the detector box. The tuning control only works above a certain level of the pick-up signal to avoid uncontrolled motion of the tuners without RF power in the cavity. The module needs a trigger pulse from the timing module and a voltage signal A_{dif} from the detector box (via the feedback control), to make sure that the regulation loop is working.

3.7.4 Fast amplitude and phase modulator

This module provides the fast (1.5 μs) regulation of the incoming phase and amplitude signals in the range of 80° and 28 dB, respectively. It is needed to compensate for changes in amplitude and phase in the cavities due to transient effects or thermal strains of the amplifier/resonator system. The stability of phase and amplitude achieved in this way is 0.2° and 10 mV at pick-up signals of typically 1.5 V (~1%).

3.7.5 Feedback control

The feedback control is the regulation module in the loop. There are two modes of operation. In the 'open loop' mode there is no regulation of phase or amplitude. In this mode the module defines only the level of the RF signal which goes from the fast amplitude and phase modulator to the preamplifier, without taking the pick-up signals into account or doing any corrections. This mode is used for system tests or conditioning of the cavities and not for acceleration. In the second, more important, mode (so-called closed-loop operation), the module sets the amplitude of the tank signal (A_{ref}) and provides the

d.c. signals for fast regulation in the fast amplitude and phase modulator. The actual values for amplitude and phase are received from the detector box.

In closed-loop operation the important values for the amplitude are A_{ref} and A_{max}. A_{max} defines the upper threshold for the RF power. It should be slightly above the value A_{ref} to leave enough tolerance for the regulation. This tolerance can be checked with the signal A_{mod}, which shows the voltage difference between pulse and pulse break. The pulse break corresponds to the value of A_{max} and should always be about 0.5 V higher than the voltage during the pulse (corresponding to A_{ref}). To illustrate the effect of the regulation, Fig. 86 shows, for comparison, the pick-up signals of the IH structure in open-loop and closed-loop operation.

The phase regulation of the system is checked with the d.c. signals PH_{tank} and PH_{mod}. The signal PH_{tank} corresponds to the phase difference between the cavity pick-up signal and the reference signal (adjusted before with a delay unit). On account of the small adjustment range of the fast amplitude and phase modulator, it should be close to zero. The signal PH_{mod} is the voltage, which corresponds to the phase set with the HRPS.

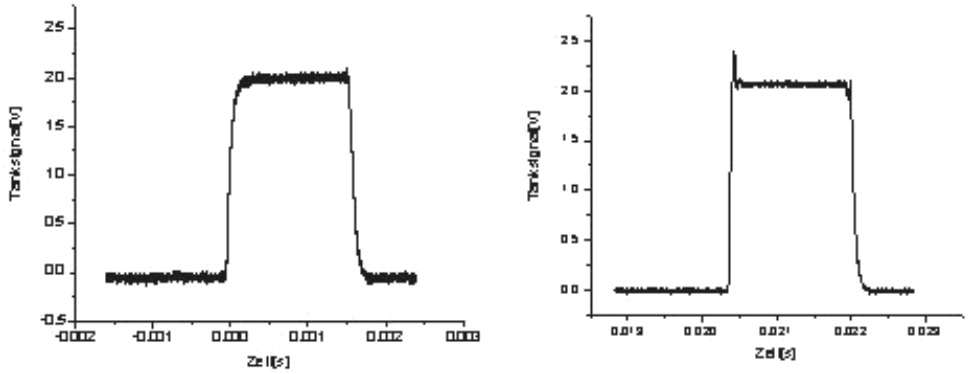

Fig. 86: IH pick-up signals. Operation in open loop (left) and in closed loop (right)

3.7.6 High-resolution phase shifter

The HRPS module digitally adjusts the phase relation between the master oscillator and the cavity. The modules define the phase relations between the different accelerator components and allow for their adjustment with high precision (~0.2°) according to the phase that the synchronous particle sees at the entrance. The HRPS for the 202.56 MHz set-up is basically a 101.28 MHz module equipped with a frequency doubler.

To avoid a thermal drift of the resonator phases due to thermal expansion of the transmission lines, the line lengths from the master oscillator to the HRPSs must be identical. The same holds for the lines from the pick-ups to the detector boxes.

3.8 Beam transport calculations

The beam-line calculations were performed with the COSY Infinity and MIRKO codes. They start from the end of the RFQ rods for the 0.3 MeV/u beam and from the end of the last gap of the seven- and nine-gap resonators for the 2.2 and the 3.0 MeV/u beam. The transport is calculated to the target in the MINIBALL beam line. The lenses included are the triplets in the matching section, the IH inner-tank triplet, the lenses in the seven-gap resonator section and the triplet lenses in front of and behind the bending magnet MD3. The names of the different elements are shown in Fig. 39.

Figure 87 shows the geometry of the REX-ISOLDE beam line. Beam diagnostics is possible at the position of diagnostic box (DB3) in front of the rebuncher of the medium-energy transport (MEBT, matching section), in DB4 just in front of the MD3 magnet and in front of the target stations (DB5 and DB6).

The specifications of the magnetic lenses are listed in Table 20. The data of the bending magnet (MD3, BEN.MD60) at the end of the accelerator line are shown in Table 21.

Table 20: Specification of the magnetic quadrupole lenses of REX-ISOLDE

Lens	**Aperture [mm]**	**Effective length [mm]**	**Separation [mm]**	**Polarity [+: x focusing]**	**Max. gradient [T/m]**
MQT1	30		50		
RFQ.MQ110		60		–	55
RFQ.MQ120		80		+	62
RFQ.MQ130		60		–	55
MQT2	30		50		
IHS.MQ30		60		+	55
IHS.MQ40		80		–	62
IHS.MQ50		60		+	55
MQT3	22		20		
IHS.MQ60		63		+	60
IHS.MQ70		104		–	60
IHS.MQ80		63		+	60
MQT4	26		30		
IHS.MQ90		85		+	55
IHS.MQ100		110		–	60
IHS.MQ110		85		+	55
MQD1	45		52		31.8
7GP.MQ10		173		–	
7GP.MQ20		173		+	
MQT5/1	40		47		30
BEN.MQ10		97.5		+	
BEN.MQ20		165		–	
BEN.MQ30		97.5		+	
MQT6, MQT7	40		47		30
BEN.MQ70		97.5		+	
BEN.MQ80		165		–	
BEN.MQ90		97.5		+	
MQT5/2	26		30		
IHS.MQ60		85		+	60
IHS.MQ70		110		–	60
IHS.MQ80		85		+	60

Table 21: Parameters of the switching magnet MD3 (BEN.MD60)

Gap size [mm]	50
Deflector angle	20°, 35°, 50°, 65°
Bending radius [mm]:	
20°, 35°	2878, 1662
50°, 65°	1182, 930
Angle between beam axis and yoke:	
20°, 35°, 50°, 65°	80°, 73°, 66°, 58°
Maximum field strength	1.14 T
I and U for B_{max}	150 A, 74 V

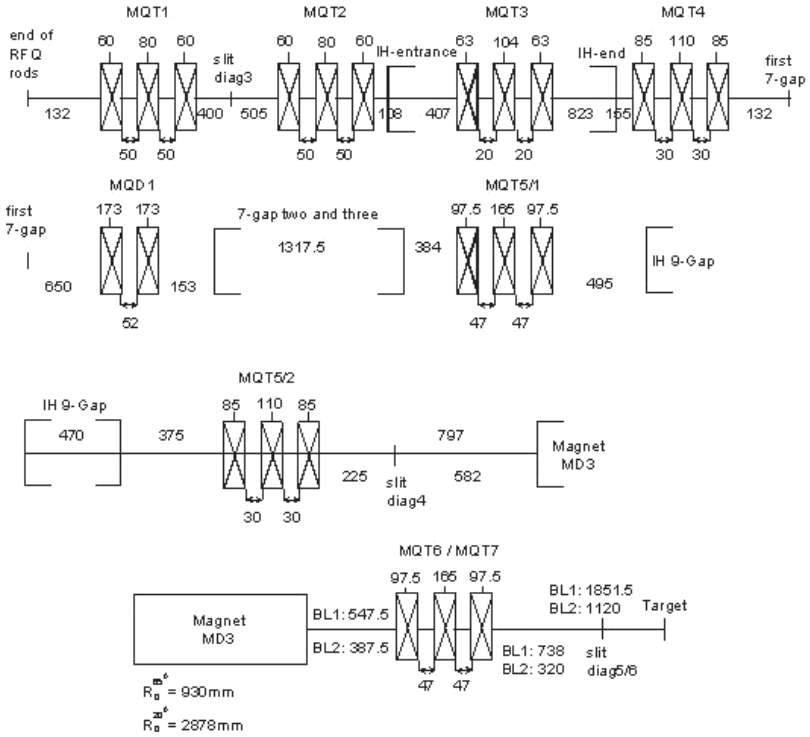

Fig. 87: Geometry of the beam line sections behind the RFQ: matching section, the IH structure, seven-gap resonators, the new IH nine-gap resonator, and the high-energy beam transport with the MD3 bending magnet

3.8.1 Transport of the 0.3 MeV/u beam towards the MINIBALL target (A/q = 4)

The results of PARMTEQ calculations, verified by emittance measurements at the University of Munich [21], are used for the start parameter of the beam-line calculations. A beam that corresponds to the acceptance of the RFQ of about 0.66 π·mm·mrad (normalized) is taken into account. This beam is larger than the beam from the EBIS by about a factor of 8–10. No losses or aberrations should occur for the real beam. The Twiss parameters and the beam emittance at the RFQ rod exit are shown in Table 22.

The values for the beam parameter definition were: x_{max} = 2.37 mm, y_{max} = 2.21 mm, x'_{max} = 14.33 mrad, y'_{max} = 14.48 mrad. A reasonable solution for the 0.3 MeV/u ion beam is shown below (Figs. 88 and 89). The magnetic field strengths for the quadrupole lenses are given in Table 23. The additional triplet behind the new nine-gap resonator was not used. A fit for a waist at diagnostic boxes 3, 4, and 5 was tried (Fig. 39).

Table 22: Beam parameters of a beam with ε_{norm} = 0.66 π·mm·mrad at the end of the RFQ rods

Parameter	**x**	**y**
α	–0.69	0.58
β [mm/mrad]	0.2	0.177
γ [mrad/mm]	7.38	7.55
ε [π·mm·mrad]	28.2	27.8

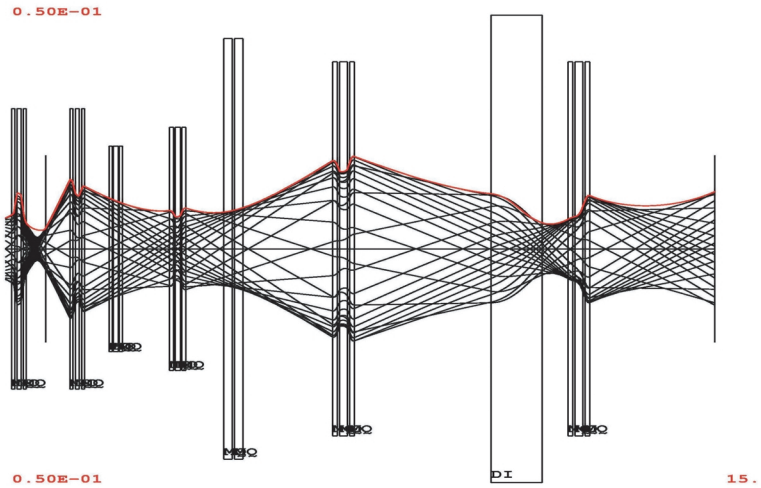

Fig. 88: Beam trajectories and envelope for transport of beams with 0.3 MeV/u to the MINIBALL beam line, X-component

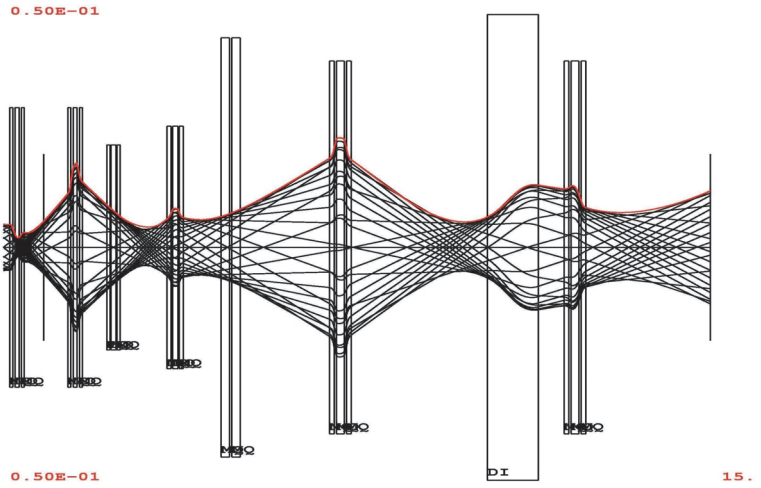

Fig. 89: Beam trajectories and envelope for transport of beams with 0.3 MeV/u to the MINIBALL beam line, Y-component

Table 23: Settings for quadrupole lenses for the transport of a 0.3 MeV/u beam

Lens	Flux density at pole tip (T)			Magnetic field gradient (T/m)		
MQT1	–0.448	+0.58	–0.552	–29.9	+48.5	–44.9
MQT2	+0.34	–0.36	+0.19	+22.7	–24	MQT3
MQT3	(not used)			(not used)		
MQT4	+0.112	–0.207	+0.145	+8.62	–15.92	+11.15
MQD1	(not used)			(not used)		
MQT5	+0.109	–0.128	+0.117	+5.45	–6.4	+5.85
MQT6	+0.17	–0.146	+0.14	+8.5	–7.3	+7

3.8.2 Injection into the IH structure (A/q = 4)

In order to match the beam from the RFQ to the IH structure, the section was analysed with the TRANSPORT code and with COSY Infinity. The gradients of the lenses involved are summarized in Table 24. The envelopes of the beam in both transverse directions, the changes of the beam angles, and the phase and energy spread are shown in Fig. 90. A key issue of the matching section is the adjustment of the beam phase spread to the IH structure requirements of ±10° phase spread.

Table 24: Settings for quadrupole lenses for injection into the IH structure

Lens	Magnetic field gradient (T/m)		
MQT1 RFQ.MQ110, RFQ.MQ120, RFQ.MQ130	–32.56	38.67	–36,82
MQT2 IHS.MQ30, IHS.MQ40, IHS.MQ50	30.3	–36.24	26.96

3.8.3 Beam transport at 1.2 MeV/u to the MINIBALL target (A/q = 4)

For the start parameter of these calculations, the results of the LORASR design calculations are used. Again a beam is taken into account which corresponds to the transverse acceptance of the IH structure of about 0.6 π·mm·mrad normalized. The Twiss parameter and the beam emittance at the exit of the IH cavity are shown in Table 25. The values for the beam parameter definition are: x_{max} = 4.58 mm, y_{max} = 2.67 mm, x'_{max} = 7.87 mrad, y'_{max} = 6.19 mrad.

Table 25: Beam parameter of a beam with $\varepsilon_{xx'}$ = 0.63 π·mm·mrad and $\varepsilon_{yy'}$ = 0.71 π·mm·mrad normalized at the exit of the IH cavity

Parameter	x	y
α	–2.738	–0.65
β [mm/mrad]	1.69	0.51
γ [mrad/mm]	5.0	2.738
ε [π·mm·mrad]	12.4	14

A solution for the beam line after acceleration to 1.2 MeV/u in the IH structure is shown in Figs. 91 and 92. The settings are listed in Table 26.

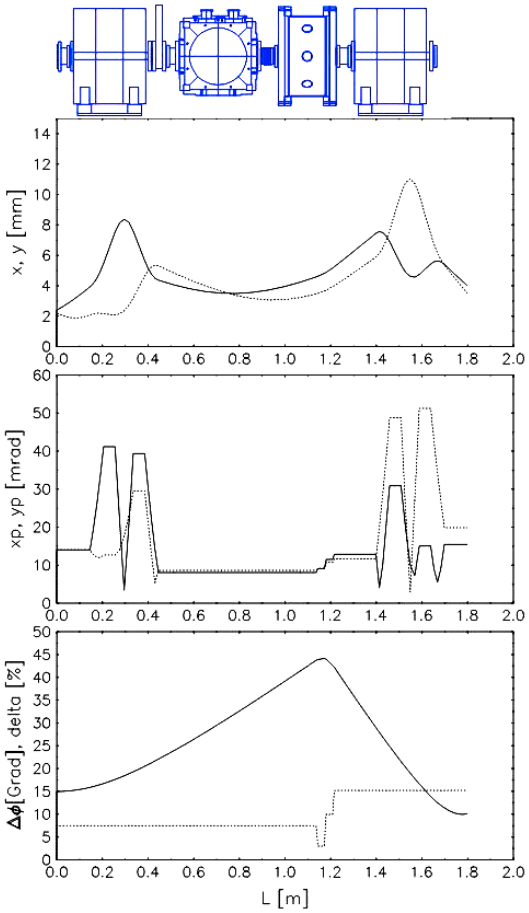

Fig. 90: Calculations of the transverse and longitudinal phase space of the matching section between RFQ and IH and of the injection at 300 keV/u into the IH structure

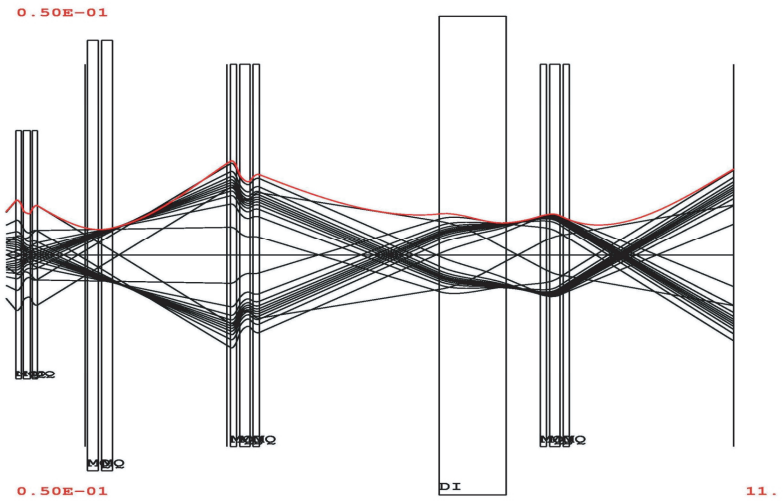

Fig. 91: After IH structure, beam trajectories and envelope, X-component

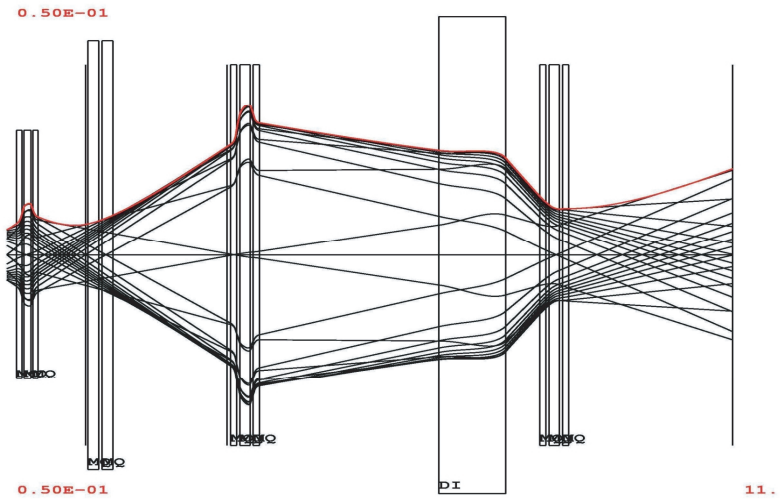

Fig. 92: After IH structure, beam trajectories and envelope, Y-component

Table 26: Settings for quadrupole lenses

Lens	Field at pole tip (T)			Magnetic field gradient (T/m)		
MQT4	+0.436	–0.523	+0.31	+33.54	–40.23	+23.85
MQD1	not used			not used		
MQT5	+0.278	–0.239	+0.163	+13.9	–11.95	+8.15
MQT6	+0.035	–0.082	+0.01	+1.75	–4.25	+0.5

3.8.4 Beam line calculations for A/q = 4 ion beams with energies of 2.2 MeV/u to the MINIBALL target

The start parameter of these calculations is derived from the linac design calculations. Again a beam is used that corresponds to the transverse acceptance of the IH structure of about 0.6 π·mm·mrad normalized. This beam has been traced through the seven-gap resonators. The Twiss parameter and the beam emittance at the exit of the third seven-gap resonator are shown in Table 27. The settings are listed in Table 28 and the envelopes are sketched in Figs. 93 and 94.

Table 27: Beam parameter of a beam with $\varepsilon_{xx'} = 0.63$ π·mm·mrad and $\varepsilon_{yy'} = 0.71$ π·mm·mrad normalized at the exit of the seven-gap 3 cavity

Parameter	x	y
α	–9.47	–1.65
β [mm/mrad]	7.2	1.8
γ [mrad/mm]	12.59	2.07
ε [π·mm·mrad]	5.0	5.0

Table 28: Settings for quadrupole lenses

Lens	Field at pole tip (T)			Magnetic field gradient (T/m)		
MQT4	+0.44	–0.538	+0.268	+33.85	–41.35	+20.62
MQD1	–0.412	+0.398		–18.3	17.7	
MQT5	+0.47	–0.455	+0.372	+23.5	–22.75	+18.6
MQT6	+0.302	0.414	+472	+15.11	20.71	+23.58

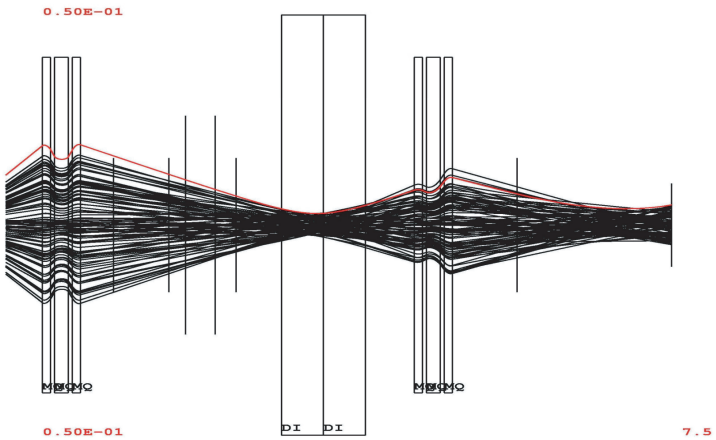

Fig. 93: Beam transport from the third seven-gap to MINIBALL at 2.2 MeV/u, X-component

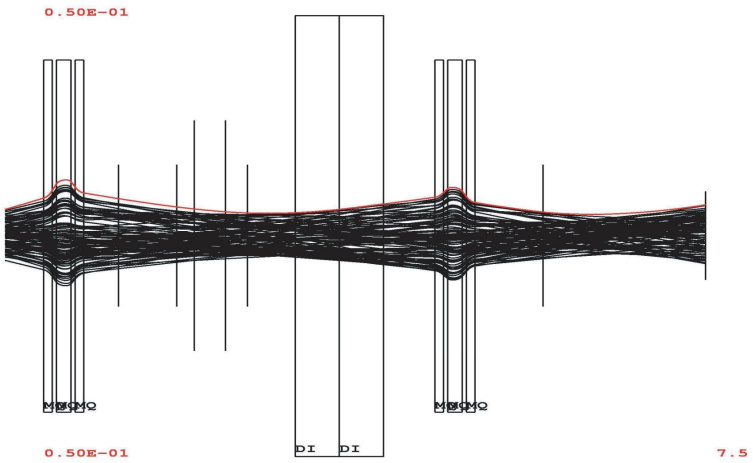

Fig. 94: Beam transport from the third seven-gap to MINIBALL at 2.2 MeV/u, Y-component

3.8.5 Beam line calculations for A/q = 4 ion beams from the third seven-gap resonator through the nine-gap resonator to the MINIBALL target with an energy of 3 MeV/u

The start parameter of these calculations is given in Table 27. Matching the beam from the third seven-gap to the nine-gap resonator is done with lens MQT5. The injection and extraction beam parameters of the nine-gap cavity are summarized in Table 29. The values are derived from the LORASR design calculations of the IH nine-gap resonator. The emittance corresponds to the acceptance of the nine-gap resonator with 20 π·mm·mrad at 2.25 MeV/u beam energy.

Table 29: Beam parameter of a beam with $\varepsilon_{xx'} = 0.63\ \pi$·mm·mrad and $\varepsilon_{yy'} = 0.71\ \pi$·mm·mrad normalized at the exit of the IH cavity

Parameter	**x**	**y**
Injection		
α	1.518	2.19
β [mm/mrad]	0.666	1.16
γ [mrad/mm]	4.96	5.0
ε [π·mm·mrad]	20	20
Extraction		
α	–1.3	–0.544
β [mm/mrad]	0.582	0.305
γ [mrad/mm]	4.64	4.25
ε [π·mm·mrad]	17.7	17.9

The settings of the magnetic quadrupole lenses for the beam transport are listed in Table 30 and the envelopes of the injection matching are sketched in Fig. 95. The beam envelopes of the transport from the nine-gap IH cavity to the MINIBALL are shown in Figs. 96 and 97.

Table 30: Settings for quadrupole lenses

Lens	**Field at pole tip (T)**			**Magnetic field gradient (T/m)**		
MQT4	+0.44	–0.538	+0.268	+33.85	–41.35	+20.62
MQD1	–0.412	+0.398		–18.31	17.7	
MQT5/1	+0.677	–0.413	+0.399	+33.85	–20.65	+19.95
MQT5/2	+0.547	–0.89	+0.629	+42.08	–68.46	+48.38
MQT6	+0.393	–0.482	+0.579	+19.65	–24.1	+28.95

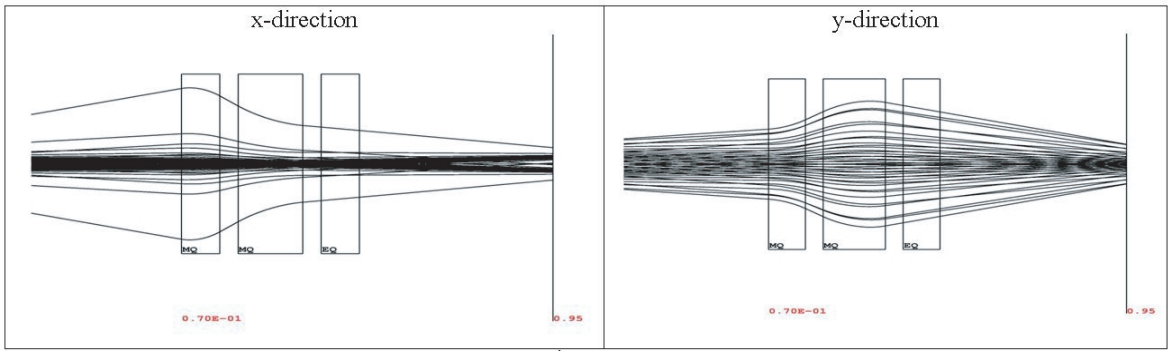

Fig. 95: Beam matching from the third seven-gap resonator to the IH nine-gap resonator

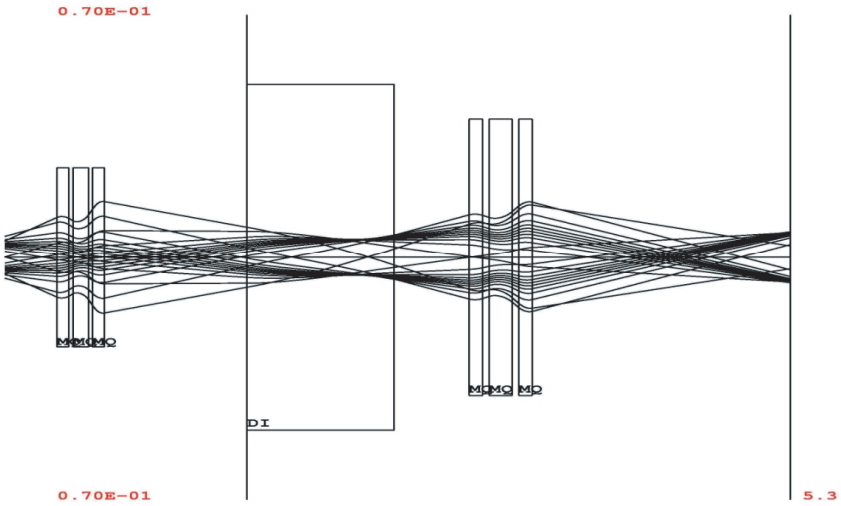

Fig. 96: Beam transport from the nine-gap IH structure to MINIBALL at 3.0 MeV/u, X-component

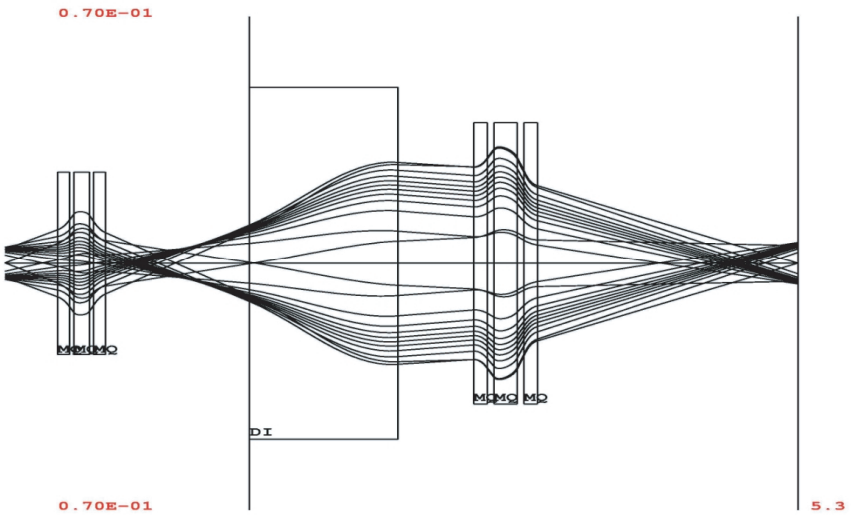

Fig. 97: Beam transport from the nine-gap IH structure to MINIBALL at 3.0 MeV/u, Y-component

3.9 Future developments and upgrades

3.9.1 REX-ISOLDE linac energy upgrade above 4 MeV/u

A major change of the linac structure will be required in order to reach energies of approximately 4.2 MeV/u. Two of the seven-gap spiral resonators with 101.28 MHz resonance frequency need to be replaced by a 1.5 m IH cavity with 202.56 MHz resonance frequency to boost the energy to the required region of 3.75 MeV/u. A seven-gap IH resonator of the MAFF type could be used to vary the final energy between 3.2 and 4.3 MeV/u (see Fig. 98).

The first seven-gap split-ring structure will be used to prepare the beam for injection into the 28-gap 202.56 MHz IH structure. The synchronous phase of the seven-gap resonator will be adjusted to –20°, which allows an exit energy of 1.53 MeV/u and a phase spread of ±10° at the entrance of the 202.56 MHz structure. The cavity will boost the energy to 3.75 MeV/u; this requires an effective acceleration voltage of 10.14 MV for ions with A/q = 4.5. With an effective shunt impedance of 180 MW/m (which is feasible for such cavities), an RF power of 380 kW is necessary. The beam

energy can be varied by ±0.5 MeV/u via the 202.56 MHz MAFF-type seven-gap resonator, which is currently serving as a nine-gap booster cavity at REX-ISOLDE.

The phase matching of the beam from the seven-gap split-ring structure towards the 28-gap resonator is critical and a minimum distance between the two structures must be guaranteed. The beam dynamics design of the cavity and the beam transport towards the target regions have been completed. The cavity design of the 28-gap resonator structure is shown in Fig. 99.

The proposed energy upgrade requires a minimum of changes to the remaining cavities, but is a rather large investment. A straightforward way of increasing the energy range to variable values between 2.5 and 5.7 MeV/u would be more efficient use of the present RF power. Additionally, other RF power amplifiers already available at CERN could be modified and used for such an upgrade. A very promising option for the linac upgrade is shown in Fig. 100.

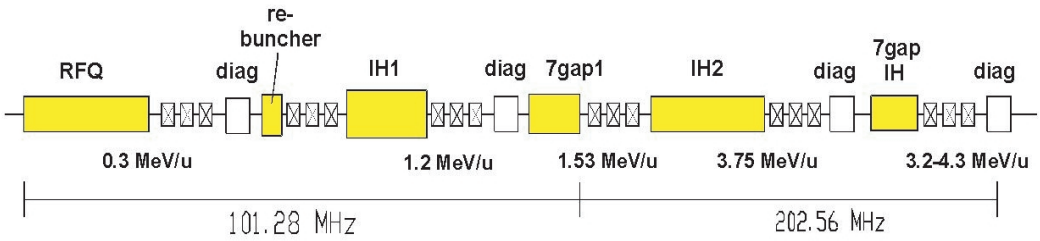

Fig. 98: First upgrade scenario for REX-ISOLDE towards 4.2 MeV/u (scheduled for 2006/2007)

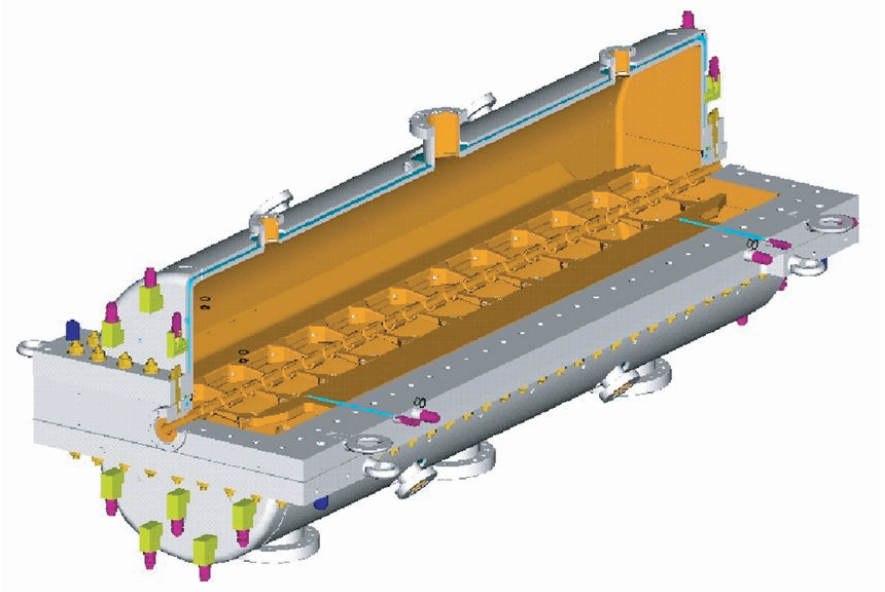

Fig. 99: Cavity design of the 202.56 MHz 28-gap IH resonator

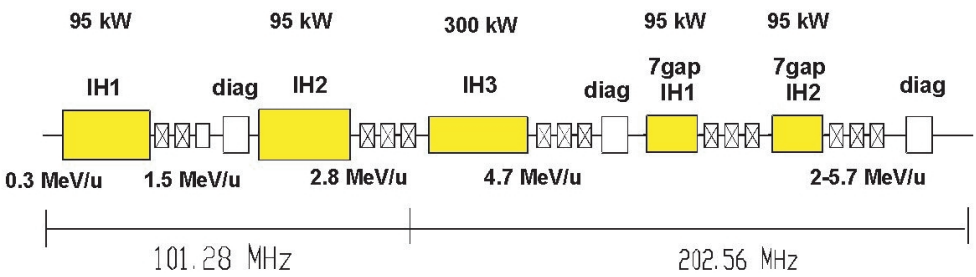

Fig. 100: Upgrade scenario for REX-ISOLDE for a maximum energy of 5.7 MeV/u

Cavity IH1 uses only 50 kW RF power to accelerate ions with A/q = 4.5. With a small change in the drift-tube structure a higher beam energy should be possible. The seven-gap split-ring structures are for energy variation, not energy boost. Thus a second IH cavity operating at 101.28 MHz would increase the energy gain tremendously—to approximately 2.8 MeV/u. A 202.56 MHz 28-gap resonator could further boost the energy towards 4.7 MeV/u. This would require 300 kW RF power. An amplifier at CERN could be modified to deliver that power with a duty cycle of 3% and 700 ms pulse duration. Two seven-gap IH cavities of the MAFF-type resonator could vary the energy between ~3.7 and 5.7 MeV/u using 95 kW RF power for ions with A/q = 4.5. These cavities could be driven by modified 101.28 MHz amplifiers that have already been used for the Heidelberg seven-gap resonators. A change in frequency is possible by purchasing new resonator cabinets for these amplifiers. The two IH seven-gap resonators could be used at the final energy of IH2 (2.8 MeV/u) to try and increase the range for energy variation. Simulations have to be performed to determine the exact range.

4 The control system and associated equipment

4.1 Introduction

The REX control system relies on three main concepts for communication between client and server machines. In this respect the system is heterogeneous. However, the guiding principle when designing the low-level control has been to rely on industrial components whenever possible. This ensures that spare parts and commercial technical documentation are available in most cases. The less-than-complete system homogeneity originates in the complexity of the machine. As mentioned above, the REX concept relies on a Penning trap and an electron-beam ion source connected in tandem, as well as on a linear accelerator used for the post-acceleration of the radioactive beam itself. The Penning trap and the trap-to-EBIS beam transfer system use the same control concept as the ISOLTRAP experiment. The EBIS, the REX mass separator, the beam optics, and the beam observation systems use a framework for Remote Procedure Call (RPC) originally developed by the PS controls group at the end of the 1990s for ISOLDE. This framework has some attractive features. It allows an operator or hardware specialist to upgrade or change control components easily, with a limited coding effort. In certain cases, changes of control equipment can be carried out by exchanging existing software modules or by parameter updates in a database. This enables very short downtimes for the replacement of faulty equipment. Control of the radio frequency amplifiers and the vacuum system has recently been developed employing OPC server techniques. This provides a quick operating solution over the period that the full system is under migration to Java applications and VME-based Device Stub Controllers (DSC).

The main computer components of the system are a file server, an OPC server, three consoles, and seven Front-End Computers (FECs). The architecture of the system is outlined in Fig. 101. Three of the front-end computers run the RPC server mentioned above. As indicated, these computers query start-up information for the hardware under their control from the database residing on the file server. The Penning trap control system is VME resident. During the development phase, the advantage of this approach has been immediate access to an existing system with real-time response for the scanning of vital parameters. The initialization parameters are read from a configuration file residing on the hard drive of the VME processor. The OPC server uses DCOM for communication between the console application and the server. The server communicates with a PLC concentrator, which is typically a Siemens CPU-315 DP processor with an Ethernet coupler. The concentrator in turn communicates with a number of sub-units, including other CPUs or slave devices. The hardware, software, and communication protocols used for REX are enlarged upon in the following sections.

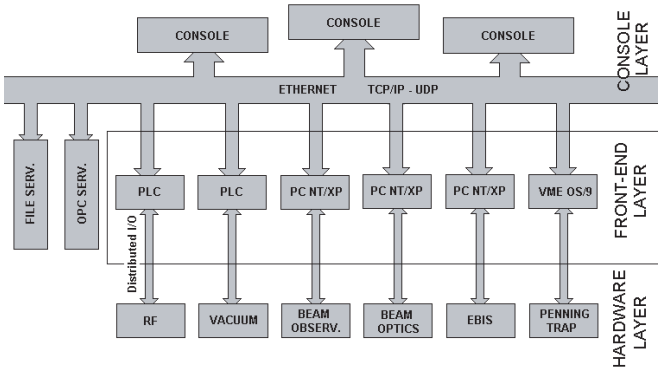

Fig. 101: General layout of the architecture of the REX-ISOLDE control system. The consoles communicate with any of the seven front-end computers that in turn control the machine hardware. Three different protocols are used for this purpose. The traditional layers of the control system are indicated on the right

4.2 The NT/XP RPC server and client model

The Windows NT/XP RPC server is used on three of the seven front-end computers. The framework was developed by I. Deloose and is described in detail in Ref. [47]. Some features are nevertheless detailed below, with emphasis on their application to the current project.

The key component of the RPC server framework is the use of Object Linking and Embedding (OLE) technology. In practice, this means that the hardware expert provides an activeX control that is loaded at start-up by the server program running on the front-end computer. The properties and methods of the activeX control correspond one-to-one to the states and actions of a specific hardware. A predefined object is added to the activeX control to connect to the server program. One purpose of this object is to identify uniquely different members of the class that describes the specific hardware. It can therefore be said to channel the data packets on the server side to the code acting on a specific piece of equipment. The name and properties of the activeX control, or the so-called equipment module, are specified in the database. As mentioned, the database is queried by the front-end computer at start-up in order to determine which modules to load on a given machine. The compiled controls are stored in a repository on the file server and read from there when the server program has queried the database. One instance of the activeX control is loaded on the front-end computer and the specific equipment using this control is tracked via its member number, which is also listed in the database. The member number is a property of the object added to the activeX control and is set by the framework after the database has been read. This means that in practice the approach is not fully object-oriented. It is possible to devise a scheme in which each piece of hardware corresponds to a separate object, but in some cases this proved unfeasible: some commercial drivers experience access conflicts if more than one process attempts to use them at a time. With the approach used here, one driver is accessed from one thread only and the member number is used to distinguish between the different pieces of equipment using this driver. Access conflicts are therefore avoided. A predefined RPC object can also be included in a standard Visual Basic (VB) executable project on the client side. In this way the application programmer does not have to fill TCP/IP packets. It is also possible to use the RPCAPI DLL directly. When the object approach is used, the type of the variable to be transferred is set as the value of a property of the object, and its numeric value is passed to the front end by activating a data transfer method. (The details of the properties and methods of this predefined object can also be found in Ref. [47].) One or several of these RPC objects may be included in the application. The approach chosen for REX has been to include one RPC object per hardware property controlled by a specific client application. In the simplest case only two objects are needed. They are used to set the Current Control Value (CCV) and to acquire (AQN) the currently active value. In some cases more than one piece of hardware is controlled from one client application and more properties or methods than the two

mentioned above are used; however, it was concluded that the application gains speed by using one RPC object per property. An obvious alternative would be to establish one RPC object per hardware object and to change the property to be transferred according to the user activity. This approach was tested but in most cases abandoned in order to gain reasonable data exchange speed: it is necessary for an application to transmit and receive data at a rate of ~5 Hz for the operator to get a real-time feel. This is not always possible if properties are changed during execution when a large number of client applications are active simultaneously.

The framework also allows for the use of the RPC object in a subscription, or so-called hotlink, mode to automatically update control parameters on the client side as they are ready to send from the front end. However, in order to maintain full control of the parameters read back from the hardware, and particularly the time intervals between data exchange, it was decided to use only the object to query and set parameters by client request. Most properties are therefore read back using timers. In this way problems with broken communication and the consequently long waiting times between detecting a non-responding subscribing client and its removal from the subscription list can be avoided. Finally, it should be mentioned that both applications and equipment modules can be written in VB or C++. A typical approach has been to provide user GUIs in VB, to do more elaborate coding in C, and to provide the functionality in a DLL.

The commercial software used includes programs for configuration and tests of data transfer on the PROFIBUS and on the VME bus. In the former case the bus controller card for the computers running NT/XP and accompanying software was purchased from Applicom. The programs can be accessed under the Applicom folder in the start-up menu on the front-end computers. The configuration program, which defines communication with the units on the bus, is the most important in this context. There is also an initialization program that downloads the configuration data. This program should be run if the configuration has been changed. A number of smaller programs for reading and writing variables of different formats from or to the hardware are available under the same heading. The PCI/VME interface used for the EBIS control is delivered with an API and some basic test programs. These can be found under the SBS folder on the EBIS front-end computer.

4.2.1 The REXEBIS control system

The REXEBIS operates in a pulsed mode and passes through stages of injection, breeding, ejection, and cleaning in a cycle that typically lasts 20 ms. The control system must therefore be capable of setting parameters on short time-scales and of maintaining static parameters that stay constant over time. The flight time of an ion from the Penning trap to the EBIS is of the order of ~10 μs. It is therefore clear that real-time response is needed to prepare the EBIS to receive an ion pulse. More specifically, when the ion beam is extracted from the Penning trap, the beam optics is set to optimize injection into the electron beam of the EBIS; during breeding the drift tubes are set to confine the ions; and finally, when the desired charge state has been reached, the drift tubes and the beam optical elements are set to new values to optimize the extraction of the beam and its passage through the mass separator. Consequently, the operator needs to optimize the beam transport and the charge breeding process not only by tuning the amplitude of the potential barriers but also by adjusting the duration of a certain process. It should be possible to accomplish this with reasonable speed so the operator can see by direct observation if a certain change makes an improvement or not. This again requires real-time feel in tuning. The solution to the microsecond real-time requirement for parameter switching has been to incorporate a number of triggered VME-resident, so-called Simple Analog Function Generators (GFAS). These are accessed from the front-end computer via a PCI/VME interface. A block diagram of the EBIS control system, including GFAS modules, can be found in Fig. 102. The function generators are triggered by a pulse that is time correlated with the opening of the Penning trap. This signal is typically sent 1 ms before the trap opens. Likewise a stop or reset signal is sent a few microseconds before the start of a new cycle. In principle, the function generators should be ready to trigger when idle. This is not the case in practice. This effect has been traced to the trigger circuitry of the GFAS and solved by including a hardware reset

signal to resynchronize the function generators before the new trigger arrives. The main trigger box in Fig. 102 should be understood to have this combined functionality. A total of eight function generators are used for REXEBIS. They control the switching of the platform potential between 60 kV and 20 kV, the setting of the potential of the four drift tubes and of the potential of two lenses. One GFAS provides timing signals for the system. The output amplitude of a normal GFAS is given with 16-bit accuracy. By programming the amplitude so that a certain bit is active for a predefined duration, starting at a given time after receiving a trigger, one can produce 16 independent Gate and Delay Generators (GDGs) from one GFAS module. The TTL level of each individual bit is available on the GFAS card. At the REXEBIS these are channelled to the equipment via Lemo connectors. These logical pulses trigger switch boxes, whose output voltages alternate between two given input voltages. They also provide sample signals for sample–hold units used in the read-back chain. An element switched between two potentials is thus controlled using a combination of static and dynamic parameters. A block diagram of the method is shown in Fig. 103. A switch box of this type takes two static voltages and a trigger signal as input.

The trigger becomes active during injection. When the trigger is passive the output voltage is set to the extraction value. Similarly, the output voltage is sampled via a sample–hold unit that receives an injection and an extraction pulse. The two voltages are maintained on the output of the sample–hold unit and are fed back into the control system via analog inputs. The REXEBIS control also comprises two Profibus Distributed Peripheral (PB DP) units at ground potential for setting and read-back of the voltages mentioned above. These units control the steering elements at the EBIS entrance. There are two similar units on the HV platform used for static parameters such as electron-beam acceleration, and extractor, collector, and suppressor voltages. There are also two drift tubes at static potential that confine contaminant ions created in the cathode region in order to avoid their mixing into the extracted beam. Some of the GUIs used for EBIS control are shown in Fig. 104.

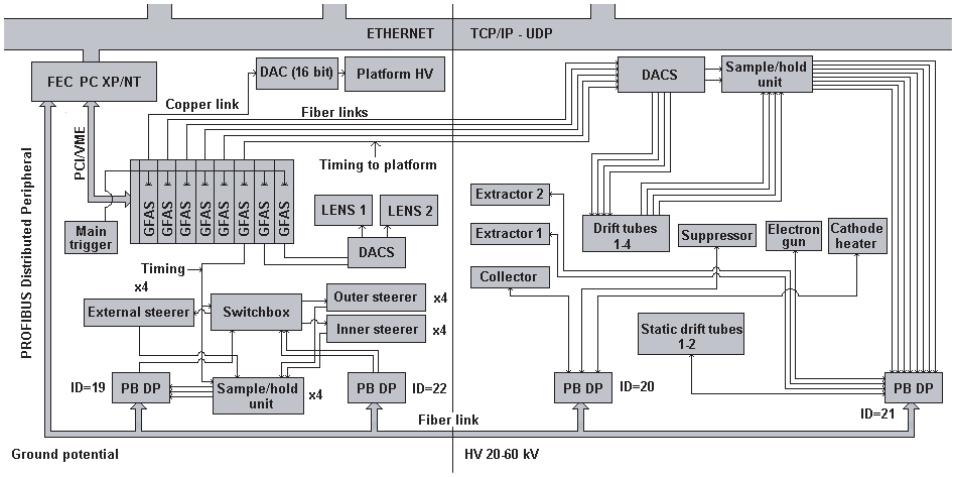

Fig. 102: Block diagram of the REXEBIS control system. The units marked PB DP represent PROFIBUS distributed peripheral equipment (so-called PROFIBUS slaves). The left part of the diagram shows equipment residing at ground potential while the right part shows equipment on the high-voltage platform. The front-end computer controlling this part of the REX machine is indicated in the upper left corner. The VME-resident GFAS modules are the standard simple analog function generators of the PS control hardware section. They are programmed via a PCI/VME interface from the front-end computer. The PROFIBUS line is controlled via a 1500 kbit controller card from Applicom

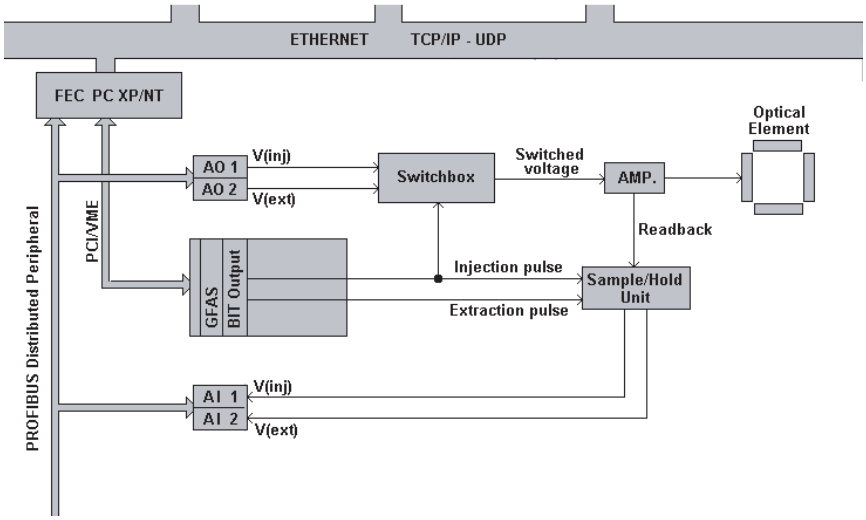

Fig. 103: Setting and read-back via a sample–hold unit for switched voltages of the REXEBIS beam optics. AI stands for analog input and AO for analog output

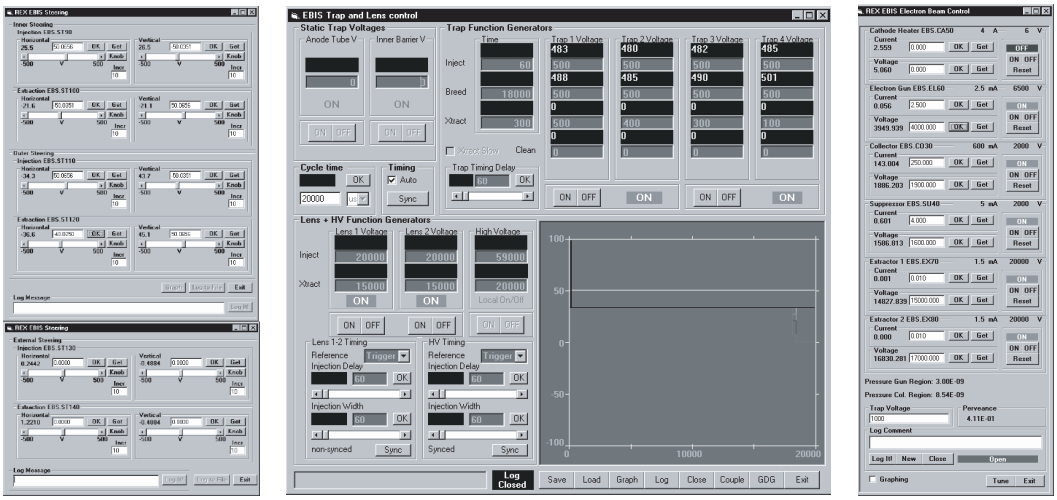

Fig. 104: Screenshots of GUIs used for REXEBIS control. The right panel controls the electron beam and the central panel the switched drift tubes, lenses, and the high voltage. The central and left panels are used for control of the beam optical elements that change potential between injection and extraction

4.2.2 Beam optics control

The second NT/XP front-end computer is used for beam optics control. Generally, beam tuning in real time requires feedback of the current beam profile and intensity readings (this is discussed further in the next section). In controlling beam optics, it is of prime importance to transfer new values to the equipment without waiting time. This is because when tuning the beam using beam position, profile, and intensity, the operator usually focuses on these readings and not on a specific voltage or current of a piece of equipment. It is therefore less important to have prompt read-back of the set current values: a fast read-back is vital, but the priority is to feed the current beam properties back to the operator and to transfer new set-values in real time. To reach this goal the equipment module for the magnet power supplies has been programmed in asynchronous mode. This means that a request to set or read back a value does not require direct access to the equipment on the bus. Instead, a timer in the equipment module triggers to read and set new values within a given time interval. As a request is received by the RPC server, the equipment module transfers the last set/read-back value from/to the calling process.

This means there is no need to wait for all values to be transferred on the bus if the operator is tuning the beam very quickly; instead, all values are picked as quickly as possible from a variable in the equipment module and sent to the hardware or passed back to the calling process. This process has been thoroughly tested and gives good results. Note also that when the operator passes a beam optimum during tuning, the beam around the optimal setting will automatically be finely adjusted. This procedure is normally carried out with greater care than the first scan to find the optimum. Consequently, the time between new set-values given by the operator will increase as an optimum is approached. The approach chosen for read-back to the calling application has been to include a timer that ticks with higher frequency when the parameter is actively tuned. When the time between transfers of new values grows longer, the timer ticks more slowly, and finally if the widget is kept open without tuning, after a preset time of 30 s, the read-back will occur once every 10 s. This should be compared to the 20 ms read-back time used during active tuning. The operator may easily restart more frequent reading by activating the widget.

The beam optics control includes two Tesla meters. These can be used in a simple mode for magnetic field measurement, and can also be used in a PID loop. Each meter has a control card connected via a fibre optical loop to the PCI-resident controller card. The PID coefficients can be adjusted using a hand-held terminal. The operator can use either a direct setting of the magnet current using analog output modules or an analog output related to the read-back field for stabilized control. These units were originally introduced to control field instability that could arise from temperature differences, for example, and to give a direct read-back of the magnetic field in the dipoles. It should be noted that these Hall probes have a preferred direction for field measurement. If turned or tilted in the field they will measure the component only in a given direction in space. Figure 105 shows a block diagram for the beam optics part of the control system.

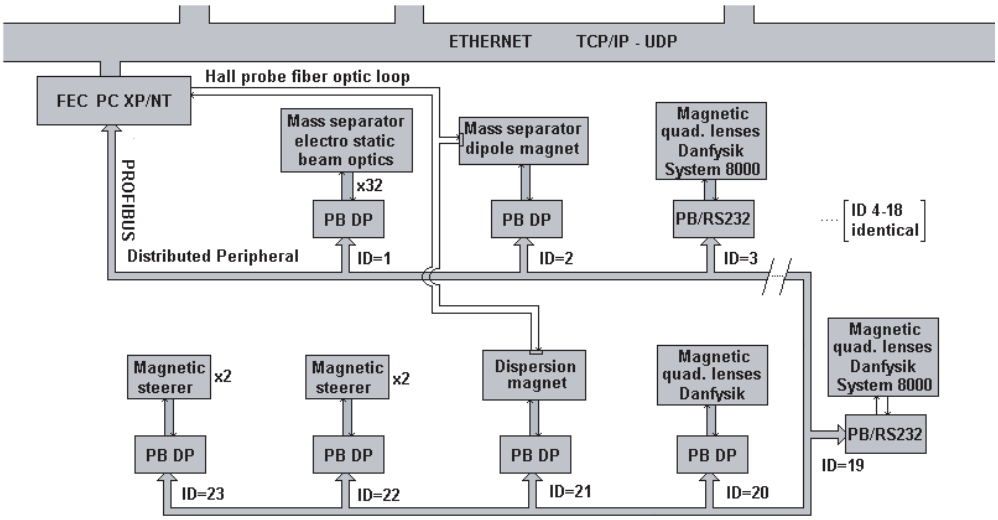

Fig. 105: Block diagram of the beam optics control system. The main control loop is a PROFIBUS line with 23 units (PB DP). The vast majority of these are PROFIBUS/RS232 interfaces for control of the magnetic quadrupoles in the linac. Five units are used for electrostatic beam optics, the two magnetic dipole magnets, and the magnetic steerers. For a detailed list see Appendix H

4.2.3 Beam observation equipment and control

The first step in the development of the general beam observation system was the design of a stand-alone system for imaging weak radioactive beams. This was undertaken by the Institute for Nuclear and Radiation Physics (IKS) at the Catholic University in Leuven, Belgium [48]. The second step was to incorporate the system into the general control scheme, and this was carried out by IKS in collaboration with CERN. The emphasis was on the transmission of images over Ethernet to make beam diagnostic

information available in the Main Control Room (MCR) of the Proton Synchrotron. Observation and diagnosis of beams from a radioactive ion-beam facility using the ISOL technique is challenging as the beam covers a wide dynamical range in energy as well as intensity. At REX the intensity varies between 10^3 and 10^9 pps, and the energy ranges from 30 keV to several MeV/u. For this reason the REX beam diagnostics includes Faraday cups for high-intensity, typically stable pilot beams for machine optimization, as well as an imaging system based on microchannel plates for observation of very weak beams. The system is capable of detecting beams from ~5 pps up to 1 nA.

The IKS system uses an aluminium plate, which is inserted in the beam to produce secondary electrons on beam impact. The electrons are accelerated by a grid onto an MCP, where the electron signal is further amplified (see Fig. 106). The amplified signal falls onto a phosphor plate, which is imaged by a CCD camera located outside the vacuum. The MCP is made by Proxitronics (model OS DD 2561 Z-V) and is equipped with a phosphor screen with a long decay time. The signal reaches 1% of the maximum amplitude after 55 ms. It is therefore possible to image the rather short beam pulses from REX, which have a typical duration of ~40 μs. The cameras are 1/3 inch monochrome CCD cameras from Philips (model VCM6650/00T) with a sensitivity of 0.1 lx. They are equipped with 8 or 12 mm CS-mount lenses. There are six beam diagnostic units mounted along the linac. These contain a Faraday cup, a low-intensity imaging system, and a stepping-motor-controlled wheel with collimators. The block diagram of the system is shown in Fig. 107.

Four units of slightly different construction are mounted in the low-energy part of the machine. These units do not include an aluminium plate for secondary electron production; the beam is instead implanted directly into the MCP. Nor do these units have a collimator wheel. Some of the units are bi-directional and all are UHV compatible. Every diagnostic unit is accompanied by an electronic control unit. The control units contain an embedded microcontroller for hardware control and an interface for communication with the control system. The units regulate the voltage of the accelerating grid (–5–0 kV), the MCP voltage (0–2.5 kV) and the phosphor screen voltage (0–5 kV). The UHV units do not contain a power supply for the grid voltage. The stepping motor control for the collimator wheel and the position control for the Faraday cup are incorporated in these units. They also provide –160 V d.c. for the secondary electron suppression of the Faraday cup and the 12 V d.c. power supply for the camera. The internal microprocessor unit is connected to an Advantech ADAM-4521 addressable RS232-RS485 converter, which is used to communicate with the front-end computer. The 10 camera images of the phosphor screens are channelled via a two-output multiplexer to two PCI frame grabbers from Matrox (Matrox Meteor and Meteor II). The multiplexer communicates with the front-end computer via the same RS485 line as the control units. The Faraday cups are connected via a low-current switchyard (Keithley 7001 switchyard main frame with two 7058 switch cards) to two Keithley 6514 electrometers. The two frame-grabber cards and two electrometers separate the beam diagnostics of the high- and low-energy beam lines. In this way the two parts of the machine can be optimized independently. The electrometers are controlled via an RS232-IEEE-488 converter (National Instruments GPIB 232 CT-A) and connected to one of the RS232 serial ports on the front-end computer. A separate trigger box can generate triggers or adapt external trigger signals to the equipment to operate the instruments in triggered mode and synchronize the measurements with the beam pulses.

There are two software equipment modules associated with the beam diagnostic system. These are Beamdiagn.ocx and FexFc.ocx. Beamdiagn.ocx communicates with the control units and grabs and processes the images from the cameras. The units are accessed asynchronously. The module continuously updates the information from the control units and passes the last read value to a querying client. The two frame grabbers also work asynchronously. The grabbed images are preprocessed to reduce the amount of data sent to the clients. First, the projection of the image is produced. Second, the pixel depth is reduced from 8 to 4 bits. Finally, the picture is compared with the camera noise and a data package is produced containing only regions where a significant number of pixels have signal above the noise level. FecFc.ocx is associated with the readout of the electrometers. As mentioned above, the

electrometers can be configured to run in a triggered or a non-triggered mode. The readout of the electrometers is asynchronous.

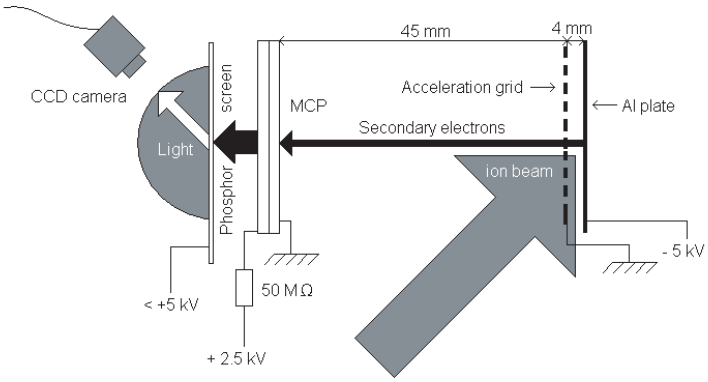

Fig. 106: Functional principle and design of the beam observation system

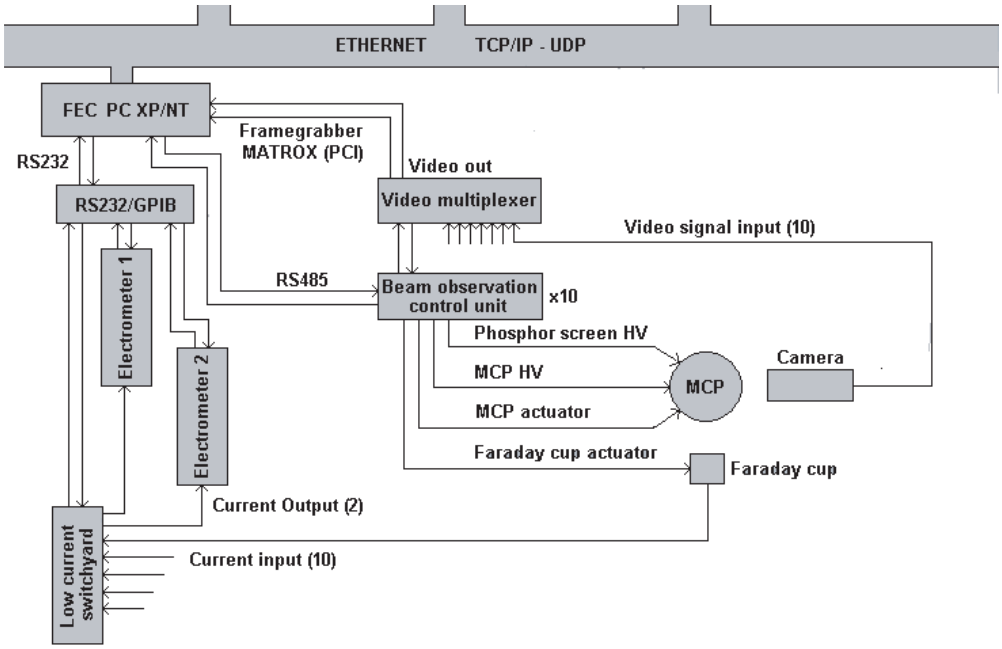

Fig. 107: Schematic of the beam diagnostic system

The client side involves three applications. The first, BDoverview, is a launch panel for the different diagnostic devices. It also shows the current status of a specific element. The second, the Profiler application (see Fig. 108), sets the parameters of the beam diagnostic units and presents the images. The parameters include the voltages mentioned above; the bin size, for reduction of the size of the transmitted data package; the region size, used to determine whether a part of the image is above noise or not; the noise level, as a percentage of pixel range; and the number of pixels in a region that should be above threshold. There are also a suppression level and a suppression number of counts that apply to the full picture to avoid flickering images when using weak pulsed beams. The third application is the Faraday cup executable. The parameters to set in this application include triggered or non-triggered readout, client and front-end computer refresh times, integration time of the electrometer and the delay time between reception of a trigger pulse and start of measurement.

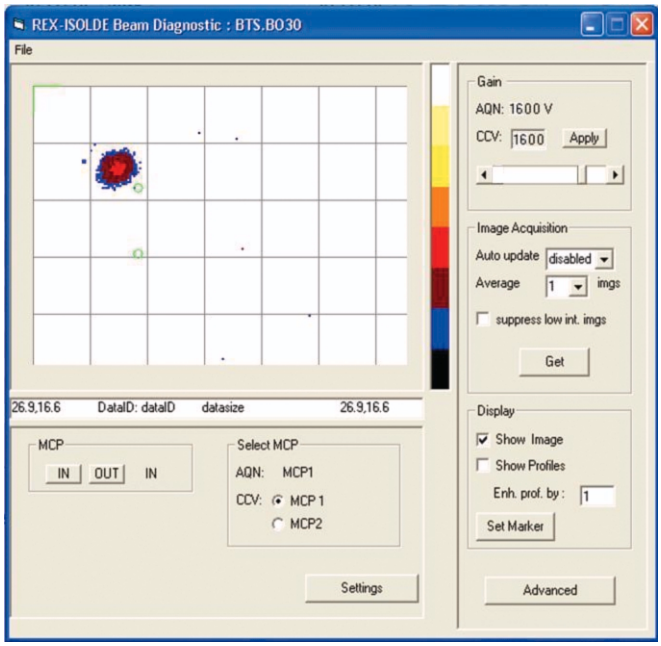

Fig. 108: The beam observation application imaging the beam after REXTRAP. This application controls one of the UHV devices. It is bi-directional. The grid lines cross at 10 mm intervals. Two circular marks can be used to note the beam spot position for comparison between different settings

4.3 The VME-OS/9 control system for REXTRAP

The REXTRAP control system is based on a system developed at the University of Mainz mainly for ion trap experiments. It has also been used by the ISOLTRAP experiment at ISOLDE. Besides its ability to control devices typically used in ion traps, it can also record data from devices such as multichannel analysers and scan different parameters. The system consists of a single-board VME Motorola 68K processor, acting as an FEC. The FEC runs the operating system OS/9 from Microware Systems Corporation. The front-end software has been developed using a cross-compiler system called Hawk. The VME processor receives calls over Ethernet and starts the different control processes via a dispatcher. There is one supervisory process running on the processor that oversees three other server processes: a device server (DevServer), a process server (ProcServer), and a data server (DataServer). The hardware configuration is shown in Fig. 109.

The VME processor is connected to the hardware via two common interfaces, PROFIBUS and GPIB. The client program requires minimum Windows NT as an operating system and is written in C++ using MS Visual Studio. The two computers are connected via Ethernet and communicate via the TCP/IP protocol. Two user interface programs are used on the PC. The first, DeviceControl, enables the setting of parameters for the devices connected to REXTRAP (power supplies, frequency generators, etc.). The second, REXTRAPControl, enables the setting of the time structure for the trap cycle, allows the scanning of parameters, and specifies which data should be taken as a function of these parameters. It also provides some graphical output for on-line data visualization.

Most of the hardware is connected to the control system via PROFIBUS. The bus is controlled by a VME-resident PROFIBUS card from Dorsch Mikrosystem that acts as bus master. Five slave units are connected: one Siemens ET200M and four WAGO I/O bus-coupler modules. The slave modules consist of a series of analog and digital input or output devices. Two slave modules on the high-voltage platform are connected to the bus master by an optical link. The more ‘intelligent’ devices, such as frequency generators, electrometers, or multichannel analysers and oscilloscopes, are connected to the FEC via GPIB and an interface card from Janz Electronic. GPIB devices on the high-voltage platform are connected via optical link.

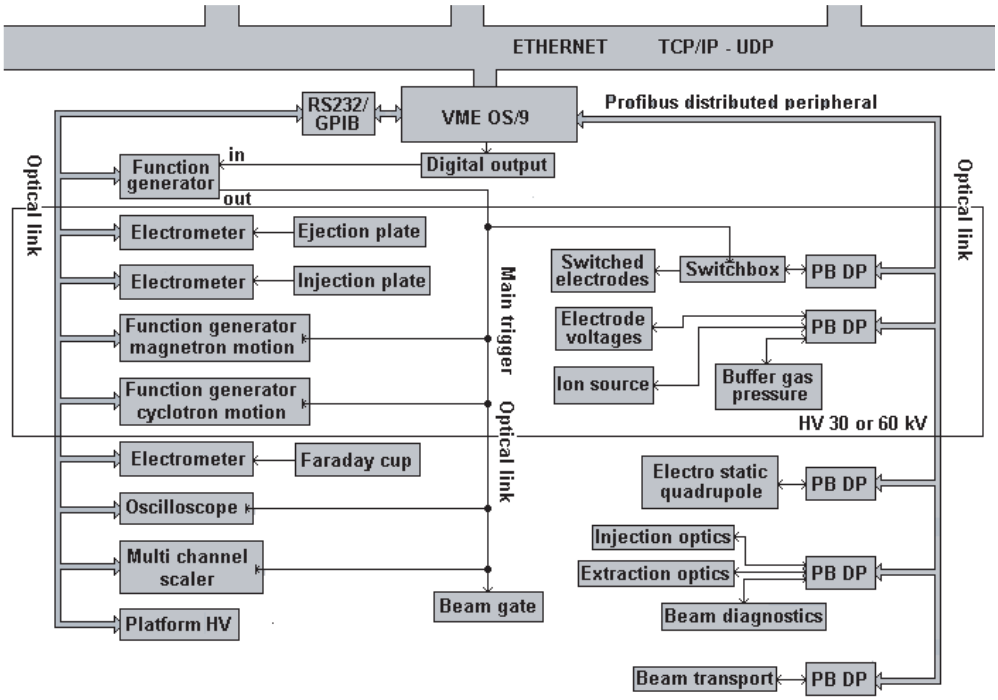

Fig. 109: Overview of the REXTRAP control

The timing of the trap operational cycle is controlled by TTL trigger signals. These are generated by a programmable 12-channel logical pattern generator (memory module) built at the University of Mainz Institute of Physics. It is programmed via a GPIB interface. The signals from the memory module are used to pulse the beam gate in front of the trap, to switch electrode voltages and the function generators for the RF signals, to trigger various data acquisition devices, and to send trigger pulses to the EBIS. The synchronization is carried out via a digital I/O interface of the VME bus. This output signal is combined by a coincidence module with the output of a common frequency generator, normally running at 49 Hz, to synchronize all REX-ISOLDE devices. Some of the applications used for Penning trap control are shown in Fig. 110.

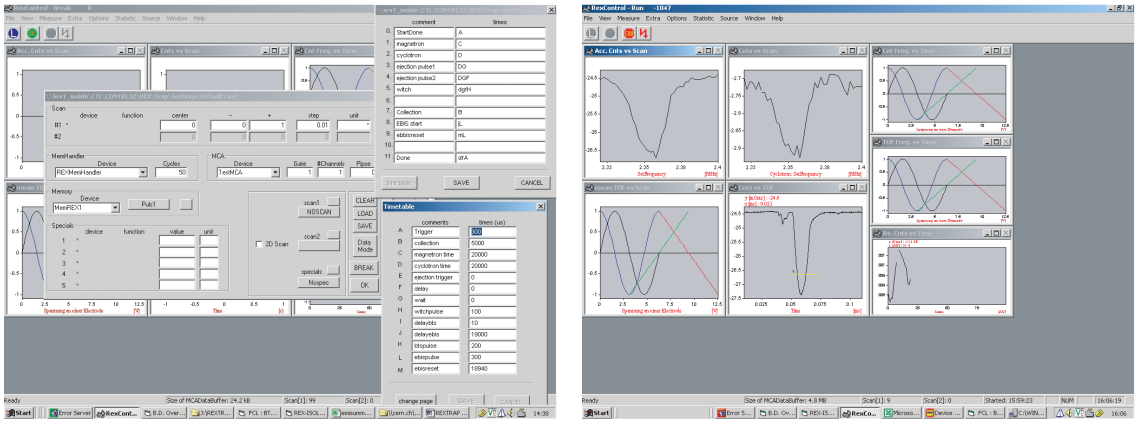

Fig. 110: Left: settings for the time signals for REXTRAP (timetable lower right); right: a typical scan. In this case the top middle panel shows a frequency scan. The bottom middle panel shows the ion signal on the MCP as a function of the time-of-flight

4.4 The OPC server approach to the RF and vacuum control systems

The RF and vacuum control systems were originally intended to be implemented using the NT/XP server model. Although equipment modules and application software were finalized, it was decided that a safer solution for first access, using simple controls for the RF system, would be to use Object Linking and Embedding for Process Control (OPC) server techniques (see Fig. 111). In particular, this approach avoids user-forced direct writing and reading of large data blocks over the bus. The equipment-specific software can be focused solely on modifying the parameters (bytes or bits) of the given equipment. In previous versions of the API provided by Siemens, the use of DP read and write functions led to situations where equipment connected to the same PROFIBUS slave would have its status data and commands re-sent, even in cases where the status of the equipment was not changed. This approach not only seemed more prone to error, but it also called for larger data transfer and decoding. The new OPC server approach from Siemens hides all such access from the user, so the user can safely access single bits and bytes of the equipment control using a tree structure for the data blocks and their components. The drawback of the current REX OPC server approach is that it does not include a database. It should be noted that the client applications can easily be adjusted to the new model and that it is planned to expand this to the vacuum control system in the near future. A widget for the vacuum system is shown in Fig. 112.

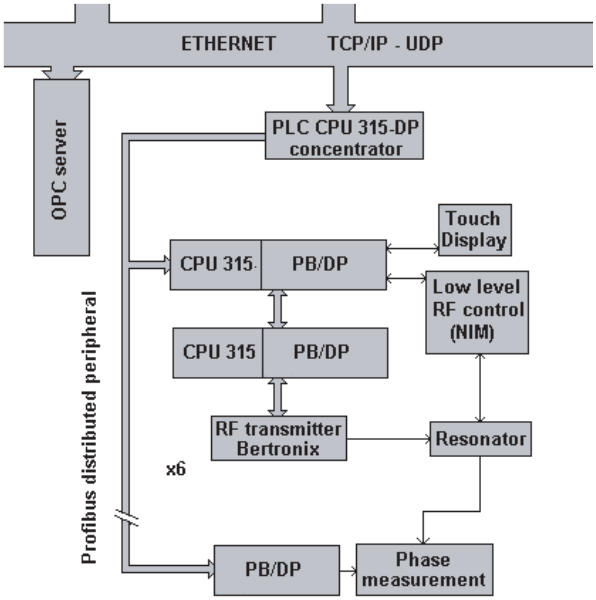

Fig. 111: The OPC RF control

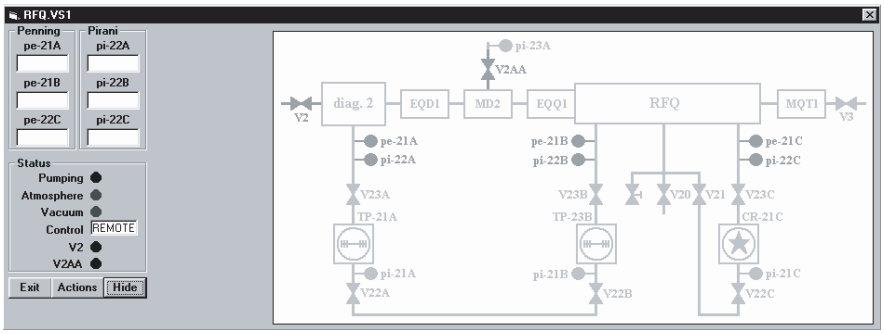

Fig. 112: Typical client control panel for the vacuum system. This shows the RFQ section

The basic architecture of the OPC RF control system involves one server, which is called from the user application using DCOM. The Siemens remote control software has to be installed on the clients before access is attempted. The OPC server maps the data blocks of a concentrator PLC, which in turn is connected via a PROFIBUS line to the rest of the equipment. In the RF case this includes six (in the near future seven) Siemens CPU 315-DPs connected to the Bertronix RF amplifiers and the NIM-based low-level control of the CERN RF group. An additional ET200M slave unit has been added to control a phase shifter unit, which automatically measures the phases between the different cavities. The update frequency of this part of the system depends on the standard timing used for the PS and is 1.2 s. The low-level RF control has also been discussed in Section 3.7.

4.5 Operator access to the control system

The main path to REX operation starts by opening a REX session. This is done by selecting REXSession under the start-up menu on one of the consoles. The REX session manager gives the option of starting several applications. The main entry into the system is either via the synoptic or the beam equipment access. The synoptic access makes it possible to start tuning panels of most equipment based at the location, whereas the equipment access option starts a program containing lists, similar to the PS working sets, of the different sections of the machine. The session manager also provides access to scanner applications. In particular it is possible to scan the separator magnet and select which isotope to post-accelerate. The trap is not currently included in this part of the software. It is possible to start a general scanning program that can scan to parameters and measure the resulting current on a Faraday cup. Which equipment to scan and where to measure the current can be freely selected. The result is presented as two projections and a colour-coded, two-dimensional plot. It is also possible to scan just one parameter, and this is the most usual application of this software. It is often used to scan the beam using the dispersion magnet to find the energy resolution of the beam.

Listed access to the equipment is made with a program named REXmonitor. This program can also scan the status of the equipment along the beam line and report any disturbances in the status of the machine. The operator is warned by a status label turning red and by a message, related to the error, being printed in a dedicated window together with the current time. The warning can also be received in audio. A dedicated application enabling an easy overview of all the linac's equipment has also been created. This can store settings to file, recall old settings, and scale settings for different A/q (starting with a known setting). These applications exist in the linac overview application as well as in REXmonitor, and settings can be shared between the two applications.

A special feature of the REX control system is the inclusion of a set of optical encoders for parameter tuning. These so-called knobs are connected to two ISA cards that decode the position of the encoders. All applications that require real-time tuning can access the position of the encoders. The current position and associated equipment of a certain encoder is also written into a shared memory segment. A special application, the so-called knobserver, can read and display this information on a panel so the user can determine which equipment is connected to which knob. This application is useful as it informs the operator which equipment is currently connected in cases where a multitude of applications are running.

Synoptic access to the vacuum system is also possible, but as low-level connection to the vacuum system is still in progress, here we note only that the option exists. A typical REX session with synoptic and list access to the equipment can be seen found in Figs. 113 and 114.

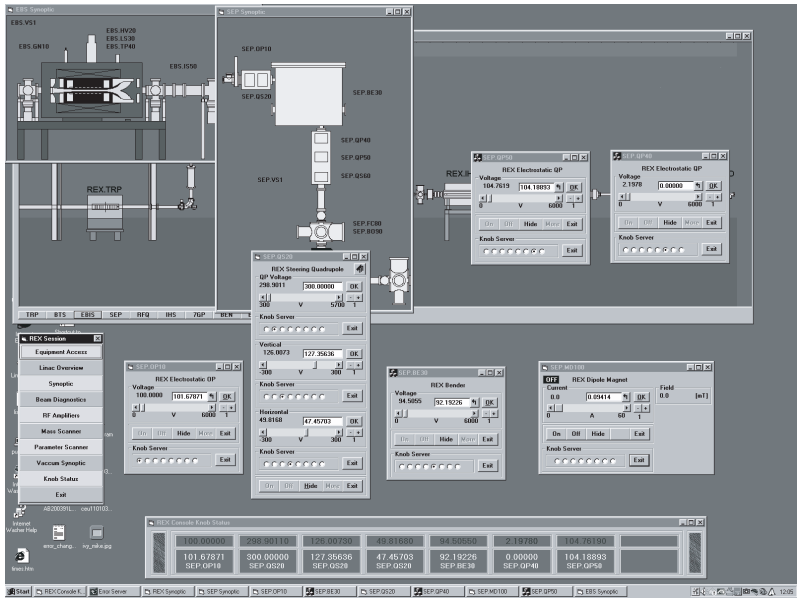

Fig. 113: A typical REX control session; the session manager in the bottom left and some of the synoptic windows at the top. A number of tuning panels are open for the separator section. Seven are connected to the optical encoders for tuning: these can be identified in the knobserver application at the bottom

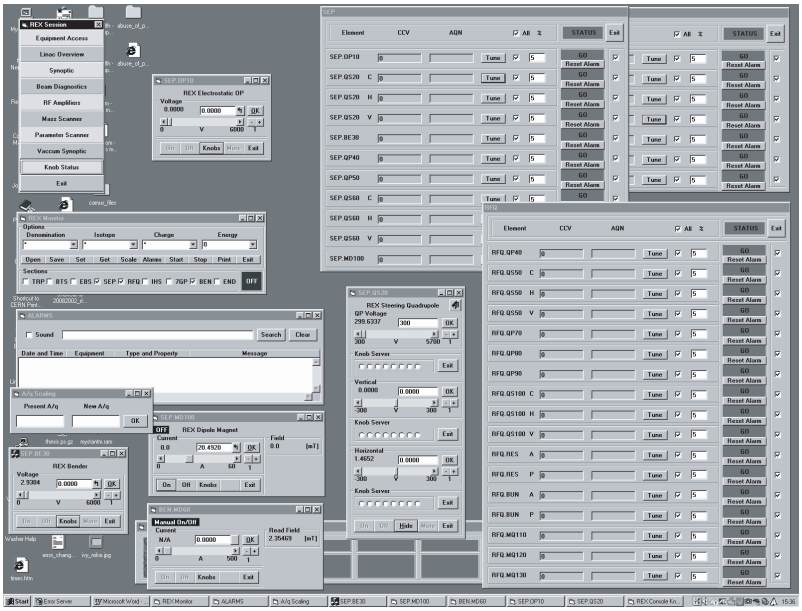

Fig. 114: List access to equipment using REXmonitor. Three sections are open. The main window of the application is immediately below the session manager in the upper left corner. Below that window is in turn the alarms window. The scaling window is open and shown on top of the alarms window. The application is not scanning for errors in this case and not too surprisingly no error messages are presented in the window. A number of tuning panels have been opened by pressing tune buttons in the section panels

References

[1] P. Schmidt, F. Ames, G. Bollen, O. Forstner, G. Huber, M. Oinonen and J. Zimmer, *Nucl. Phys.* **A701** (2002) 550c.

[2] M. König, G. Bollen, H.-J. Kluge, T. Otto and J. Szerypo, *Int. J. Mass Spectrom. Ion Process.* **142** (1995) 95.

[3] H. Raimbault-Hartmann, D. Beck, G. Bollen, M. König, H.-J. Kluge, E. Schark, J. Stein, S. Schwarz and J. Szerypo, *Nucl. Instrum. Methods Phys. Res.* **B126** (1997) 378.

[4] D.H.E. Dubin and T.M. O'Neil, *Rev. Mod. Phys.* **71** (1999) 87;
J.J. Bollinger, D.J. Heinzen, F.L. Moore, Wayne M. Itano, D.J. Wineland and D.H.E. Dubin, *Phys. Rev.* **A48** (1993) 525;
F. Anderegg, X.-P. Huang, E. Sarid and C.F. Discroll, *Rev. Sci. Instrum.* **68** (1997) 2367.

[5] SIMION 3D Vers. 7.0 (2000) Idaho National Engineering and Environmental Lab., Idaho Falls, USA.

[6] A. Wilfart, Diploma thesis, LMU, Munich, 2002.

[7] M. Beck *et al.*, *Nucl. Instrum. Methods Phys. Res.* **A503** (2003) 567.

[8] P. van Duppen *et al.*, *Nucl. Instrum. Methods Phys. Res.* **B93** (1994) 378.

[9] B. Visentin, *Nucl. Instrum. Methods Phys. Res.* **B101** (1995) 275.

[10] F. Wenander *et al.,* REXEBIS, the electron beam ion source for the REX-ISOLDE project: Design and simulations, CERN OPEN-2000-320 (2000).

[11] J.H. Billen and L.M. Young, Proc. 1993 Particle Accelerator Conference, Washington, 1993 (IEEE, New York, 1993), vol. 2, p. 790.

[12] R. Rao and F. Wenander, *Nucl. Instrum. Methods Phys. Res.* **A416** (1998) 210.

[13] H. Nishihara, M. Tereda, *J. Appl. Phys.* **39** (1968) 4573;
H. Nishihara, M. Tereda, *J. Appl. Phys.* **41** (1970) 3322.

[14] FEI Company, Beam Technology Division, Technical Bulletin No. 3, FEI Co., US. http://www.feibeamtech.com/ .

[15] SAES Getters, S.p.A., Milan, Italy. http://www.saesgetters.com/ .

[16] A.O. Nier and T.R. Roberts, *Phys. Rev.* **81** (1951) 507.

[17] R. Rao *et al.*, *Nucl. Instrum. Methods Phys. Res.* **A427** (1999) 170.

[18] H. Wollnik, *Optics of Charged Particles* (Academic Press, San Diego, 1987).

[19] H. Matsuda *et al.*, *Nucl. Instrum. Methods Phys. Res.* **A258** (1987) 310.

[20] O. Kester *et al.*, *Nucl. Instrum. Methods Phys. Res.* **B204** (2003) 20.

[21] T. Sieber, 'Entwicklung von 4-Rod- und IH-Radio Frequenz Quadrupol (RFQ)-Beschleunigern für radioaktive Ionenstrahlen bei REX-ISOLDE und MAFF', Ph.D. thesis, LMU München, May 2001.

[22] S. Emhofer, 'Aufbau und Vermessung der HF-Eigenschaften des REX-ISOLDE-IH-Beschleunigers', Diploma thesis, LMU München, December 1999.

[23] H. Podlech *et al.*, Proc. Seventh European Particle Accelerator Conference, Vienna, 2000 (EPS, Geneva, 2000), p. 572.

[24] K. U. Kühnel, Diploma thesis, IAP Frankfurt, 1999.

[25] K.R. Crandall *et al.*, PARMTEQ, LA-UR-96-1836.

[26] U. Ratzinger, LORASR, GSI/INT/0791.

[27] M. Griesser, LINAC2.0, MPI-K Heidelberg.

[28] B. Franczak, MIRKO Version 5.13 Handbuch, GSI Darmstadt, 1989.

[29] K. Makino and M. Bertz, COSY Infinity version 8, *Nucl. Instrum. Methods Phys. Res.* **A427** (1999) 338.

[30] O. Kester *et al.*, Proc. 2003 Particle Accelerator Conference, Portland, Oregon, 2003 (IEEE, New York, 2003) p. 2872.

[31] Marc Dietrich, SSP Eu exp. 2003 (INTC proposal).

[32] R.H. Stokes, T.P. Wangler, *Annu. Rev. Nucl. Part. Sci.* **38** (1989) 97.

[33] A. Schempp *et al., Nucl. Instrum. Methods Phys. Res.* **B10/11** (1985) 831.

[34] D.C. Carey, Third order TRANSPORT, SLAC-R-95-462.

[35] U. Ratzinger, N. Angert and J. Klabunde, GSI Scientific Report 1987.

[36] D. Warner *et al.*, CERN Heavy-Ion Facility Design Report, CERN 93-01.

[37] http://www.cst.de .

[38] U. Ratzinger, 'Effiziente Hochfrequenz-Linearbeschleuniger für leichte und schwere Ionen', Habilitationsschrift, Uni Frankfurt, 1998.

[39] R. von Hahn *et al.*, *Nucl. Instrum. Methods Phys. Res.* **A328** (1993) 270.

[40] D. Habs *et al.*, *Nucl. Instrum. Methods Phys. Res.* **B204** (2003) 739.

[41] H. Bongers, 'Untersuchung eines IH-7-Spalt-Resonators zur Energievariation beschleunigter radioaktiver Strahlen', Ph.D. thesis, LMU München, April 2003.

[42] O. Kester, 'A short IH cavity for the energy variation of radioactive ion beams', Proc. Eighth European Particle Accelerator Conference, Paris, 2002 (EPS, Geneva, 2002), p. 915.

[43] O. Kester *et al.*, *Nucl. Instrum. Methods Phys. Res.* **B139** (1998) 28.

[44] T. Sieber *et al.*, Tests and First Experiments with the new REX-ISOLDE 200 MHz IH structure, Proc. LINAC2004, 2004, Lübeck, Germany.

[45] Bertronix Manual KB/SVS-101/100-P.

[46] Bertronix Manual KB/SVS-202/100-P.

[47] I. Deloose, PS/CO Note 96-44, PC/CO Note 97-29, PS/CO Note 98-33.

[48] K. Kruglov *et al.*, *Nucl. Phys.* **A 701** (2002) 193.

Bibliography

Eurisol report 2003 and references therein, www.ganil.fr/eurisol/Final_Report.html .

NSAC ISOL task force report and experimental programme for an advanced ISOL facility and references therein, www.sc.doe.gov/henp/np/nsac/harrison/harrison.html .

Appendix A: REXTRAP devices

Table A1: Control devices for REXTRAP

Name	Description	Model/type	Interface	Functions	Comments
HV	high voltage for platform	FUG +PROBUS 65 000 V 2 mA	GPIB	set voltage read voltage set current read current on/off	modified for 10^{-5} stability
RA0.QP	quadrupole steering triplet	6 x ISOLDE +/–3500 V	analog	SetQP1 SetQP2 SetQS3Quadrupole SetQS3offset SetQS3Horizontal SetQS3Vertical ReadQP1 ReadQP2 ReadQS3	
Injection kicker	horizontal / vertical kicker	ISOLDE +/–3500 V ISOLDE +/–700 V	analog	SetHorizV SetVertV ReadHorizV ReadVertVU ReadVertVD	upper electrode can be connected as beam gate
Injection lens	repeller for electrons	ISOLDE +/–700V	analog	set voltage read voltage	
Deceleration pot	first step for deceleration	FUG –12500 V 0.5 mA	analog	set voltage read voltage read current	
Transfer pot	intermediate potential	FUG –3500 V 2 mA	analog	set voltage read voltage read current	
Injection steerer	x/y steerers	E Lab Mainz 2 of 4 channels +/–200 V	analog	set horizontal voltage set vertical voltage read horizontal voltage read vertical voltage	output on transfer potential
Electrode 01	Einzel lens	FUG –3500 V 2 mA	analog	set voltage read voltage read current	
Electrode 02	intermediate voltage	ISOLDE –3500 V	analog	set voltage read voltage	
Electrode 03	intermediate voltage	ISOLDE –3500 V	analog	set voltage read voltage	
Electrode 05	maximum of potential well	FUG 3500 V 2 mA	analog	set voltage read voltage read current	upper voltage for voltage divider
Electrode 16	minimum of linear part of potential well	FUG 3500 V 2 mA	analog	set voltage read voltage read current	lower voltage for voltage divider

Name	Description	Model/type	Interface	Functions	Comments
Electrode 17	inner trap electrode switching possible	amplifier +/– 200 V Munich electronic	analog + switchbox	set voltage1 set voltage2	pulsed
Electrode 18	inner trap electrode switching possible	amplifier +/– 200 V Munich electronic	analog + switchbox	set voltage1 set voltage2	pulsed 2 fold segmented electrode
Electrode 20	central trap electrode switching possible	amplifier +/– 200 V Munich electronic	analog + switchbox	set voltage1 set voltage2	8 fold segmented electrode no static voltage connected
Electrode 24	inner trap electrode switching possible	amplifier +/– 200 V Munich electronic	analog + switchbox	set voltage1 set voltage2	pulsed 2 fold segmented electrode
Electrode 26	inner trap electrode switching possible	amplifier +/– 200 V Munich electronic	analog + switchbox	set voltage1 set voltage2	pulsed
Electrode 27	inner trap electrode switching possible	amplifier +/– 200 V Munich electronic	analog + switchbox	set voltage1 set voltage2	pulsed
Electrode 28	inner trap electrode switching possible	amplifier +/– 200 V Munich electronic	analog + switchbox	set voltage1 set voltage2	pulsed
Electrode 29	outer trap electrode switching possible	TREK +/–750 V	analog + switchbox	set voltage1 set voltage2	pulsed
Electrode 32	outer trap electrode switching possible	TREK +/–750 V	analog + switchbox	set voltage1 set voltage2	pulsed
Electrode 33	outer trap electrode switching possible	TREK +/–750 V	analog + switchbox	set voltage1 set voltage2	pulsed
Electrode 36	maximum of potential well	TREK +/–750 V	analog + switchbox	set voltage1 set voltage2	pulsed
Electrode 37	intermediate voltage	ISOLDE –3500 V	analog	set voltage read voltage	
Electrode 38	intermediate voltage	ISOLDE –3500 V	analog	set voltage read voltage	
Electrode 39	intermediate voltage	ISOLDE –3500 V	analog	set voltage read voltage	
Electrode 40	Einzel lens	–7500 V 1 mA	analog	set voltage read voltage	

Name	Description	Model/type	Interface	Functions	Comments
Electrode steerer	x/y steerers	E Lab Mainz 2 of 4 channels +/–200 V	analog	set horizontal voltage set vertical voltage read horizontal voltage read vertical voltage	output on transfer potential
Acceleration pot	first step for acceleration	FUG –12500 V 0.5 mA	analog	set voltage read voltage read current	
Ejection lens	repeller for electrons	ISOLDE +/–700 V	analog	set voltage read voltage	
Ejection kicker	steerer on ground potential	ISOLDE +/–700 V	analog	set horizontal voltage set vertical voltage read horizontal voltage read vertical voltage	
Einzel lens	lens	FUG 65000 V 2 mA	analog	set voltage read voltage read current	
Magnetron	function generator	Stanford DS345	GPIB	SetFrequency SetAmplitude Setoffset SetWaveform SetPhase SetDelay SetGate SetPulse SetRamp GaussMod	
Cyclotron	function generator	Stanford DS345	GPIB	SetFrequency SetAmplitude Setoffset SetWaveform SetPhase SetDelay SetGate SetPulse SetRamp GaussMod EnableSweep SetStartFrequency SetStopFrequency SetSweepRate SetModulationType SetModulationWave SetTriggerSrc	
Beam gate	switch	WAGO	digital	In/Out	beam gate remote controlled or open

Appendix B: Beam transfer system devices

Table B1: BTS devices

Name	Description	Model/type	Interface	Functions	Comments
BTS.KI10	kicker supply	+3500 V 1 mA –3500 V 1 mA	analog	set voltage read voltage	
BTS.BE40	electrostatical bender	+7500 V 1 mA –7500 V 1 mA	analog	set voltage read voltage	sets voltages for spherical bender
BTS.QT50	quadrupole steering triplet	2 x +3500 V 1 mA 2 x –3500 V 1 mA 4 x +7500 V 1 mA 4 x –7500 V 1 mA	analog	SetQP1 SetQP2 SetQS3Quadrupole SetQS3offset SetQS3Horizontal SetQS3Vertical ReadQP1 ReadQP2 ReadQS3	
BTS.QT100	quadrupole steering triplet	2 x +3500 V 1 mA 2 x –3500 V 1 mA 4 x +7500 V 1 mA 4 x –7500 V 1 mA	analog	SetQP1 SetQP2 SetQS3Quadrupole SetQS3offset SetQS3Horizontal SetQS3Vertical ReadQP1 ReadQP2 ReadQS3	
BTS.BE130	electrostatical bender	+7500 V 1 mA –7500 V 1 mA	analog	set voltage read voltage	sets voltages for spherical bender
BTS.KI140	kicker supply	+3500 V 1 mA –3500 V 1 mA	analog	set voltage read voltage	

Appendix C: REXTRAP offline ion source devices

Table C1: REXTRAP offline ion source devices

Name	Description	Model/type	Interface	Functions
IonSource	ion source	Xantrex 12 V 100 A FUG 3500 V 2 mA	analog /digital	SetHeatingC ReadHeatingC FanOn FanOff SetOffsetV ReadOffsetV ReadOffsetC
SourceSteerer	x/y steerer	ISOLDE +/- 700 V	analog	SetHorizV SetVertV ReadHorizVL ReadHorizVR ReadVertVU ReadVertVD
SourceBenderPos	positive bender voltage	FUG 6500 V 1 mA	analog	SetVoltage ReadVoltage ReadCurrent
SourceBenderNeg	negative bender voltage	FUG 6500 V 1 mA	analog	SetVoltage ReadVoltage ReadCurrent

Appendix D: REXEBIS devices

Table D1: REXEBIS hardware. S&H stands for sample and hold unit

Device	Function	Mode	Type	Control function
Gun platform	Cathode heater voltage	R/W	analog d.c.	PROFIBUS
	Cathode heater current	R	analog d.c	PROFIBUS
	Collector voltage	R/W	analog d.c	PROFIBUS
	Collector current	R	analog d.c	PROFIBUS
	Suppressor voltage	R/W	analog d.c	PROFIBUS
	Suppressor current	R	analog d.c	PROFIBUS
REXEBIS platform	Trap 1 voltage	R/W	µs switching	Function generator controlled, R:S&H
	Trap 2 voltage	R/W	µs switching	Function generator controlled, R:S&H
	Trap 3 voltage	R/W	µs switching	Function generator controlled, R:S&H
	Outer barrier voltage	R/W	µs switching	Function generator controlled, R:S&H
	Cathode voltage	R/W	analog d.c.	PROFIBUS, R:S&H
	Cathode current	R/W	analog d.c.	PROFIBUS, R:S&H
	Extractor voltage 1	R/W	analog d.c.	PROFIBUS
	Extractor current 1	R/W	analog d.c.	PROFIBUS
	Extractor voltage 2	R/W	analog d.c.	PROFIBUS
	Extractor current 2	R/W	analog d.c.	PROFIBUS
	Inner Einzel lens voltage	R/W	ms switching	W:PROFIBUS, R:S&H
	Outer Einzel lens voltage	R/W	ms switching	W:PROFIBUS, R:S&H
	Gun vacuum, Pe	R	analog	PROFIBUS
	Collector vacuum, Pe	R	analog	PROFIBUS
	OVC vacuum full range	R	analog	ISOLDE controlled
	2 gate valves	R/W	digital	ISOLDE controlled
	2 turbos	R/W	digital	ISOLDE controlled
Ground potential	HV platform switching	W	µs switching	Function generator controlled
	2 inner deflector x voltage	R/W	ms switching	PROFIBUS, R:S&H
	2 inner deflector y voltage	R/W	ms switching	PROFIBUS, R:S&H
	2 outer deflector x voltage	R/W	ms switching	PROFIBUS, R:S&H
	2 outer deflector y voltage	R/W	ms switching	PROFIBUS, R:S&H
	3 cooling water flow	R/W	digital	ISOLDE controlled
	Optics turbo	R/W	analog	ISOLDE controlled
	Prevacuum turbo	R/W	analog	ISOLDE controlled
	Gate valve	R/W	analog	ISOLDE controlled
	Leak valve	R/W	analog	ISOLDE controlled
	End valve	R/W	analog	ISOLDE controlled
	Rough valves	R/W	analog	ISOLDE controlled
	Optics vacuum, Pe and Pi	R	analog	ISOLDE controlled
	Preturbo vacuum, full range	R	analog	ISOLDE controlled

Appendix E: Cooling circuit of the IH structure

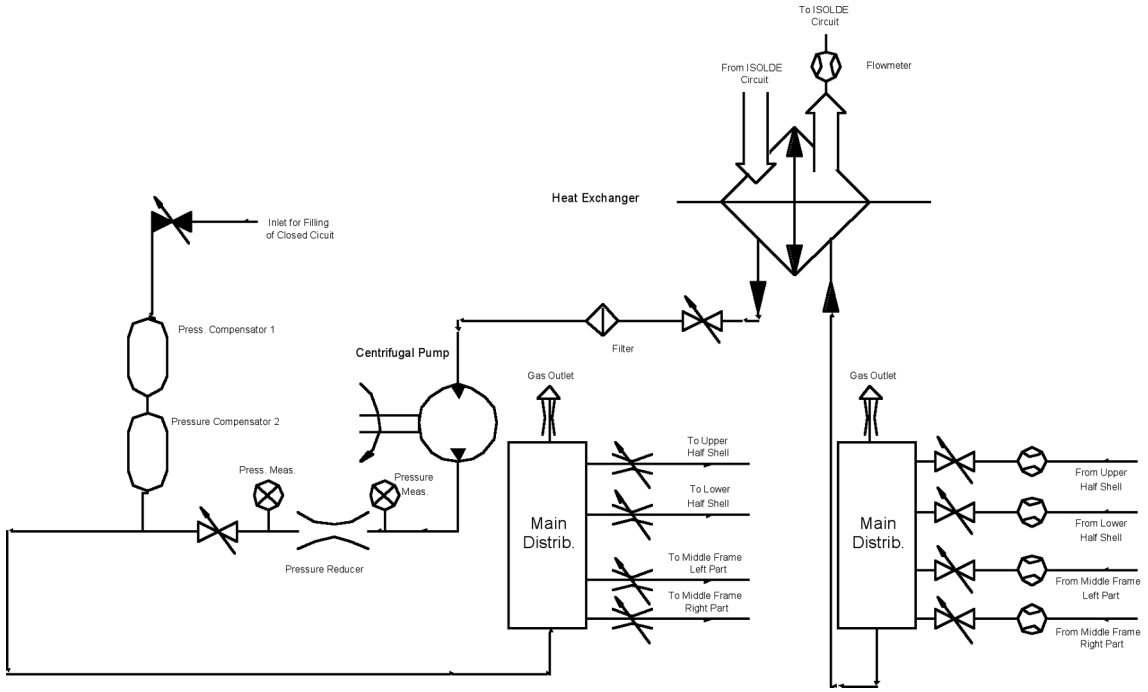

Fig. E1: IH black steel cooling circuit

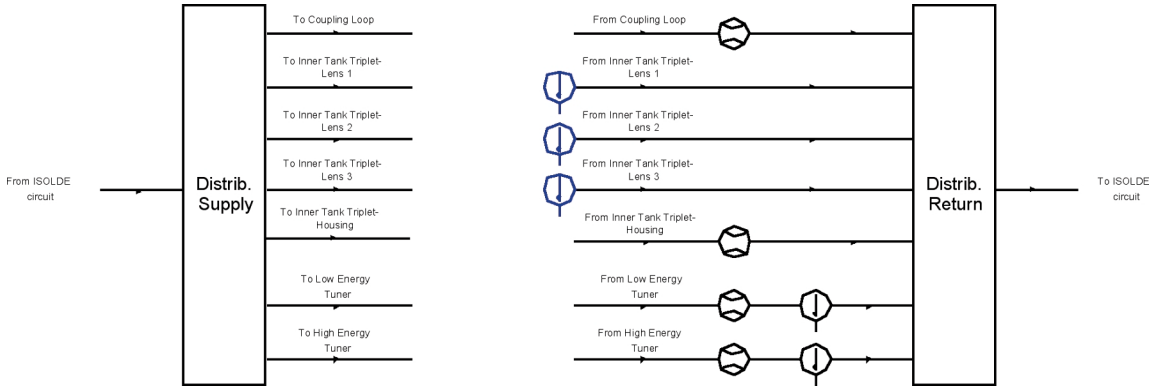

Fig. E2: IH stainless-steel cooling circuit

Appendix F: Magnetic field–current dependence of the REX magnets

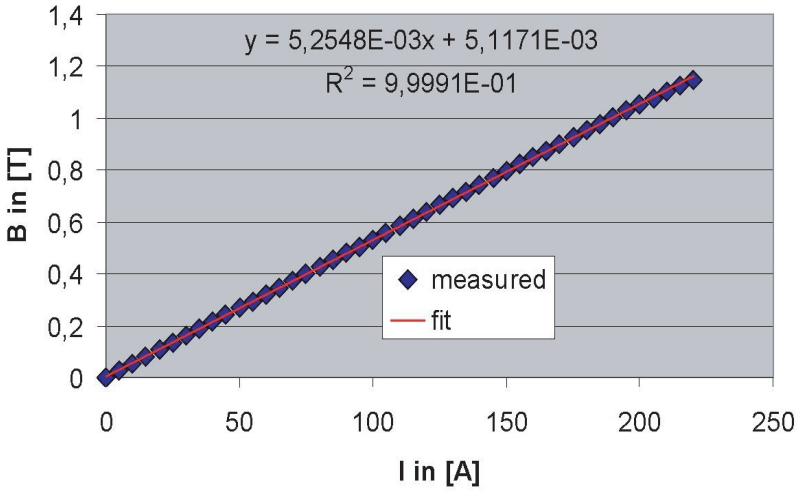

Fig. F1: B vs I for BEN.MD60

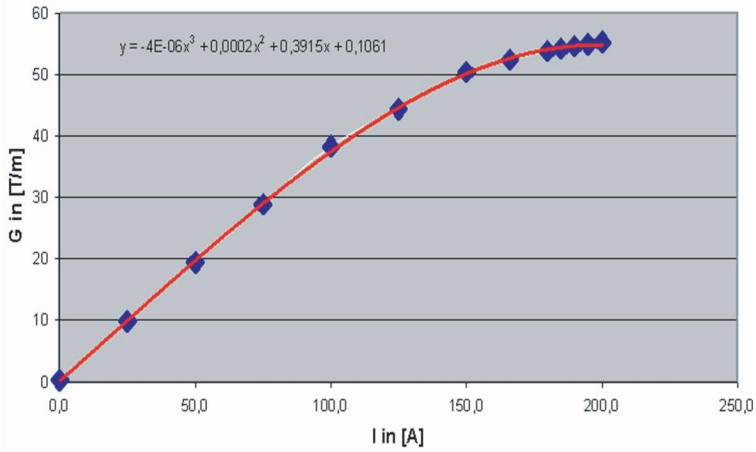

Fig. F2: Gradients for RFQ.MQ110, RFQ.MQ130, IHS.MQ30 and IHS.MQ50

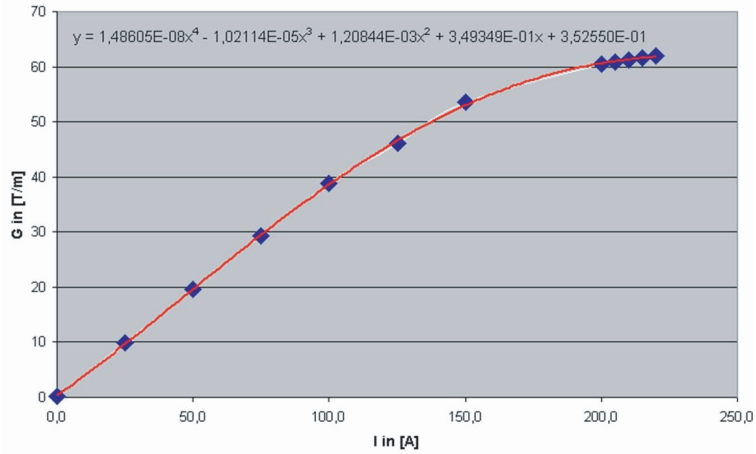

Fig. F3: Gradients for RFQ.MQ120 and IHS.MQ40

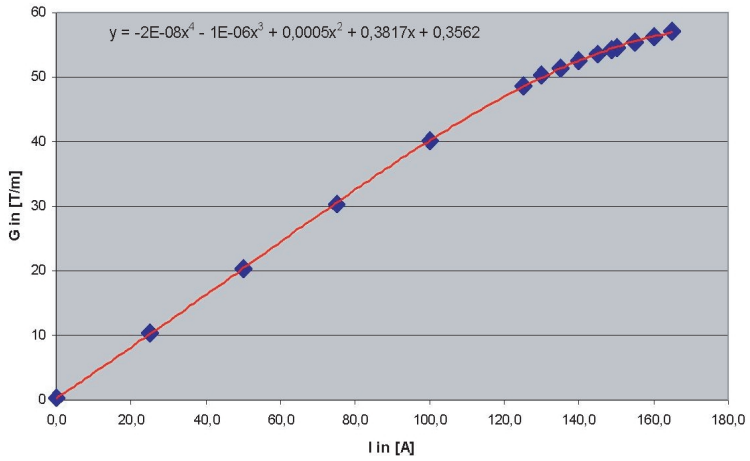

Fig. F4: Gradients for IHS.MQ60 and IHS.MQ80

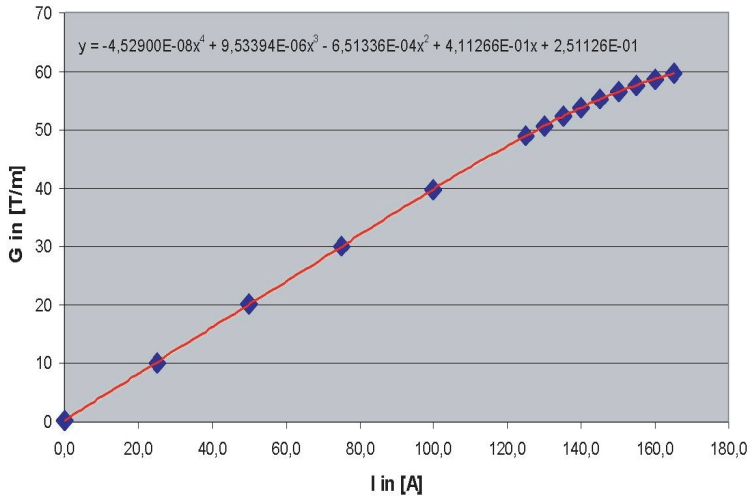

Fig. F5: Gradient for IHS.MQ70

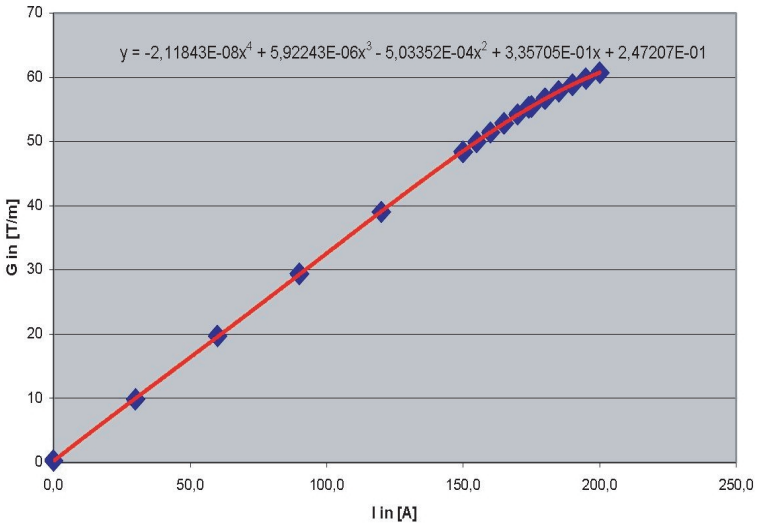

Fig. F6: Gradients for IHS.MQ90 and IHS.MQ110

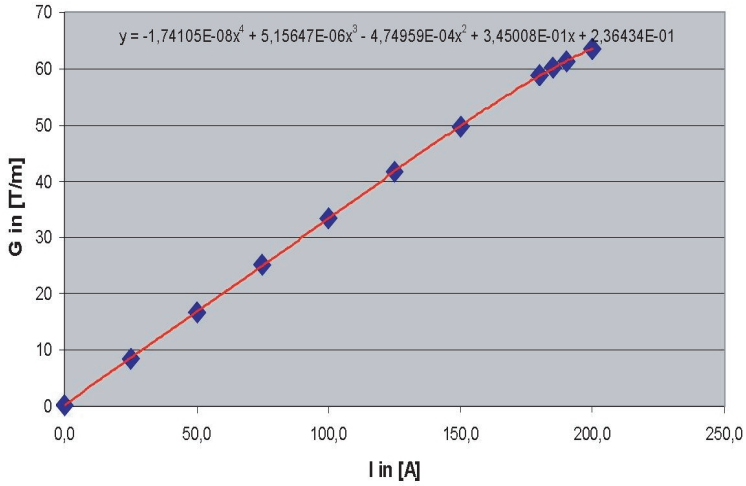

Fig. F7: Gradient for IHS.MQ100

Appendix G: Mass separator beams

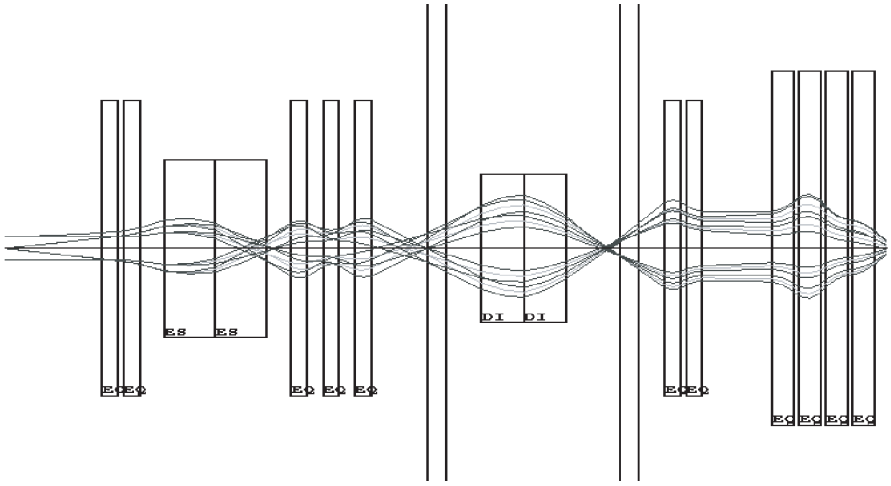

Fig. G1: Beam in x-(dispersive) direction through the mass separator

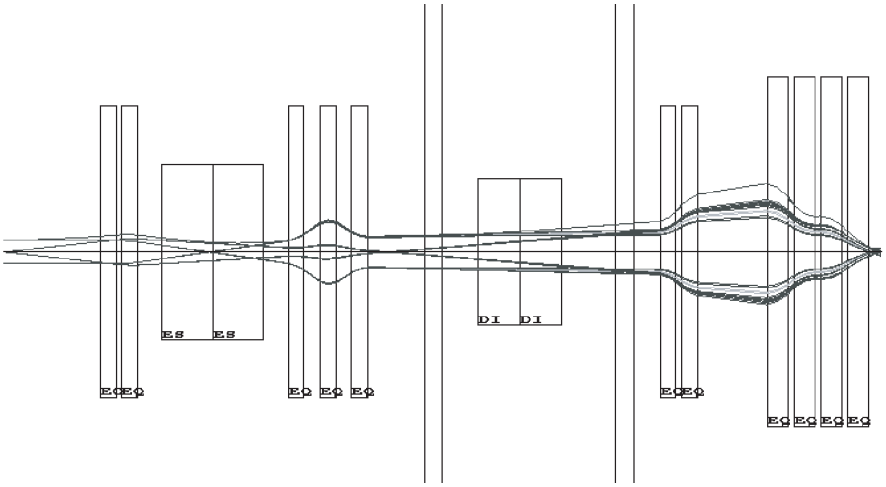

Fig. G2: Beam in y-direction through the mass separator

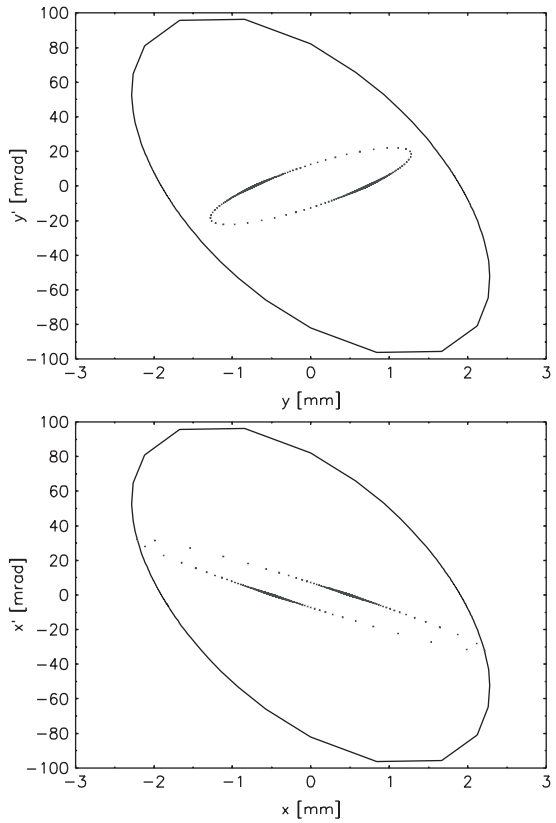

Fig. G3: Third-order calculation of the injection emittances of the separator into the RFQ in comparison with the RFQ acceptance

Appendix H: Control system devices

Table H1: Description of PROFIBUS slave number 19 controlling REXEBIS hardware.
In particular this slave controls switched voltages for beam steering.
Note that input and output use separate address spaces

Equipment name	Description	Period	Element	Address	Module	Function
EBS.ST90 EBS.GDG07	inner steering	injection	top	8	750-456	analog input 0–10V
EBS.ST90 EBS.GDG07	inner steering	injection	bottom	10	750-456	analog input 0–10V
EBS.ST90 EBS.GDG07	inner steering	injection	left	12	750-456	analog input 0–10V
EBS.ST90 EBS.GDG07	inner steering	injection	right	14	750-456	analog input 0–10V
EBS.ST100 EBS.GDG08	inner steering	extraction	top	24	750-456	analog input 0–10V
EBS.ST100 EBS.GDG08	inner steering	extraction	bottom	26	750-456	analog input 0–10V
EBS.ST100 EBS.GDG08	inner steering	extraction	right	28	750-456	analog input 0–10V
EBS.ST100 EBS.GDG08	inner steering	extraction	left	30	750-456	analog input 0–10V
EBS.ST110 EBS.GDG09	outer steering	injection	top	0	750-456	analog input 0–10V
EBS.ST110 EBS.GDG09	outer steering	injection	bottom	2	750-456	analog input 0–10V
EBS.ST110 EBS.GDG09	outer steering	injection	right	4	750-456	analog input 0–10V
EBS.ST110 EBS.GDG09	outer steering	injection	left	6	750-456	analog input 0–10V
EBS.ST120 EBS.GDG10	outer steering	extraction	top	16	750-456	analog input 0–10V
EBS.ST120 EBS.GDG10	outer steering	extraction	bottom	18	750-456	analog input 0–10V
EBS.ST120 EBS.GDG10	outer steering	extraction	right	20	750-456	analog input 0–10V
EBS.ST120 EBS.GDG10	outer steering	extraction	left	22	750-456	analog input 0–10V
EBS.ST130 EBS.GDG11	extern. steering	injection	left	32	750-456	analog input 0–10V
EBS.ST130 EBS.GDG11	extern. steering	injection	right	34	750-456	analog input 0–10V
EBS.ST130 EBS.GDG11	extern. steering	injection	top	36	750-456	analog input 0–10V

Equipment name	Description	Period	Element	Address	Module	Function
EBS.ST130 EBS.GDG11	extern. steering	injection	bottom	38	750-456	analog input 0–10V
EBS.ST140 EBS.GDG12	extern. steering	extraction	left	40	750-456	analog input 0–10V
EBS.ST140 EBS.GDG12	extern. steering	extraction	right	42	750-456	analog input 0–10V
EBS.ST140 EBS.GDG12	extern. steering	extraction	top	44	750-456	analog input 0–10V
EBS.ST140 EBS.GDG12	extern. steering	extraction	bottom	46	750	analog input 0–10V
EBS.ST130	extern. steering	injection	top	10	750-556	analog output 0–10 V
EBS.ST130	extern. steering	injection	left	12	750-556	analog output 0–10 V
EBS.ST130	extern. steering	injection	right	14	750-556	analog output 0–10 V
EBS.ST130	extern. steering	injection	down	16	750-556	analog output 0–10 V
EBS.ST140	extern. steering	extraction	top	0	750-556	analog output 0–10 V
EBS.ST140	extern. steering	extraction	left	2	750-556	analog output 0–10 V
EBS.ST140	extern. steering	extraction	right	4	750-556	analog output 0–10 V
EBS.ST140	extern. steering	extraction	down	6	750-556	analog output 0–10 V
GDG not activated	extern. steering	injection		48	750-456	analog input 0–10 V
GDG not activated	extern. steering	extraction		50	750-456	analog input 0–10 V
GDG not activated	extern. steering	injection		52	750-456	analog input 0–10 V
GDG not activated	extern. steering	extraction		54	750-456	analog input 0–10 V

Table H2: Description of PROFIBUS slave number 20 controlling REXEBIS hardware.
The hardware is used for electron beam creation, manipulation and collection.
Input and output use separate address spaces

Equipment name	Description	Period	Address	Module	Function
EBS.CO30	collector V	static	0	750-468	analog out 0–10 V
EBS.CO30	collector I	static	2	750-468	analog out 0–10 V
EBS.SU40	suppressor V	static	4	750-468	analog out 0–10 V
EBS.SU40	suppressor I	static	6	750-468	analog out 0–10 V
EBS.CA50	cathode heat.V	static	8	750-468	analog out 0–10 V
EBS.CA50	cathode heat. I	static	10	750-468	analog out 0–10 V
	spare	static	12	750-468	analog out 0–10 V
	spare	static	14	750-468	analog out 0–10 V
EBS.CO30	collector enable	static	12	750-514	relay output module
EBS.SU40	collector enable	static	12, bit 1	750-514	relay output module
EBS.CA50	cath. heat. enable	static	12, bit 2	750-514	relay output module

Equipment name	Description	Period	Address	Module	Function
EBS.CO30	collector V	static	12, bit 3	750-550	analog input ±10 V
EBS.CO30	collector I	static	2	750-550	analog input ±10 V
EBS.SU40	suppressor V	static	4	750-550	analog input ±10 V
EBS.SU40	suppressor I	static	6	750-550	analog input ±10 V
EBS.CA50	cathode heat.V	static	8	750-550	analog input ±10 V
EBS.CA50	cathode heat. I	static	10	750-550	analog input ±10 V

Table H3: PROFIBUS slave number 21 controlling REXEBIS hardware. The slave controls the electron gun acceleration voltage, the extractor voltages, and the read-back of the switched drift-tube voltages, which are set with the VME-resident function generators (GFAS). Input and output use separate address spaces

Equipment name	Description	Period	Address	Module	Function
EBS.EL60	electron gun V	static	0	750-468	analog input 0–10 V
EBS.EL60	electron gun I	static	2	750-468	analog input 0–10 V
EBS.EX70	extractor 1 V	static	4	750-468	analog input 0–10 V
EBS.EX70	extractor 1 I	static	6	750-468	analog input 0–10 V
EBS.EX80	extractor 2 V	static	8	750-468	analog input 0–10 V
EBS.EX80	extractor 2 I	static	10	750-468	analog input 0–10 V
	spare		12	750-468	analog input 0–10 V
	spare		14	750-468	analog input 0–10 V
EBS.EL60	electron gun V	static	0	750-556	analog output 0–10 V
EBS.EL60	electron gun I	static	2	750-556	analog output 0–10 V
EBS.EX70	extractor 1 V	static	4	750-550	analog output 0–10 V
EBS.EX70	extractor 1 I	static	6	750-550	analog output 0–10 V
	spare		8	750-550	relay output module
	spare		10	750-550	relay output module
	spare		12	750-550	relay output module
	spare		14	750-550	relay output module
EBS.EL60	electron gun enable	static	16, bit 1	750-550	relay output module
EBS.EX70	extractor 1 enable	static	16, bit 2	750-550	relay output module
EBS.EX80	extractor 2 enable	static	16, bit 3	750-550	relay output module
	spare		16	750-550	relay output module
EBS.GDG05	drift-tube 1 V	injection	16	750-456	analog input ±10 V
EBS.GDG05	drift-tube 2 V	injection	18	750-456	analog input ±10 V
EBS.GSD05	drift-tube 3 V	injection	20	750-456	analog input ±10 V
EBS.GDG05	drift-tube 4 V	injection	22	750-456	analog input ±10 V
EBS.GDG05	used in switched mode		24	750-456	analog input ±10 V
EBS.GDG05	used in switched mode		26	750-456	analog input ±10 V

Equipment name	Description	Period	Address	Module	Function
EBS.GDG05	used in switched mode		28	750-456	analog input ±10 V
EBS.GDG05	used in switched mode		30	750-456	analog input ±10 V
EBS.GDG06	drift-tube 1 V	breeding	32	750-456	analog input ±10 V
EBS.GDG06	drift-tube 2 V	breeding	34	750-456	analog input ±10 V
EBS.GDG06	drift-tube 3 V	breeding	36	750-456	analog input ±10 V
EBS.GDG06	drift-tube 4 V	breeding	38	750-456	analog input ±10 V
EBS.GDG06	used in switched mode		40	750-456	analog input ±10 V
EBS.GDG06	used in switched mode		42	750-456	analog input ±10 V
EBS.GDG06	used in switched mode		44	750-456	analog input ±10 V
EBS.GDG06	used in switched mode		46	750-456	analog input ±10 V
EBS.GDG17	currently not in use			750-456	analog input ±10 V
EBS.GDG17	currently not in use			750-456	analog input ±10 V
EBS.GSD17	currently not in use			750-456	analog input ±10 V
EBS.GDG17	currently not in use			750-456	analog input ±10 V
EBS.GDG17	used in switched mode			750-456	analog input ±10 V
EBS.GDG17	used in switched mode			750-456	analog input ±10 V
EBS.GDG17	used in switched mode			750-456	analog input ±10 V
EBS.GDG17	used in switched mode			750-456	analog input ±10 V
EBS.EX80	extractor 2 V		8	750-550	analog output 0-10 V
EBS.EX80	extractor 2 I		10	750-550	analog output 0-10 V

Table H4: Description of PROFIBUS slave number 22 controlling REXEBIS hardware. This slave provides the set voltages for the final steering elements used to match the incoming beam to the EBIS acceptance. The values currently held by the hardware are read back in slave 19

Equipment name	Description	Period	Element	Address	Module	Function
EBS.ST110	outer steering	injection	down	6	750-556	analog output
EBS.ST120	outer steering	extraction	down	4	750-556	analog output
EBS.ST110	outer steering	injection	up	2	750-556	analog output
EBS.ST120	outer steering	extraction	up	0	750-556	analog output
EBS.ST110	outer steering	injection	right	14	750-556	analog output
EBS.ST120	outer steering	extraction	right	12	750-556	analog output
EBS.ST110	outer steering	injection	left	10	750-556	analog output
EBS.ST120	outer steering	extraction	left	8	750-556	analog output
EBS.ST90	inner steering	injection	down	22	750-556	analog output
EBS.ST100	inner steering	extraction	down	20	750-556	analog output

Equipment name	Description	Period	Element	Address	Module	Function
EBS.ST90	inner steering	injection	up	18	750-556	analog output
EBS.ST100	inner steering	extraction	up	16	750-556	analog output
EBS.ST90	inner steering	injection	right	30	750-556	analog output
EBS.ST100	inner steering	extraction	right	28	750-556	analog output
EBS.ST90	inner steering	injection	left	26	750-556	analog output
EBS.ST100	inner steering	extraction	left	24	750-556 750-612	analog output supply module
		interlock		0	750-414	digital input 5 V
		interlock		2	750-414	digital input 5 V
		interlock		4	750-414	digital input 5 V
		interlock		6	750-414	digital input 5 V

Table H5: Description of PROFIBUS slave number 1 controlling electrostatic beam optical elements used for matching the beam to the acceptance of the RFQ

Equipment name	Description	Period	Polarity	Address	Module	Function
SEP.OP10	octupole	static	negative	0	750-550	analog output
SEP.OP10	octupole	static	positive	2	750-550	analog output
SEP.QS20a	steering quad.	static	positive	4	750-550	analog output
SEP.QS20b	steering quad.	static	positive	6	750-550	analog output
SEP.QS20a	steering quad.	static	positive	8	750-550	analog output
SEP.QS20b	steering quad.	static	positive	10	750-550	analog output
SEP.BE30	bender	static	negative	12	750-550	analog output
SEP.BE30	bender	static	positive	14	750-550	analog output
SEP.QP40	quadrupole	static	negative	16	750-550	analog output
SEP.QP40	quadrupole	static	positive	18	750-550	analog output
SEP.QP50	quadrupole	static	negative	20	750-550	analog output
SEP.QP50	quadrupole	static	positive	22	750-550	analog output
SEP.QS60a	steering quad.	static	negative	24	750-550	analog output
SEP.QS60b	steering quad.	static	negative	26	750-550	analog output
EBS.QS60a	steering quad.	static	positive	28	750-550	analog output
EBS.QS60b	steering quad.	static	positive	30	750-550	analog output
RFQ.QP40	quadrupole	static	negative	32	750-550	analog output
RFQ.QP40	quadrupole	static	positive	34	750-550	analog output
RFQ.QS50a	steering quad.	static	negative	36	750-550	analog output
RFQ.QS50a	steering quad.	static	negative	38	750-550	analog output

Equipment name	Description	Period	Polarity	Address	Module	Function
RFQ.QS50a	steering quad.	static	positive	40	750-550	analog output
RFQ.QS50b	steering quad.	static	positive	42	750-550	analog output
RFQ.QP70	quadrupole	static	negative	44	750-550	analog output
RFQ.QP70	quadrupole	static	positive	46	750-550	analog output
RFQ.QP80	quadrupole	static	negative	48	750-550	analog output
RFQ.QP80	quadrupole	static	positive	50	750-550	analog output
RFQ.QP90	quadrupole	static	negative	52	750-550	analog output
RFQ.QP90	quadrupole	static	positive	54	750-550	analog output
RFQ.QS100a	steering quad.	static	negative	56	750-550	analog output
RFQ.QS100a	steering quad.	static	negative	58	750-550	analog output
RFQ.QS100b	steering quad.	static	positive	60	750-550	analog output
RFQ.QS100b	steering quad.	static	positive	62	750-550	analog output

Table H6: PROFIBUS slave number 2 controlling the dipole magnet of the REX mass separator

Equipment name	Description	Address	Module	Function
SEP.MD100	on = 1, off = 0	4, bit 1	750-513	digital output
SEP.MD100	0.5 s = 1 ≥ on	4, bit 2	750-513	digital output
SEP.MD100	not used	4, bit 3	750-513	digital output
SEP.MD100	not used	4, bit 4	750-513	digital output
SEP.MD100	not used	4, bit 5	750-513	digital output
SEP.MD100	not used	4, bit 6	750-513	digital output
SEP.MD100	not used	4, bit 7	750-513	digital output
SEP.MD100	not used	4, bit 8	750-513	digital output
SEP.MD100	magnet I (coarse)	0	KL4132	a.o. 16 bit ±10 V
SEP.MD100	magnet I (fine)	2	KL4132	a.o. 16 bit ±10 V
SEP.MD100	magnet I (coarse)	0	750-468	analog input
SEP.MD100	magnet I (fine)	2	750-468	analog input
SEP.MD100	not used	4	750-468	analog input
SEP.MD100	not used	6	750-468	analog input
SEP.MD100	on = 1, off = 0	8	750-401	digital input

Table H7: Description of PROFIBUS slave number 20 controlling the magnetic quadrupole triplet in front of the target station

Equipment name	Description	Address	Module	Function
spare	I	0	750-468	analog input
BEN.MQ70	I	2	750-468	analog input
BEN.MQ80	I	4	750-468	analog input
BEN.MQ90	I	6	750-468	analog input
spare		0	750-550	analog output
BEN.MQ70	I	2	750-550	analog output
BEN.MQ80	I	4	750-550	analog output
BEN.MQ90	I	6	750-550	analog output
spare	on	30	750-514	relay output
BEN.MQ70	on	32	750-514	relay output
spare	off	34	750-514	relay output
BEN.MQ70	off	36	750-514	relay output
BEN.MQ80	on	38	750-514	relay output
BEN.MQ90	on	40	750-514	relay output
BEN.MQ80	off	42	750-514	relay output
BEN.MQ90	off	44	750-514	relay output
		46	750-608	power supply
spare	water interl. p.s.	48	750-414	digital output
spare	temp. interl. p.s	50	750-414	digital output
spare	phase error	52	750-414	digital output
spare	power off	54	750-414	digital output
spare	channel on	56	750-414	digital output
spare	water interl. mag.	58	750-414	digital output
spare	temp. interl. mag.	60	750-414	digital output
spare	over current p.s.	62	750-414	digital output
BEN.MQ70	water interl. p.s.	48	750-414	digital output
BEN.MQ70	temp. interl. p.s	50	750-414	digital output
BEN.MQ70	phase error	52	750-414	digital output
BEN.MQ70	power off	54	750-414	digital output
BEN.MQ70	channel on	56	750-414	digital output
BEN.MQ70	water interl. mag.	58	750-414	digital output
BEN.MQ70	temp. interl. mag.	60	750-414	digital output
BEN.MQ70	over current p.s.	62	750-414	digital output

Equipment name	Description	Address	Module	Function
BEN.MQ80	water interl. p.s.	48	750-414	digital output
BEN.MQ80	temp. interl. p.s	50	750-414	digital output
BEN.MQ80	phase error	52	750-414	digital output
BEN.MQ80	power off	54	750-414	digital output
BEN.MQ80	channel on	56	750-414	digital output
BEN.MQ80	water interl. mag.	58	750-414	digital output
BEN.MQ80	temp. interl. mag.	60	750-414	digital output
BEN.MQ80	over current p.s.	62	750-414	digital output
BEN.MQ90	water interl. p.s.	48	750-414	digital output
BEN.MQ90	temp. interl. p.s	50	750-414	digital output
BEN.MQ90	phase error	52	750-414	digital output
BEN.MQ90	power off	54	750-414	digital output
BEN.MQ90	channel on	56	750-414	digital output
BEN.MQ90	water interl. mag.	58	750-414	digital output
BEN.MQ90	temp. interl. mag.	60	750-414	digital output
BEN.MQ90	over current p.s.	62	750-414	digital output

Table H8: Description of PROFIBUS slave number 21 controlling the dispersion magnet bending the beam towards the target station(s)

Equipment name	Description	Address	Module	Function
BEN.MD60	magnet I	0	KL4132	a.o. 16 bit ±10 V
BEN.MD60	magnet I	2	KL4132	a.o. 16 bit ±10 V
BEN.MD60	magnet I	0	750-467	analog input
BEN.MD60	magnet I	2	750-467	analog input

Table H9: Description of PROFIBUS slave number 22 controlling the magnetic steering in the seven-gap section

Equipment name	Description	Address	Module	Function
7GP.ST10X	water interl. p.s.	0	750-556	a.o. ±10 V
7GP.ST20X	temp. interl. p.s	2	750-556	a.o. ±10 V
7GP.ST20Y	phase error	4	750-556	a.o. ±10 V
7GP.ST20Y	power off	6	750-556	a.o. ±10 V
7GP.ST10X	channel on	0	750-456	a.i. ±10 V
7GP.ST20X	water interl. mag.	2	750-456	a.i. ±10 V
7GP.ST20Y	temp. interl. mag.	4	750-456	a.i. ±10 V

Equipment name	Description	Address	Module	Function
7GP.ST20Y	over current p.s.	6	750-456	a.i. ±10 V

Table H10: Description of PROFIBUS slave number 22 controlling the bender section

Equipment name	Description	Address	Module	Function
BEN.ST10X	water interl. p.s.	0	750-556	a.o ±10 V
BEN.ST20X	temp. interl. p.s	2	750-556	a.o ±10 V
BEN.ST20Y	phase error	4	750-556	a.o ±10 V
BEN.ST20Y	power off	6	750-556	a.o ±10 V
BEN.ST10X	channel on	0	750-456	a.i. ±10 V
BEN.ST20X	water interl. mag.	2	750-456	a.i. ±10 V
BEN.ST20Y	temp. interl. mag.	4	750-456	a.i. ±10 V
BEN.ST20Y	over current p.s.	6	750-456	a.i. ±10 V